PREDICTABILITY OF CURRENT AND FUTURE MULTI-RIVER DISCHARGES: GANGES, BRAHMAPUTRA, YANGTZE, BLUE NILE, AND MURRAY-DARLING RIVERS

A Dissertation
Presented to
the Academic Faculty

by

Jun Jian

In Partial Fulfillment
of the Requirements for the Degree
Doctor of Philosophy in the
School of Earth and Atmospheric Sciences

Georgia Institute of Technology
December 2007

PREDICTABILITY OF CURRENT AND FUTURE MULTI-RIVER DISCHARGES: GANGES, BRAHMAPUTRA, YANGTZE, BLUE NILE, AND MURRAY-DARLING RIVERS

Approved by:

Dr. Peter J. Webster, Advisor
School of Earth & Atmospheric Sciences
Georgia Institute of Technology

Dr. Marc Stieglitz
School of Civil & Environmental Engineering
Georgia Institute of Technology

Dr. Judith Curry
School of Earth & Atmospheric Sciences
Georgia Institute of Technology

Dr. Robert Black
School of Earth & Atmospheric Sciences
Georgia Institute of Technology

Dr. Rong Fu
School of Earth & Atmospheric Sciences
Georgia Institute of Technology

Date Approved: September 18, 2007

ACKNOWLEDGEMENTS

First and most sincerely I want to give my most gratefulness to my advisor Dr. Peter J. Webster. During over five years he has lead and support me in academic, social, grammar, and other areas, without his great constitution I can not begin, insist on, and finish this study.

Hai-Ru Chang, Carlos D. Hoyos, Violeta Toma, Paula Agudelo, and other colleagues in our research group shared their knowledge and experiences with generosity and provided a good atmosphere. I appreciated that.

I want to thank all the professors who are in my defense committee or have taught me in class. Their instructions are great treasures to me. I want to thank all the people who took the time to review this paper and comment on it.

I wish to thank my friends Dan Collins, Claire M Cosgrove, Yanping He, Thomas Hopson, Arsineh Hecobian, and many others. Without their kindness, compassion, and patience I would have a hard time as an international student.

At last, I want to thank my father Guoshu Jian and mother Lifang Su, and my wife Zhongying Wu. Their support in soul kept me going through this long way.

TABLE OF CONTENTS

LIST OF TABLES

LIST OF FIGURES

SUMMARY

Determining river discharge is of critical importance to many societies as they struggle with fresh water supply and risk of flooding. In Bangladesh, floods occur almost every year but with sufficient irregularity to have adverse social and economical consequences. Important goals are to predict the discharge to be used for the optimization of agricultural practices, disaster mitigation and water resource management. The aim of this study is to determine the predictability of river discharge in a number of major rivers on time scale varying from weeks to a century. We investigated predictability considering relationship between SST and discharge. Next, we consider IPCC model projections of river discharge while the models are statistically adjusted against observed discharges. In this study, we consider five rivers, the Ganges, the Brahmaputra, the Yangtze, the Blue Nile, and the Murray-Darling Rivers.

On seasonal time scales, statistically significant correlations are found between mean monthly equatorial Pacific sea surface temperature (SST) and the summer Ganges discharge with lead times of 2-3 months due to oscillations of the El Niño-Southern Oscillation (ENSO) phenomena. In addition, there are strong correlations in the southwest and northeast Pacific. These, too, appear to be tied to the ENSO cycle. The Brahmaputra discharge, on the other hand, shows somewhat weaker relationships with tropical SST. Strong lagged correlations relationships are found with SST in the Bay of Bengal but these are the result of very warm SSTs and exceptional Brahmaputra discharge during the summer of 1998. When this year is removed from the time series, relationships weaken everywhere except in the northwestern Pacific for the June

discharge and in areas of the central Pacific straddling the equator for the July discharge. The relationships are relative strong, but they are persistent from month to month and suggest that two different and sequential factors influence Brahmaputra river flow.

Second goal is to project the behavior of future river discharge forced by the increasing greenhouse gases (GHGs) and aerosols from natural and anthropogenic sources. Three more rivers, the Yangtze, Blue Nile, and Murray-Darling rivers are considered. It is meaningful to people living within the watershed, which would experience flooding or drought in the next 100-years. The original precipitation output from the third phase of Coupled Model Inter-comparison Project (CMIP3) project has large inter-model variability, which limits the ability to quantify the regional precipitation or runoff trends.

With a basic statistical Quantile-to-Quantile (Q-Q) technique, a mapping index was built to link each modeled precipitation averaged over river catchment and observational discharge measured close to the mouth. Using the climatological annual cycle to choose the "good" models, the observational river discharges are well reproduced from the 20th century run (20C3M) model results. Furthermore, with the same indices, the future 21st century river discharge of the Yangtze, the Ganges, the Brahmaputra, and the Blue Nile are simulated under different SRES scenarios. The Murray-Darling River basin does not have the similar seasonal cycle of discharge with modeled precipitations. So we choose to build the link between satellite imaged and modeled precipitations and use it to simulate the future precipitation.

The Yangtze, Ganges, Brahmaputra River mean wet season discharges are projected to increase up to 15-25% at the end of the 21st century under the most abundant GHGs

scenarios (SRESA1B and SRESA2). The risks of flooding also reach to a high level throughout the time. Inter-model deviations increase dramatically under all scenarios except for the fixed-2000 level concentration (COMMIT). With large uncertainty, the Blue Nile River discharge and Murray-Darling River basin annual precipitation do not suggest a sign of change on multi-model mean.

CHAPTER 1

INTRODUCTION

Societies with large populations exist within river watersheds obtaining water for social purpose, agriculture, and industrial production. For those societies, river discharge is the major source for water supply which eventually depends on precipitation. However, during a wet season when the river flow rate is large, the flood risk also increases.

The river discharge of the Ganges and Brahmaputra is of critical importance to India and Bangladesh with both rivers sustaining thriving agriculture societies. Each year, short-lived flooding occurs throughout the summer and early autumn but with sufficient irregularity to have adverse agricultural and societal consequences. These conditions also occur in other monsoon-affected river basins such as Yangtze and Mekong Rivers located in East and Southeast Asia.

Major flooding events occur in Bangladesh at least every 5 years. The devastating floods in 1998 killed 2,379 people and left 60% of Bangladesh under water for three months (Mirza et al. 2003, Chowdhury 2003). This year (2007), as of August 8, extreme flooding has already killed more than 1,500 in India and Bangladesh and forced millions from their homes (Seattle Times 2007). In China, flooding and associated disasters killed 4,150 people in 1998 (Wikipedia: China flooding), 1,292 in 2005 (China Daily 2005), and 652 till July 29, 2007 (People's Daily 2007). The water source of these floods is mainly from the precipitation occurring during the South East Asian monsoon which has marked oscillations on seasonal and intraseasonal time scales (e.g. Webster et al. 1998, Hoyos and Webster 2007).

On the other hand, extreme drought may also have great socioeconomic consequences. In 1980s, the catastrophic drought in the Horn of Africa region which includes the Blue Nile River basin caused over one million people to face famine (Hubbard et al. 1992). In December 2006, it was declared that Murray-Darling River basin had experienced a once in a 1000-year drought (New Zealand Herald 2006).

Occasionally, flooding is especially long-lived and destructive. Thus, an important challenge for the scientific community is to predict the discharge of these rivers for both minor and major flooding (and for significant reductions in discharge) to be used in the optimization of agricultural practices, disaster mitigation and water resource management.

Webster et al. (2004, 2006) have established a three-tier forecast for both Ganges and Brahmaputra River discharge on short-term (1-10 day), medium term (20-30 days), and long-term range (1-6 month) using post-processed European Centre for Medium Range Weather Forecasts (ECMWF) operational forecasts for the short term (Hopson 2005) and post-processed climate forecasts for the long-term (Hopson 2005, Hopson and Webster 2007). The intermediate forecast uses a physically-based Bayesian scheme developed by Webster and Hoyos (2004). The real-time forecasts can be found at http://cfab2.eas.gatech.edu/

1.1 Sea surface temperature (SST) as a climatic predictor

The surface layer of the tropical ocean absorbs the majority of the incoming solar radiation. A warm sea surface acts as a source of energy and moisture that helps drive the global atmosphere circulation. As a substantial lower boundary for atmosphere, the sea surface temperature (SST) is dominant in the genesis and maintenance of meteorological and oceanographic processes such as monsoon depressions and subsequent floods.

Furthermore, tropical Pacific SST is modulated by El Niño-Southern Oscillation (ENSO) events, which are robust coupled atmosphere-ocean phenomena. An ENSO event is the most dominant source for interannual variability in weather and climate.

In order to build a forecasting model, the general procedure is to find possible predictor variables from the complicated climate-hydrology system. SST anomalies, as well as snow cover, and upper and lower circulation anomalies, (Shukla 1987, Livezey 1990, Hastenrath 1987, Webster et al. 1998) are often used as climate predictors in empirical schemes to generate seasonal forecasts of summer monsoon strength and related river discharge for the Ganges and Brahmaputra basin. In addition to the above variables, precipitation, outgoing longwave radiation (OLR), sea level pressure (SLR), soil moisture, and others are used in sub-seasonal discharge forecasts (Webster and Hoyos 2004).

Given the societal impact of floods in the tropics, it is surprising how few fundamental studies have been undertaken to develop schemes for their prediction. Those that do exist have concentrated on seasonal prediction. For example, Amarasekera et al. (1997) found that the Amazon and Congo discharges were essentially uncorrelated with Pacific SST variability. In addition, higher correlations were found between subtropical rivers such as the Nile and the Parana and with ENSO. The Nile appears to be the most extensively studied river basin with the development of a number of predictive schemes (e.g., Wang et al. 1999, Tawfik 2003, Eldaw et al. 2003) all of which show similar relationships as Amarasekera et al. (1997). However, few studies have concentrated on the Ganges-Brahmaputra system.

1.2 Trends in current and future river discharges

Global warming is often used to refer to the global averaged near-surface temperature increase observed in recent decades and its possible future trend. Many studies have concentrated on studying the global warming and its associated climate change (La Treut et al. 2007 IPCC-AR4 WG1 page 103-121, Hegerl et al. 2007 IPCC-AR4 WG1 page 704-705).

From the 1970s, the global SSTs have been observed to posses an increasing trend (La Treut et al. 2007 IPCC-AR4 WG1 page 100-102, Agudelo and Curry 2004, Webster et al. 2005). During the same period, the Asian monsoon appears to have entered a decreasing trend (Wu 2005, Xu et al. 2006), which caused a downward trend of annual rainfall in those monsoon-affected area. Over a 120-year period, average correlation between the equatorial Pacific SST and seasonal All-India Rainfall Index (AIRI) is relatively strong at -0.64 (Webster et al. 1998). However, this large-scale and long-period ENSO-monsoon relationship is statistically non-stationary. The relationship has weakened during the early part of the 20^{th} century and possibly during the last few decades (Troup 1965, Kumar et al. 1999, Torrence and Webster 1998, 1999, Stephenson et al. 1999, Clark et al. 2000, 2003). In addition, while the reduction of seasonal rainfall results in a decrease of the river mean discharge, extreme flooding events have still occurred.

Given that the mean surface air temperature (SAT) is projected to rise in the next 100 years (e.g. Meehl et al. 2007 IPCC-AR4 WG1 page 749), it is important to consider the possible consequences of surface warming on weather and climate phenomena. Perhaps one of the most relevant questions from the societal point of view is whether or not river

discharge will increase or decrease dramatically. At the current stage, the numerical models are the only robust approach we could follow to estimate future climate. Most coupled climate models show an ENSO-like interannual variability in the past and in the future (Meehl et al. 2007 IPCC-AR4 WG1 page 751, Yukimoto et al 2000). However, the changes in future ENSO interannual variability differ from model to model. On the other hand, the monsoon trend is not simulated in a straightforward manner in the third phase of Coupled Model Inter-comparison Project (CMIP3), which consists of 23 atmosphere-ocean global circulation models (AOGCM). The multi-model mean Asian monsoon precipitation is projected to increase (Meehl et al. 2007 IPCC-AR4 WG1 page 778-779). However, the associated tropical Hadley, Walker and monsoon circulation is projected weakening as suggested by Tanaka et al. (2005).

With the highest global population density within their basins (Figure 1.1), the Ganges, Brahmaputra, Yangtze Rivers have large seasonal flow rates, which are mostly provided by Asian summer monsoon precipitation. The Blue Nile and Murray-Darling rivers, with much smaller flow rates, also provide water supply for people living in broad areas. In each of these basins, precipitation is related to strong monsoon circulations (except for Murray-Darling River) and modulated by SST anomalies. These river basins were chosen because of their importance to regional societies, as well as their relative differences to the Ganges, Brahmaputra, and Yangtze rivers and the availability of relatively long data records. The time series of annual mean river discharges are shown in Figure 1.2. A summary of the river discharge data in each basin are shown in Table 1.1. Detailed discussion can be found in Chapter 2 (for the Ganges and Brahmaputra rivers) and Chapter 3 (for the Yangtze, Blue Nile, and Murray-Darling rivers)

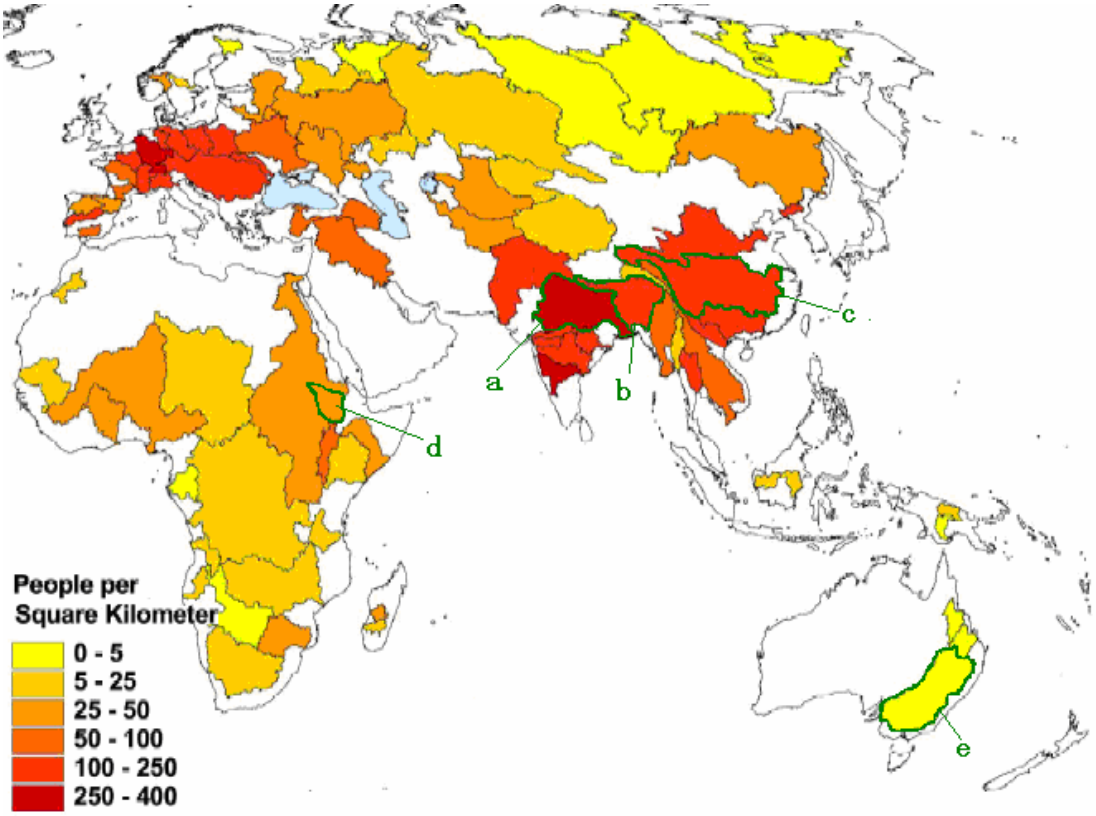

Figure 1.1 River watershed locations in the African, Asian, and Oceania continents discussed in the text are circled with thick green contours (a) the Ganges, (b) the Brahmaputra, (c) the Yangtze, (d) Blue Nile branch of the Nile River, and (e) the Murray-Darling River. The colors indicate the basin-average population density. High-population densities are found in Western Europe, South and East Asia. The Ganges, Brahmaputra and Yangtze River basins are located in the latter area, highly affected by Asian monsoon, and ranked among the top 10 largest rivers in the world (applied from World Resource Institute, http://earthtrends.wri.org/maps_spatial/watersheds/index.php).

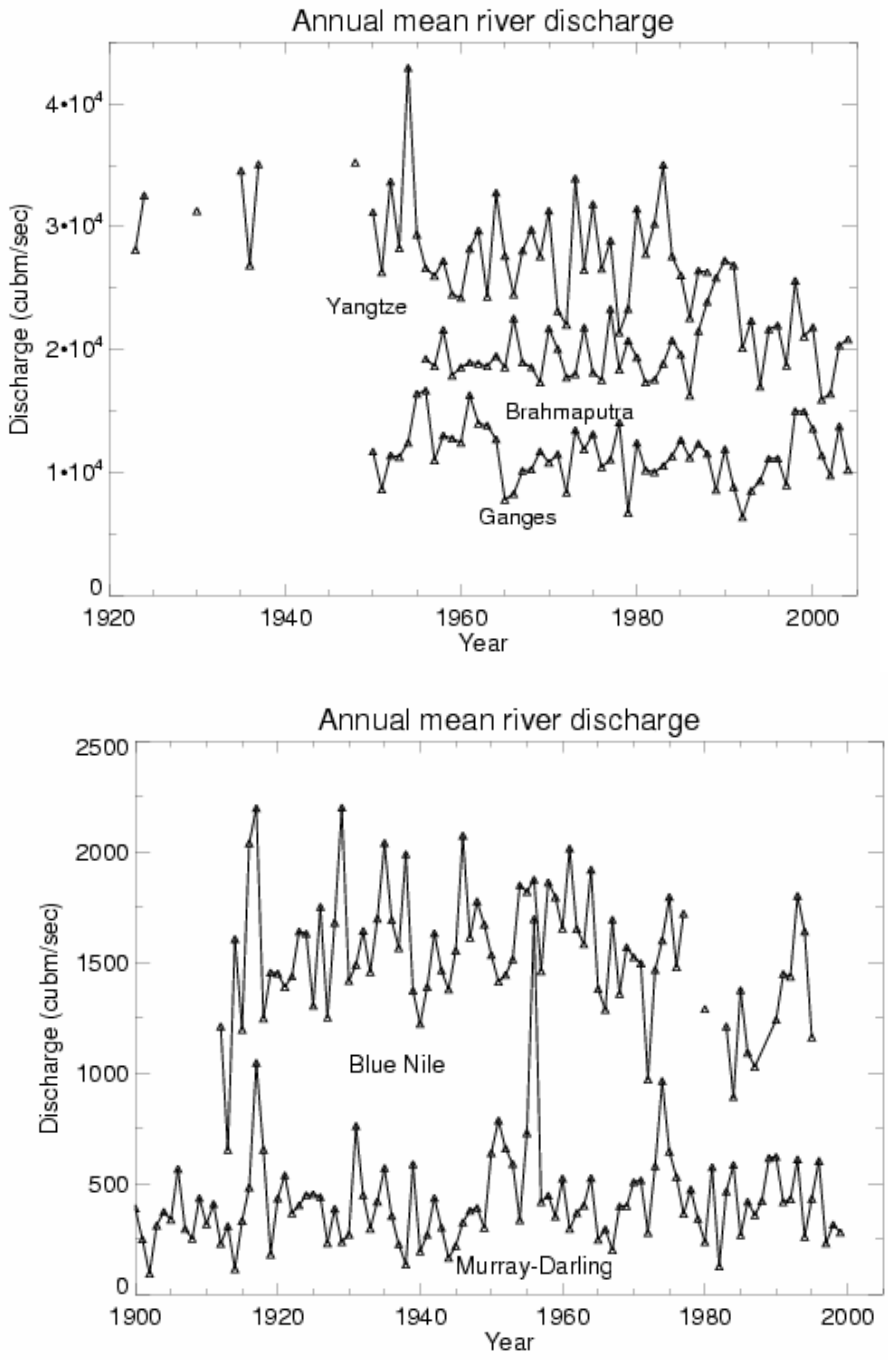

Figure 1.2 Observational annual mean river discharges of the Yangtze, the Ganges, the Brahmaputra (upper panel) and the Blue Nile rivers (bottom panel) over the 20th century. The modeled Murray-Darling annual mean discharge series are shown in the bottom panel. The rivers in the upper panel exceed by one order in magnitude than the others.

Table 1.1 Characteristics of the observational discharge dataset of the five rivers (partially from Global Runoff Data Centre website 2007).

Discharge Features	Blue Nile	Ganges	Brahma-putra	Yangtze	Murray-Darling
Station location	Roseires Dam (34.4°E, 11.8°N)	Hardinge Bridge (24.08°N, 89.03°E)	Bahadurabad (25.18°N, 89.17°E)	Datong station (30.77°N, 117.62°E)	Downstream of Lock 1, close to (34°S, 141°E)
Catchment area (km^2)	210,000	846,300	636,130	1,705,383	> 991,000
Start and end date	1912-1995	1950-2004	1956-2004	1922-1988	1891-2000
Missing data percentage	1.2%	2%	6%	21%	0
Area where IPCC-AR4 modeled precipitation are averaged	34°E-39°E, 9°N-12°N	77°E-88°E, 24°N-29°N	89°E-96°E, 26°N-31°N	99°E-117°E, 26°N-32°N	140°E-151°E, 27°S-38°S
Approximate population	<80million	Totally > 500 million		400 million	2 million
Annual flow rate	1536 $m^3 s^{-1}$	11400 $m^3 s^{-1}$	20100 $m^3 s^{-1}$	28700 $m^3 s^{-1}$	423 $m^3 s^{-1}$
Note					Hydrological model results

The use of climate model projections is the most robust and perhaps the only approach we have to project future climate change and associated impacts in the hydrological cycle. The Intergovernmental Panel on Climate Change (IPPC) model runs made for the recent 4th assessment report (AR4) CMIP3 models provide simulated precipitation for both 20th and 21st centuries. Climate models should be evaluated by their ability to simulate past climate before they are used for estimations of future climate change. However, the quantitative measurement of large-scale precipitation starts during

the late 1970s with the satellite-based technology. On the other hand, measurements of discharge from in-situ gauges, which can be interpreted at the first order as an integration of precipitation over its catchment, are available for a much longer time.

1.3 Thesis outline

Given the importance of river discharges for the inhabitants of river basins, it is important to find answers for the following questions: (i) Is there any statistically significant relationship between the SST variability and the intraseasonal and seasonal variability of the river discharge, i.e. will SST variation contribute to the predictability of intraseasonal and seasonal river discharge anomalies? (ii) What is the river discharge projection for the next 100 years under different climatic forcings introduced by greenhouse gases (GHGs) and aerosols from natural or anthropogenic sources?

This work consists of two major parts. In the first part, we examine whether there are useful antecedent SST signals for Ganges and Brahmaputra River discharges in the evolving climate system on time scales ranging from intraseasonal to seasonal. Such finding would potentially help in the improvement of prediction and understanding the river discharge variability in the Ganges- Brahmaputra River delta.

The second part of this study constitutes an effort to obtain an objective and quantitative estimation (via coupled climate models) of rivers' response to increased GHGs concentrations. The extra GHGs in the atmosphere are assumed to be the results of increased anthropogenic activities after the revolution of industrialization and increase of population.

In the second part of this study, different statistical techniques are used. In particular, a Quantile-to-Quantile (Q-Q) technique enables the adjustment of the biases in the

coupled climate models to a reasonable level for a quantitative study. Unlike the other purely statistical analysis (Allen and Tett 1999, Palmer 2000, Craig et al. 2001), the climatological annual cycle of precipitation is used to evaluate the different coupled climate models from a physical point of view.

The emphasis of this study is to project the future discharges of the Ganges, the Brahmaputra, the Yangtze, the Blue Nile, and Murray-Darling rivers. The same goal, when we predict the discharge of Ganges and Brahmaputra River flooding, is valid toward other rivers as well as it could be used in long time inter-governmental industry and agriculture productivity optimization, population mitigation and water resource management.

CHAPTER 2

PREDICTABILITY OF THE GANGES AND BRAHMAPUTRA RIVER DISHCARGE ON INTRASEASONAL AND SEASONAL TIME SCALES

2.1 Introduction

Accurate and timely forecasts of river flow have the potential of providing critical information for water resource management, agriculture optimization and disaster mitigation. Nowhere is the need for reliable and timely forecasts more urgent than in the Bangladesh delta, which is fed by two of the largest river systems in the world: the Brahmaputra and Ganges (Figure 2.1a). The catchment area of the Ganges system extends across the great plains of northern India beginning in Nepal and along the southern slopes of the Himalaya. The Brahmaputra basin, on the other hand, extends northward through Assam and Bhutan and then westward into the Himalayas and the Tibetan Plateau. River flow through Bangladesh, located at the confluence of these two great rivers, is fed by a combined catchment area that ranks tenth in size on the planet. In terms of discharge, the combined climatological flow is only surpassed by the Amazon and the Congo.

Each year, Bangladesh has short-lived flooding occurs from July to September with sufficient irregularity to have disruptions to social and agricultural activities and claim lives. For example, the summers of 1987 and 1988 also brought devastating flood of similar extent and duration. Given the consequences of major flooding, the rationale for

developing accurate forecast schemes is obvious. Furthermore, forecasting of the location and timing of the smaller floods 10-30 days in advance can allow advantageous changes in planting, harvesting, fertilizing and pest control (Subbiah 2004, Webster et al. 2006).

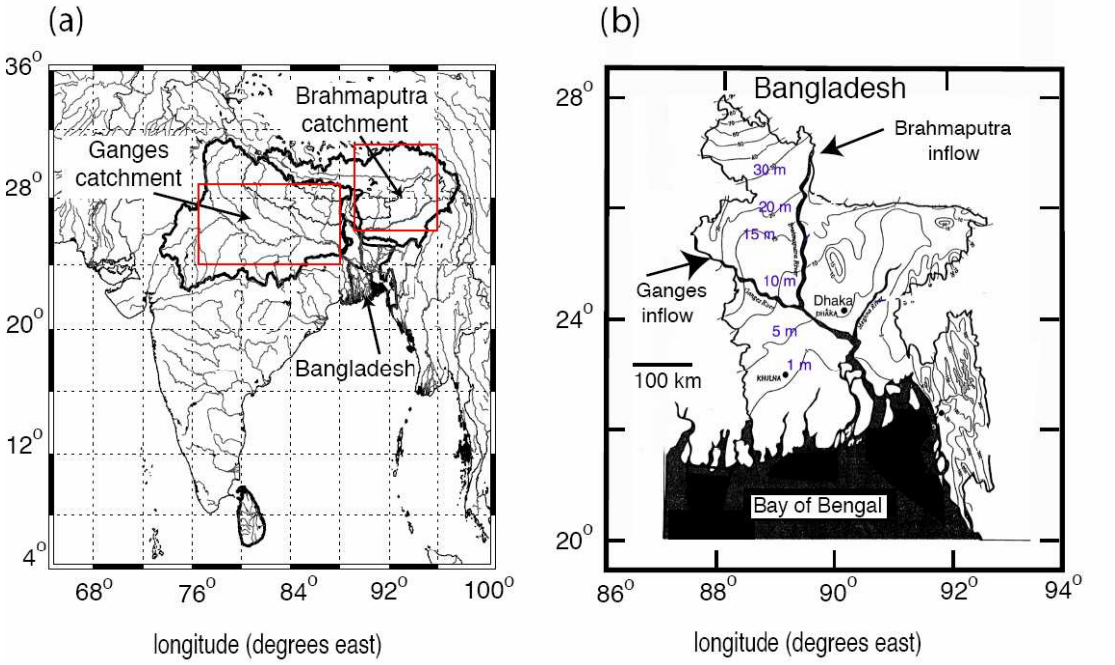

Figure 2.1 Geography of locations discussed in the text. (a) The catchment areas of the Brahmaputra and Ganges rivers (solid outlines), and (b) Detailed map of Bangladesh and the entrance points of the Brahmaputra and Ganges rivers into the country where river flow measurements are made. The two staging stations are at Bahadurabad and Hardinge Bridge, respectively. Isopleths show elevation above mean sea level (m). Red boxes in (a) indicate the area where the climate model data are retrieved for discussion in Chapter 5.

The Bangladesh prediction problem is especially acute because no upstream river flow data, either current or historical, is available from India within which the catchments of the Ganges and Brahmaputra largely reside. Furthermore, only a limited amount of precipitation data is made available to Bangladesh. The only information of river discharge is that which is measured directly by the Bangladeshis themselves at the

locations where the two rivers enter Bangladesh from India (Figure 2.1b). As a result, authorities in Bangladesh have been restricted to issuing forecasts extending out to 2 days which is the river transit time for water through Bangladesh. Despite efforts to produce longer term forecasts of river discharge, the lack of upstream data has been crippling. From Bangladeshi perspective, the upstream Ganges and Brahmaputra catchments must be considered as the two largest un-gauged river basins on the planet. Without upstream data, short-term forecasting of river discharge (1-10 days) requires forecasting precipitation and other weather variables over the entire extent of the basins to initialize hydrological models. Because of this, it is important to see if longer term empirical forecasts are possible through associations with climatic oscillations that possess some predictability themselves.

Most studies seeking predictable elements of river discharge with large scale and easily identifiable climate indices have concentrated on the association of the Southern Oscillation Index (SOI). Amarasekera et al. (1997), for example, related interannual Pacific Ocean SST variability with the discharge of two tropical rivers, the Congo and the Amazon, and two subtropical rivers, the Parana and the Nile. The Amazon and Congo appeared weakly and negatively correlated with the SOI but with only 10% of the variance explained. The Nile and Parana, on the other hand, had twice the variance explained by the SOI, correlating negatively with the Nile and positively for the Parana. Berri et al. (2002) studied the Parana-La Plata complex and noting that during the El Ninos of 1983, 1992 and 1998 excessive flooding occurred requiring the evacuation of hundreds of thousands of people. Labat et al. (2004, 2005) using wavelet techniques showed that the Amazon, Parana, Orinoco and Congo river flows were influenced by the

SOI on a 3-6 year time scale in keeping with the earlier study of Amarasekera et al. (1997), while longer term variability was influenced by a combination of the Pacific Decadal Oscillation and the North Atlantic Oscillation.

Whitaker et al. (2001), concentrating on the Ganges, found a relatively strong relationship at the 95% significance level between annual river flow and indices of the extremes of El Nino Southern Oscillation (ENSO) and whether the SOI was increasing or decreasing, suggesting that there existed a basis for prediction. These encouraging results are in keeping with the relatively strong relationship between total Indian rainfall and ENSO (e.g., Yasunari 1990, Shukla and Paolino 1983, Shukla 1995).

Extensive analyses over wider time scales were conducted by Chowdhury (2003) and Chowdhury and Ward (2004) and extended to the Brahmaputra and the Meghna (Figure 2.1). Shamon et al. (2005), concentrating on the Brahmaputra, included an assessment of the importance of springtime Himalayan and Tibetan Plateau snow pack. Chowdhury and Ward found correlations between rainfall in the upper reaches of the Ganges and Brahmaputra catchment areas and the subsequent river discharge into Bangladesh. However, there was no categorization in terms of seasonal monsoon modes (e.g., “active” and “break” periods) and the lags that may occur in discharge relative to the extrema in the monsoon intraseasonal cycle (Lawrence and Webster 2001, 2002). Given that the active and break sequences follow a relatively robust pattern (Lawrence and Webster 2000) and possess considerable predictable (Webster and Hoyos 2004), the determination of a relationship between the phase of the monsoon intraseasonal variability and river discharge would appear to be potentially fruitful.

Chowdhury and Ward (2004) also correlated river discharge in different months with simultaneous distributions of SST in the Indo-Pacific region. Two general results were found: (i) The Ganges River flow correlates negatively with eastern-central Pacific SSTs and positively with the western Pacific SSTs, probably related to the El Nino-La Nina factor. (ii) The Brahmaputra discharge does not appear to have any direct relationship with the central–eastern Pacific SSTs, a result substantiated by Shaman et al. (2005), for both the river discharge and Bangladesh rainfall. These results appear consistent with Shukla (1995) who found decreasing correlations between the SOI and rainfall from the western par of the Ganges Valley (maximum) to Bangladesh (minimum). Positive correlations were found by Chowdhury and Ward (2004) between Brahmaputra discharge and the SSTs in northern Indian Ocean and western Pacific SSTs. Later we will study the robustness of the relationship with the former region. Finally, although limited by a short data record (9 years), Shaman et al. suggested that the Brahmaputra discharge was related to Himalayan snow depth during the previous spring.

2.2 Dataset used in this chapter

Ganges and Brahmaputra River discharge data come from observations made at staging stations at Bahadurabad on the Brahmaputra, and at Hardinge Bridge on the Ganges. Both stations lie close to the Bangladesh-Indian border (marked with arrows in Figure 2.1b). Daily Ganges and Brahmaputra River discharge data used in the study extend from 1950 to 2003 and 1956 to 2003, respectively. Short isolated missing data points (less than one per month) are interpolated linearly. Longer missing periods (several winters and from April 1971 to March 1972) were replaced by climatology mean

values. Data was obtained from the Bangladesh Flood Forecast and Warning Center in Dhakar, Bangladesh.

SST data was retrieved from NOAA Extended reconstructed SST dataset (Smith et al. 2003). It was constructed using the most recently available Comprehensive Ocean-Atmosphere Data Set (COADS) SST data and improved statistical methods that allow for stable reconstruction of sparse data. This monthly analysis begins January 1854 and extends to December 2003 with a resolution of two degrees latitude by two degrees longitude. In this research, only data for the period from 1950 to 2003 are considered to match the discharge data.

Daily and monthly rainfall products of the global merged precipitation analysis (GPCP; Huffman et al. 1997, Huffman et al. 2001, Adler et al. 2003) were used in this work. The pentad and monthly precipitation dataset cover the period over 1979 to 2004. This product, with 2.5 degrees spatial resolution, is based on many direct precipitation measures, including microwave and infrared retrievals, covering different periods within the entire data record (Huffman et al. 1997, Huffman et al. 2001, Adler et al. 2003). This dataset is obtainable from http://data.cdc.noaa.gov

2.3 Temporal variability in Ganges and Brahmaputra discharge

Figure 2.2a shows 11 years of the 50 plus years of Brahmaputra and Ganges discharge data described above. The time series shows high magnitude interannual variability and, within each year, subseasonal variance. The inset panel shows the annual cycles of both river flows measured at the India-Brahmaputra border from 1956 onwards.

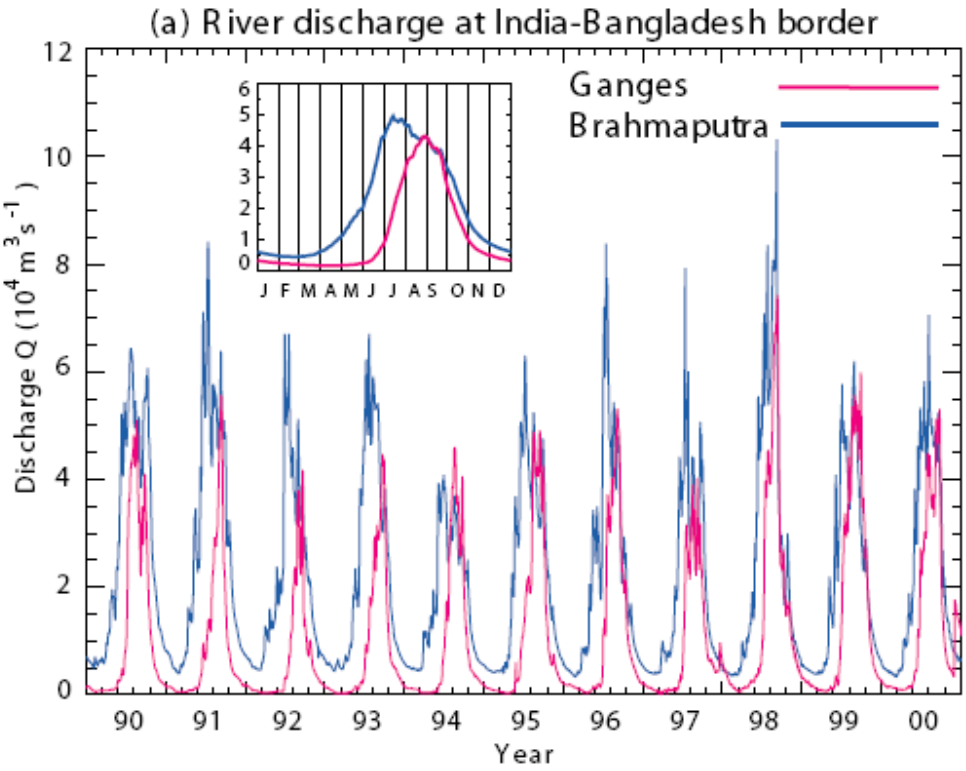

Figure 2.2 (a) The discharges of the Brahmaputra (blue) and the Ganges (red) rivers measured at Bahadurabad and Hardinge Bridge, respectively, for the eleven-year period. Inset shows the mean annual cycle of discharge calculated over the entire length of the dataset.

The annual cycles of discharge (inset: Figure 2.2 a) indicates significant phase differences. The Brahmaputra flow increases rapidly in late spring ahead of the Ganges by about two months. The earlier Brahmaputra discharge probably occurs because for two reasons. First, there is springtime snowmelt from the Himalayas and Tibetan Plateau that runs fairly unattenuated to the Bay of Bengal. Early Ganges discharge also depends on snowmelt in the Nepalese Himalaya which occurs at roughly the same time as at the head of the Brahmaputra basin. But, residing between Nepal and Hardinge Bridge within the Ganges Valley are 10% of the global population which uses much of the early Ganges discharge for irrigation and the refilling of dams and other water diversions. Thus, part of

the differences in the annual cycles of the two rivers is probably the signature of extreme human active, plus the different basin time scales. The second reason is that rains occur in Assam (to the northeast of Bangladesh) some weeks earlier than over the Ganges catchment (Webster et al. 1998, Lawrence and Webster 2002). It should be noted that the differences in the annual cycles of the two rivers cannot be solely explained in terms of the isochrone analysis. To explain the differences in the timing of the springtime build-up of discharge, the isochrone analysis in the Brahmaputra would have to be in error by a factor of 8.

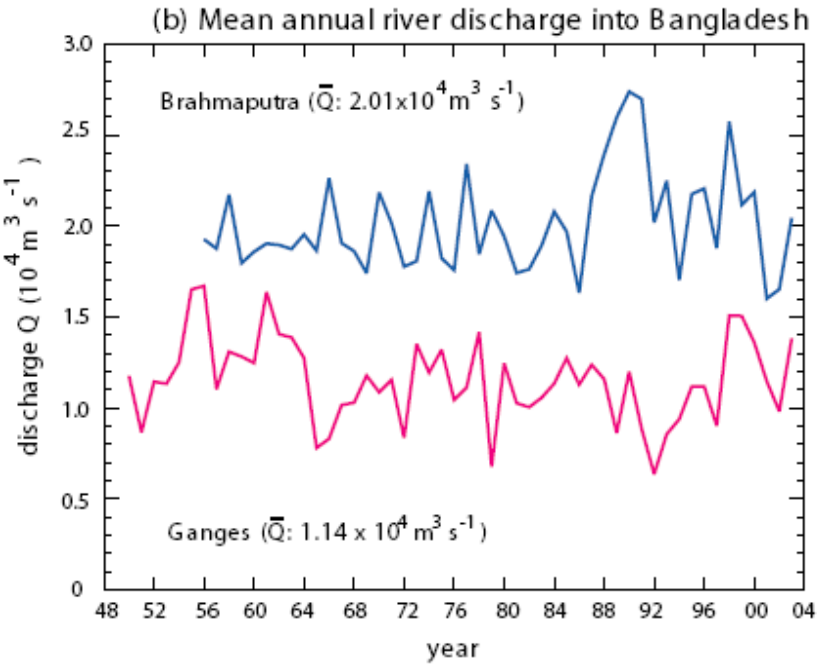

Figure 2.2 (b) Mean annual discharge of the Brahmaputra (blue) and Ganges (red) for the periods 1950 to 2003 and 1956 to 2003, respectively.

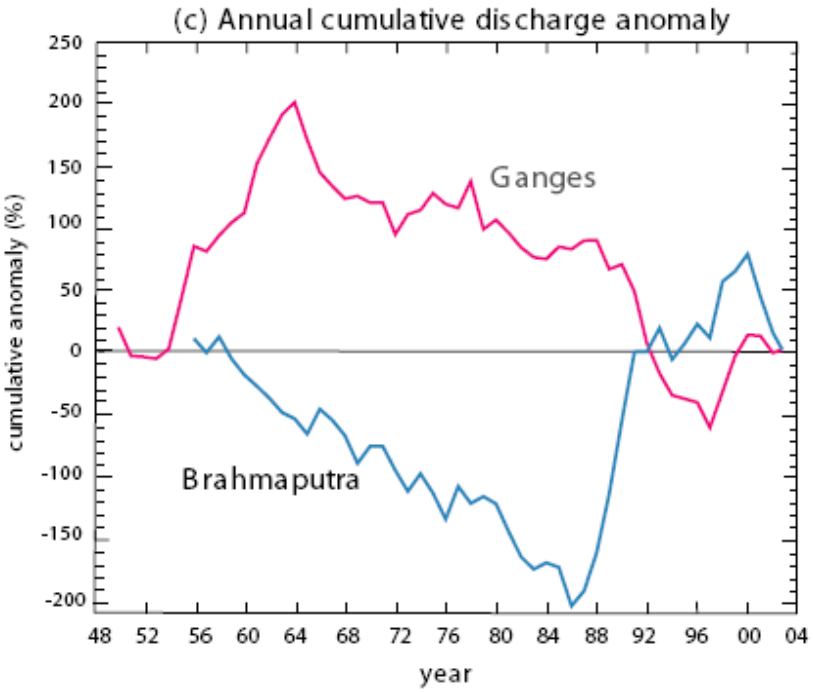

Figure 2.2 (c) Cumulative river discharge for the Brahmaputra (blue) and Ganges (red)

A time series of annual mean discharge for each of the rivers is shown in Figure 2.2 (b). The long-term mean annual discharge for the Brahmaputra is 2.01×10^4 m^3 s^{-1} compared to $1.14 \times 10^4 m^3$ s^{-1} for the Ganges. The cumulative discharge time series shown in Figure 2.2 (c) indicates considerable interannual variability in the discharge of both the Ganges and the Brahmaputra rivers. Between 1988 and the present, the Brahmaputra discharge has been well above average. The Ganges, on the other hand, has shown a steady decrease in discharge since the 1960s. The decrease in the Ganges discharge appears to be consistent with the decrease in the strength of the overall Indian monsoon since the early 1970s (e.g., Webster et al. 1998). Years of excessive discharge can be seen to correspond to above average discharge (1987, 1988, and 1998).

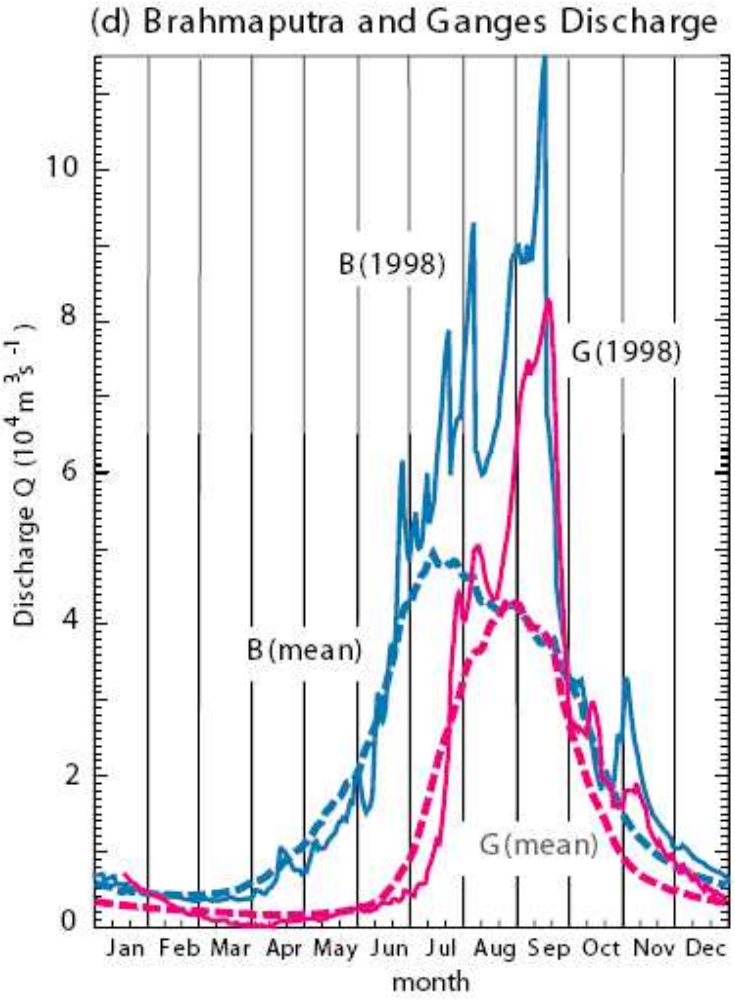

Figure 2.2 (d) Detail of the Brahmaputra a (blue) and Ganges (red) for 1998 measured at Bahadurabad and Hardinge Bridge. Besides exceeding the long-term averages considerably and possessing maximum amplitudes of twice the mean annual cycle, there is evidence of intraseasonal variability in the discharge.

River streamflow is highly correlated with precipitation occurring at locations higher up in the catchment basin as shown by Chowdhury and Ward (2004). In the Southeast Asian monsoon region, rainfall shows strong intraseasonal variability (30-80 days) during the wet season that results in active and break phases of the monsoon (e.g. Sikka and Gadgil 1980, Webster et al. 1998, Lawrence and Webster 2000, 2002). Discharge of rivers Ganges and Brahmaputra also shows variability in the intraseasonal band which explains about 10% of the daily discharge variance, which is a considerable amount considering the large amplitude of the annual cycle. Figure 2.2d shows details of the year 1998 for both rivers. Both rivers had early season discharges that were close to climatology. However, by mid-June, the Brahmaputra continued upward so that by the end of July the discharges was almost twice climatology. Peak flows occurred in mid-September with discharges nearly three times the September climatological values. The Ganges also peaked at the same time with double climatological values. Superimposed on both curves are distinct peaks throughout the summer.

2.4 Intraseasonal variability of Ganges and Brahmaputra discharge

Composite analysis of daily intraseasonal discharge variability reveals an almost in-phase relationship between the intraseasonal variability of both Ganges and Brahmaputra River flows (Figure 2.3). The composite time series were constructed based on 27 active events of Ganges discharge from 1996 to 2004 obtained from filtered daily time series in the 40-100 day spectral band. An active event is defined as a period of maximum

discharge in the 20-60 day band with a magnitude greater than one standard deviation of the mean variance within the band.

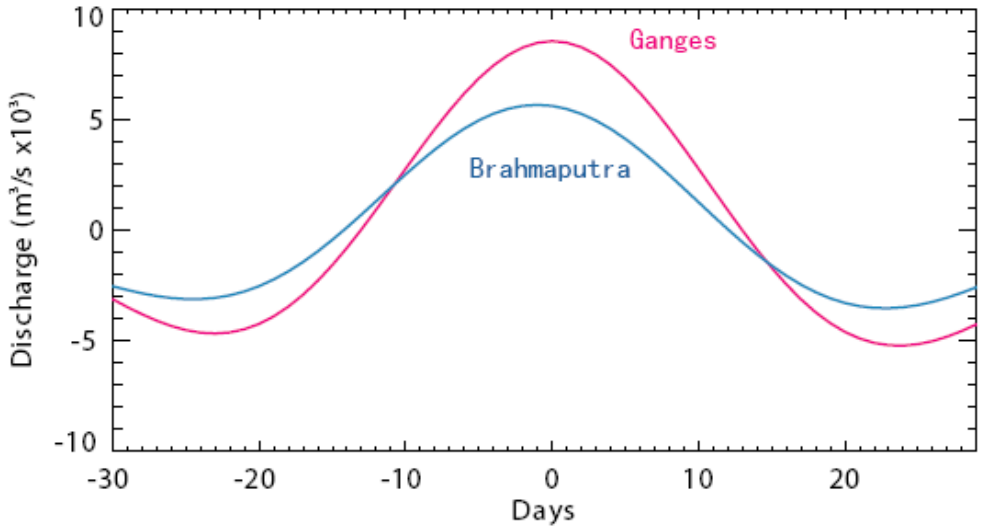

Figure 2.3 Composite analysis of daily intraseasonal discharge of the Ganges (red)-Brahmaputra (blue) rivers. A three-day lag is evident (from Jian et al. 2007).

The spatial progression of the rainfall anomalies provides an explanation of the low-pass filter introduced by the basin and the related change in the intraseasonal spectral peak. The basin acts not only as an integrator of the rainfall but also as a moving average operator of the rainfall time series. The composites show that the river discharge in both basins lags about 20 days the peak ISO rainfall over the Bay of Bengal, which, in itself is useful for discharge prediction. The memory introduced by the basin relative to the arrival of the large-scale intraseasonal active event should be taken into account when designing empirical forecasting schemes for Ganges and Brahmaputra discharge.

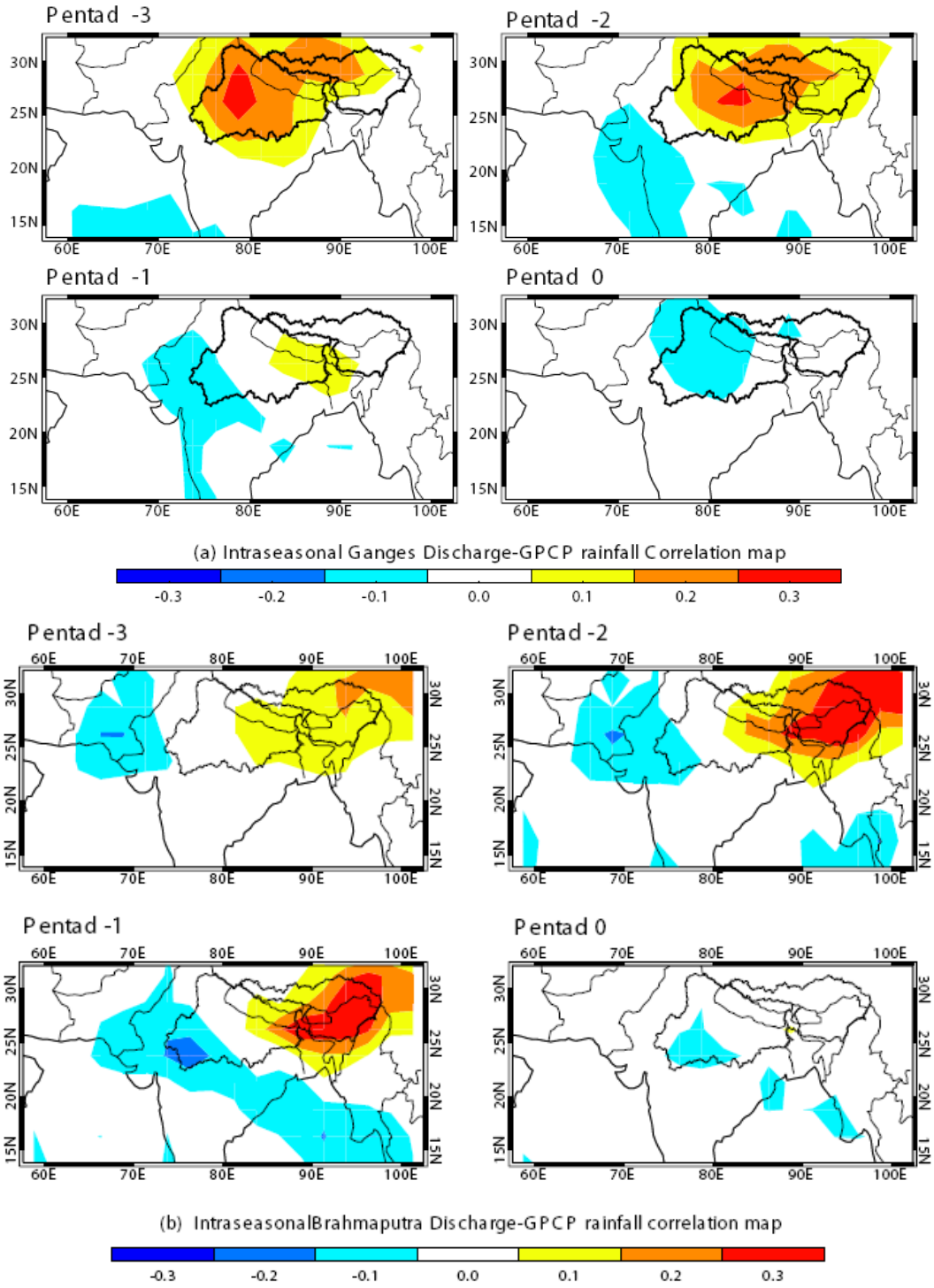

Figure 2.4 Spatial correlations between pentad Ganges (a) and Brahmaputra River (b) discharge and pentad precipitation in the intraseasonal band from pentad -3 to pentad 0. Both data series are filtered in 1-15 pentad band. High correlation is observed in upstream river basin and moves toward downstream with less lags.

The results of the composite analysis are confirmed by correlation analysis between pentad river discharge and pentad GPCP precipitation from 1979 to 2004. Figure 2.4 a shows the correlation between Ganges River discharge and precipitation in the 1-15 pentad intraseasonal band (5-60 days) for lag -3 to 0 pentads. The results indicate that the highest positive correlation between Ganges discharge and precipitation takes place over the Ganges basin with a lag of 3 pentads (15 days) with the rainfall leading discharge. We note also that there is an in-phase relationship between rainfall over the two basins. For example, at lags -3 and -2 pentads, the Ganges basin and upstream Brahmaputra basin show maximum precipitation. However, in Figure 2.4 (b), the precipitation over Brahmaputra Basin is in out-phase with upstream Ganges Basin at lags -3 and -2 pentads. Also we notice that the precipitation over Brahmaputra basin has stronger correlation with pentad discharge.

Hoyos (2006) has built basin isochrone maps for interpretation of river flow rates and the determination of hydrological time-scales for the two basins. During that process, a flow routing algorithm (Ramírez and Vélez 2002) and a digital elevation model are applied to the region to find the path and the distance of every grid cell to the outflow of the basin. For detailed applications, further hydraulic and terrain considerations are necessary to estimate the network flow velocity that is probably different at every grid cell. However, for both basins given their slope and land cover, the simplest way to estimate isochrones is by assuming constant average velocity of flow (here 1 m s^{-1}) within the entire basin network, including hill slopes and channels. Figure 2.5 shows isochrones in units of days for both the Ganges and Brahmaputra basins. Isochrones

should be interpreted as indicative of the average time it takes a parcel of liquid water located in some location within the basin to reach the outlet of the basin.

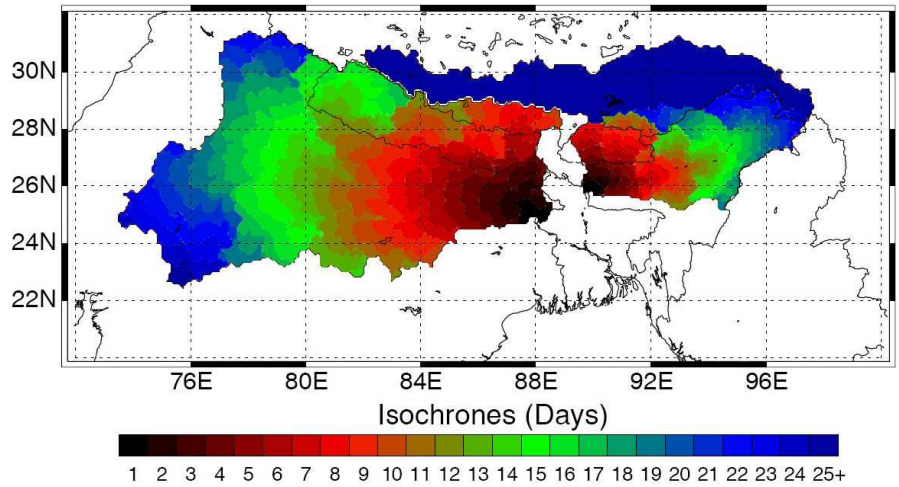

Figure 2.5 Isochrones (days) for the Brahmaputra and Ganges basins. The contours provide an estimate of the time it takes for water in a particular location in the basin to pass by Bahadurabad and Hardinge Bridge (from Jian et al. 2007).

The isochrones provide hydrologic support to the features observed in the composites. There is high degree of spatial coherency of the distribution of positive rainfall anomalies and their temporal occurrence (composite day) with the isochrones map. For example, for the Ganges basin, the geographic location of the rainfall anomalies at pentad -3 correspond almost one-to-one with isochrones of 17 to 23 days. Similar correspondence occurs in the Brahmaputra basin.

2.5 Seasonal variability

2.5.1 Seasonal discharge variability and SST

Figure 2.6 a shows correlations between the mean seasonal (July to September; JAS) Brahmaputra River discharge into Bangladesh and tropical Indo-Pacific SST on different seasonal lags using all years of available data. Shaded areas denote regions with correlation coefficients greater than 0.2. The 95% confidence level (r = 0.29) is marked by a solid black line. The figures from bottom to top in panel (a) show the simultaneous correlations, the JAS discharge and the prior April through June (AMJ) SST, and the JAS discharge with the prior January through March (JFM) SST, respectively. Overall, Figure 2.6 a shows very strong and significant broad scale correlations especially over the Indian Ocean. These are similar to the correlations found by Chowdhury (2003) and Chowdhury and Ward (2004). However, from Figure 2.2 c we note that the Brahmaputra discharge was very much stronger than average during the excessive flood year of 1998. The correlations were recalculated with the exclusion of 1998. These new correlations are shown in Figure 2.6 b indicating severely reduced correlations indicating that 1998 contributed an overridingly strong bias to the correlations. As it turns out, the summer of 1998 was an exceptional year in terms of the magnitude of the north Indian Ocean SST anomaly (Webster et al. 1999 and Saji et al. 1999) which reached an unprecedented 1.5°C above normal and occurred at the time of the 1997-1998 El Niño. Whereas there is usually a warming of the Indian Ocean associated with the declining phase of an El Niño, the anomaly is generally much weaker than that which occurred during the summer of 1998.

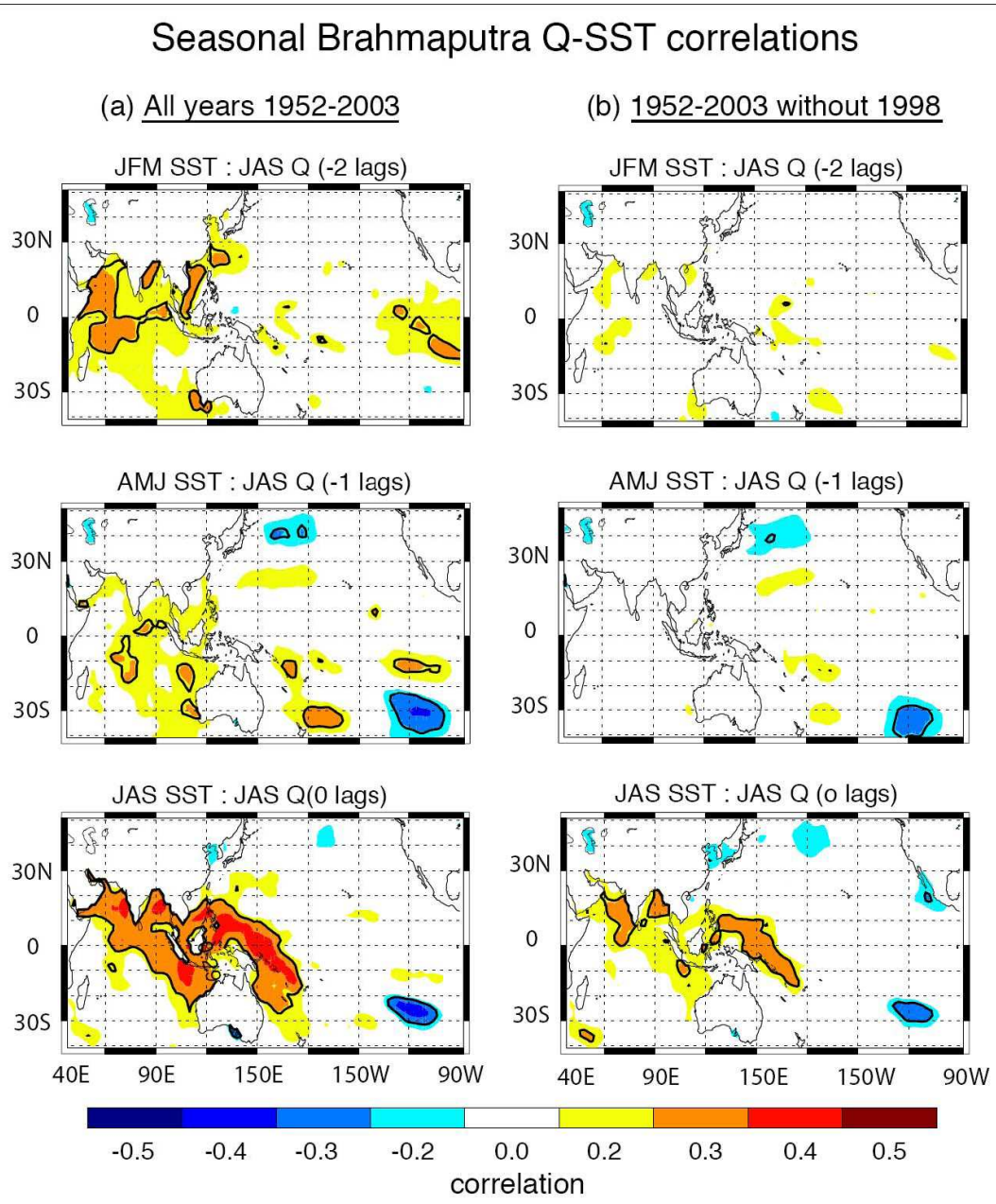

Figure 2.6 (a) Correlation map of JAS Brahmaputra River discharge with simultaneous SST, one-season lead (AMJ) SST, two-season lead (JFM) SST. (b) Same as (a) but with the omission of year 1998's value. A reduced correlation in all areas is observed with this omission.

In summary, with 1998 excluded, the SST-Brahmaputra discharge relationship is reduced to moderate regional simultaneous correlations in the Bay of Bengal. At lags, no significant correlation appears to exist. Statistically, the 1998 data represents an outlier that provides little contribution to the determination of long-term predictability. We can conclude that Brahmaputra River discharge is not significantly connected to ocean SST variance over long periods. Whether or not the unique and anomalous state of the Indian Ocean during the 1998 period resulted in the excessive discharge is unclear. This question would require experimentation with numerical climate models. Irrespective of the answer, it is clear that 1998 is not representative of the long-term predictability of the Brahmaputra River discharge.

The relationship between the Ganges discharge and regional SST is very different from those found for the Brahmaputra. Maps of correlations for the same lags are displayed in Figure 2.7. In the middle and bottom panels (lag -1 and lag 0), strong negative correlations occur in the central equatorial Pacific and also eastward and the north of the equator. On the other hand, strong positive correlations occur in the western and southwest Pacific Ocean. The strong positive correlations over the southwest Pacific Ocean (to the east of Australia) persist throughout the correlation period commencing, in embryonic form, at -2 lags or -6 months. In addition, relatively strong relationships exist with the equatorial northwest Pacific SST. These out-of-phase correlations between the Nino 3.4, the southwest Pacific and the northwest Pacific Ocean match the SST anomaly patterns associated with the ENSO cycle and are similar to the patterns constructed by Chowdhury et al. (2004). Overall, the strong SST-discharge correlations one season

ahead appear to suggest that useful predictability may exist for the Ganges River discharge.

It is interesting to note that there is a relative absence of correlations between SST in the Indian Ocean and the Ganges River discharge on the time scales considered in this section. In addition, unlike the Brahmaputra River case, the exclusion of 1998 makes little difference to the correlations shown in Figure 2.7. The absence of a link with the regional SST seems strange because the Indian Ocean plays an integral part in the dynamics of the monsoon circulation through heat and moisture transfer (e.g., Webster et al. 1998, Fasullo and Webster 2002). Also, the result is not in keeping with the modest relationships between Indian Ocean SST and All-India rainfall found by Harzallah et al. (1997) and Clark et al. (2000, 2002). Given that river discharge is essentially the integral of rainfall over the area of a catchment, one would expect stronger relationships with regional SST variability than that displayed in Figure 2.7. However, Harzallah et al. (1997) and Clark et al. (2000) both sought correlations of SSTs with the All-India Rainfall Index (AIRI), the large-scale measure of total rainfall over the entire subcontinent of India. It may be that the use of such a gross rainfall index is misleading. In fact, Webster and Hoyos (2004) noted that when district rainfall distributions were compared at the extremes of + or -1 standard deviation of the mean AIRI that there were large spatial variability of the anomalies, with states having negative anomalies in wet years and vice versa. In addition, Shukla (1995) has shown that the eastern part of the Ganges Valley is less correlated with the AIRI than the western part. In fact, towards Bangladesh the correlation actually reverses.

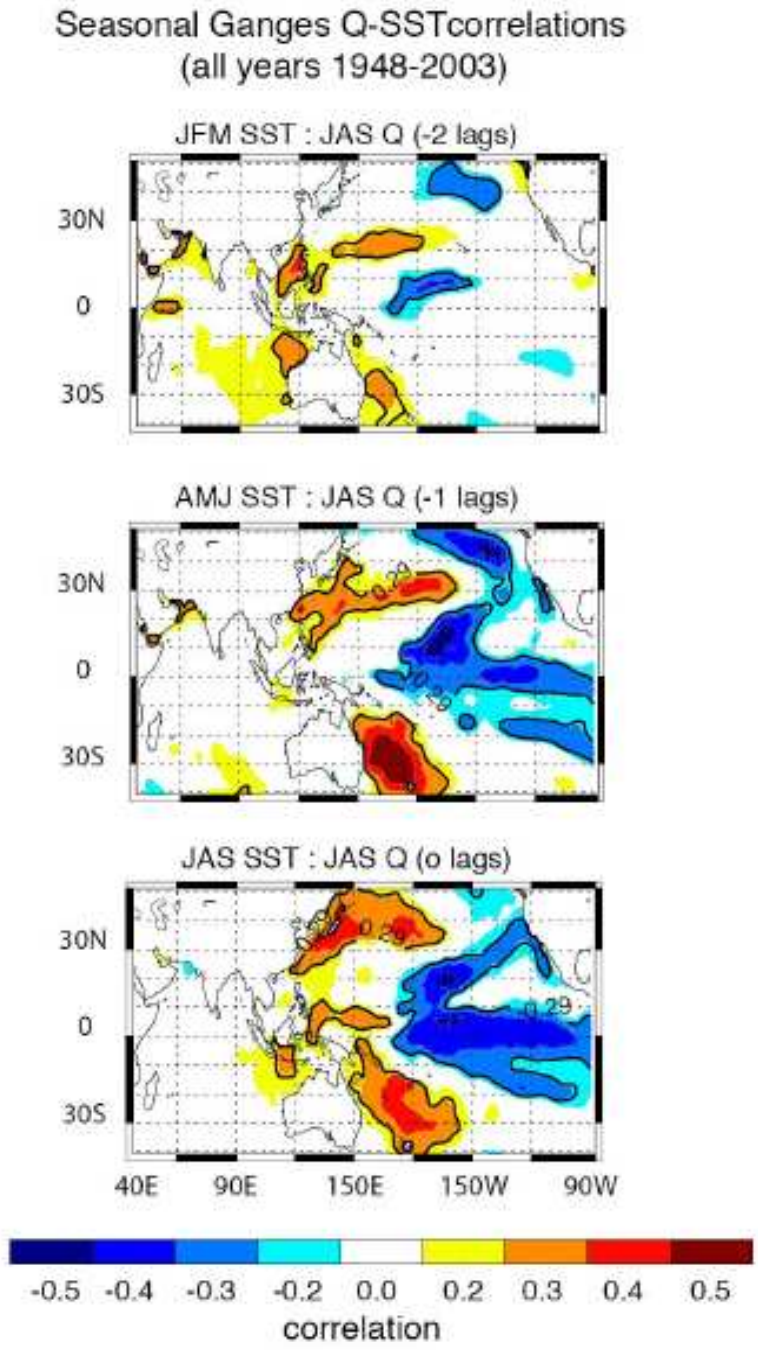

Figure 2.7 Same as Figure 2.6 (a) but with JAS Ganges River discharge

2.5.2 Monthly discharge variability and SST

The analysis is extended by correlating monthly Ganges discharge with monthly SST at different lags. The July Ganges discharge is correlated with the July (0 lag), June (-1 lags) and May (-2 lags) SSTs (Figures 2.8 a) and the August discharge with August (0), July (-1) and June (-2) SSTs (Figures 2.8 b). The correlation patterns are similar to those found in the seasonal calculations. The regions of high negative (positive) correlation in the central equatorial (southwest) Pacific exist for lags -2 months to lag 0. In addition, the moderate northwest Pacific correlations also persist. The highest correlation value observed is greater than 0.6 and occurs in the southwest Pacific Ocean between the May SST and the July Ganges flow. A similar analysis was conducted for the Brahmaputra discharge but regions of significance were not found.

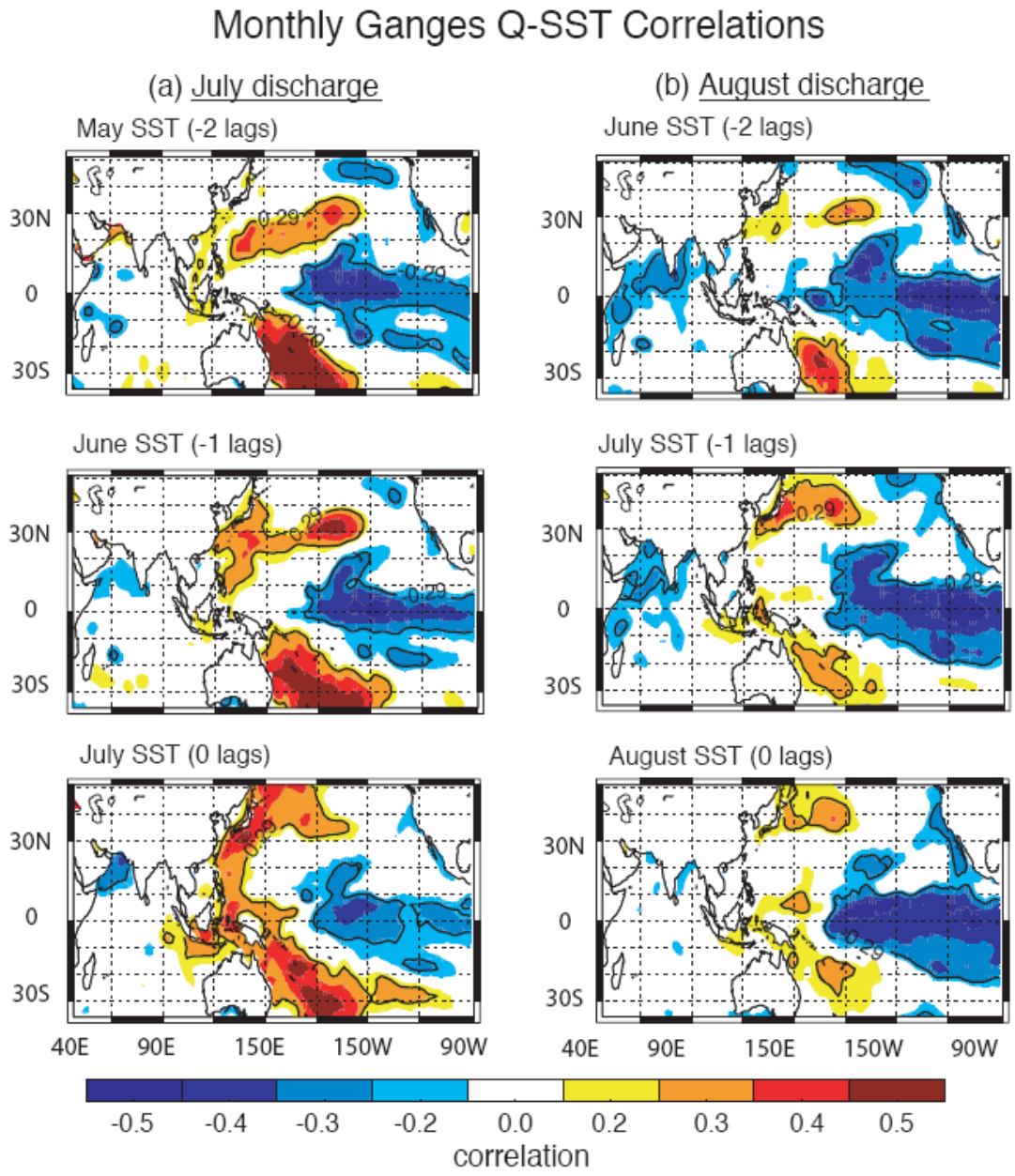

Figure 2.8 Correlation map of (a) July Ganges discharge with SSTs of July, June, and May (b) August Ganges discharge with SSTs of August, July, and June.

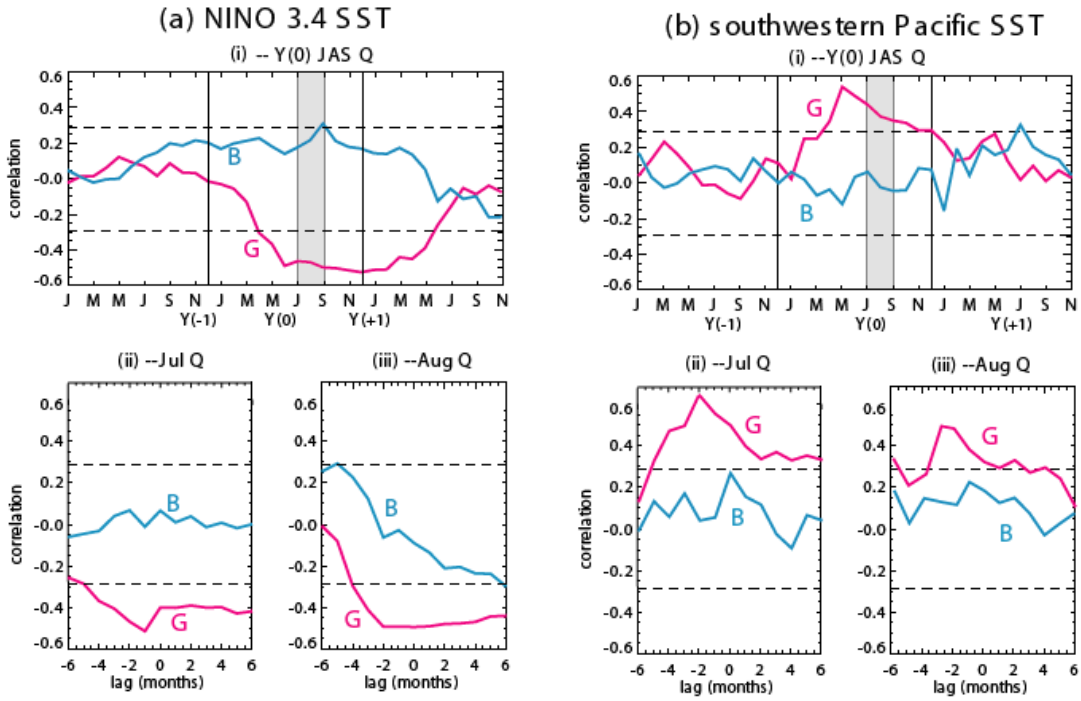

Figure 2.9 Systematic lagged correlations between two river (i) seasonal (ii) July ,and (iii) August discharges and (a) Nino 3.4 SST (b) southwestern Pacific SST.

Figure 2.9 presents lead-lag correlations between Ganges and Brahmaputra river discharge and the SST in areas of significant correlation found in Figures 2.6 - 2.8. Figure 2.9a refers to associations between the discharge of the two rivers with the Nino 3.4 SST variability (120°W-179°W and 5°N-5°S) and Figure 2.9 b with the SST in the southwestern Pacific Ocean (160˚E-180˚E, 30˚S-20˚S). The Nino 3.4 region was chosen following Trenberth (1997) as particularly sensitive to El Nino variability. The first panels (i) of both figures show lagged correlations over a three-year period. The composites are plotted relative to the peak Nino 3.4 SST anomaly shown in the upper part of the two panels. Thus Y(-1) refers here to the year preceding the January extreme in SST anomaly and Y(+1) refers to the year following the January extreme. The black

dash lines denote the 95% confidence interval deduced using Monte Carlo methods. The second and third panels show the correlations between monthly discharge (panel (ii) for July discharge and panel (iii) for August discharge) for lags of 6 months prior to and after the discharge.

For all lags and in all regions considered, the Brahmaputra River discharge and SST relationships do not exceed the 95% confidence level. The Ganges, on the other hand, possesses stronger and more widespread relationships. For example, Figure 2.9 a(i) shows that the JAS Ganges discharge is significantly correlated with the Nino 3.4 SST from March of Y(0) through March of Y(+1). That is, there appears to be predictability of the JAS discharge four months in advance. Similar predictability appears in the southwest Pacific Ocean SST (Figure 2.9 b(ii)). Figure 2.9 a(i) is similar to the lag relationships found by Yasunari (1990) between the eastern equatorial Pacific SST anomaly and Indian monsoon rainfall anomaly. Similar lag-lead relationships are found between the Ganges River discharge and the southwest Pacific Ocean SST. The major difference between the two regions is the shape of the correlation curves. The Nino 3.4 correlations tend to increase slowly with time through year Y(0) whereas the southwest Pacific Ocean correlation change rapidly during the early spring of Y(0).

The correlations between monthly discharge and SST (panels (ii) and (iii), Figure 2.9 a-b) show similar correlations patterns. The strongest relationship occurs between the southwest Pacific Ocean SST and the July Ganges discharge (Figure 2.9 (b), panel ii). At -4 lags, there is a highly significant relationship.

To demonstrate that the relationships between Pacific SST and the Ganges River discharge are not the result of individual large anomaly events or the influence of

statistical outliers such as found for the Brahmaputra in 1998, scatter plots of July Ganges discharge and the SST in the two regions are shown in Figure 2.10. The statistics appear to be well-behaved with La Nina being associated with strong Ganges discharge and El Nino with weak discharge. This is in keeping with the relatively strong relationship between ENSO and precipitation in the upper Ganges catchment area (Shukla 1995, Chowdhury 2003, Chowdhury and Ward 2004). Reversed and slightly stronger correlations exist between the Ganges discharge and the southwestern Pacific Ocean SST. It should be noted, however, that not all of the variance can probably be explained in terms of El Nino and La Nina. There are a number of extreme discharge years that occur during non-extreme ENSO years.

Noting that there appears to be very little relationship between the ENSO phenomenon and Brahmaputra discharge we extend the analysis to see if there are relationships with extra-tropical SST anomalies. Figure 2.11a shows that the June Brahmaputra River flow correlated beyond the 95% level with SST in the extra-tropical northwest Pacific Ocean to the east of Japan (150˚E-180˚E, 35˚N-45˚N) during the preceding winter and spring. Of some note is that the patterns are very similar for each of the lags. The maps of correlation contours and the scatter points (from May to February) are shown as a series of panels on the right-hand-side in the same format as Figure 2.11. Unlike with the Brahmaputra-Indian Ocean SST relationships, the correlations are not defined by outliers. The correlations are significant at the 95% level although the variance explained is relatively small (15-20%). Figure 2.11b shows SST correlations in the Indo-Pacific region for March through June but relative to the July Brahmaputra discharge. The positive correlations in the northwest Pacific have now become negative

and there are substantial areas of positive correlation spanning the equator in the central Pacific.

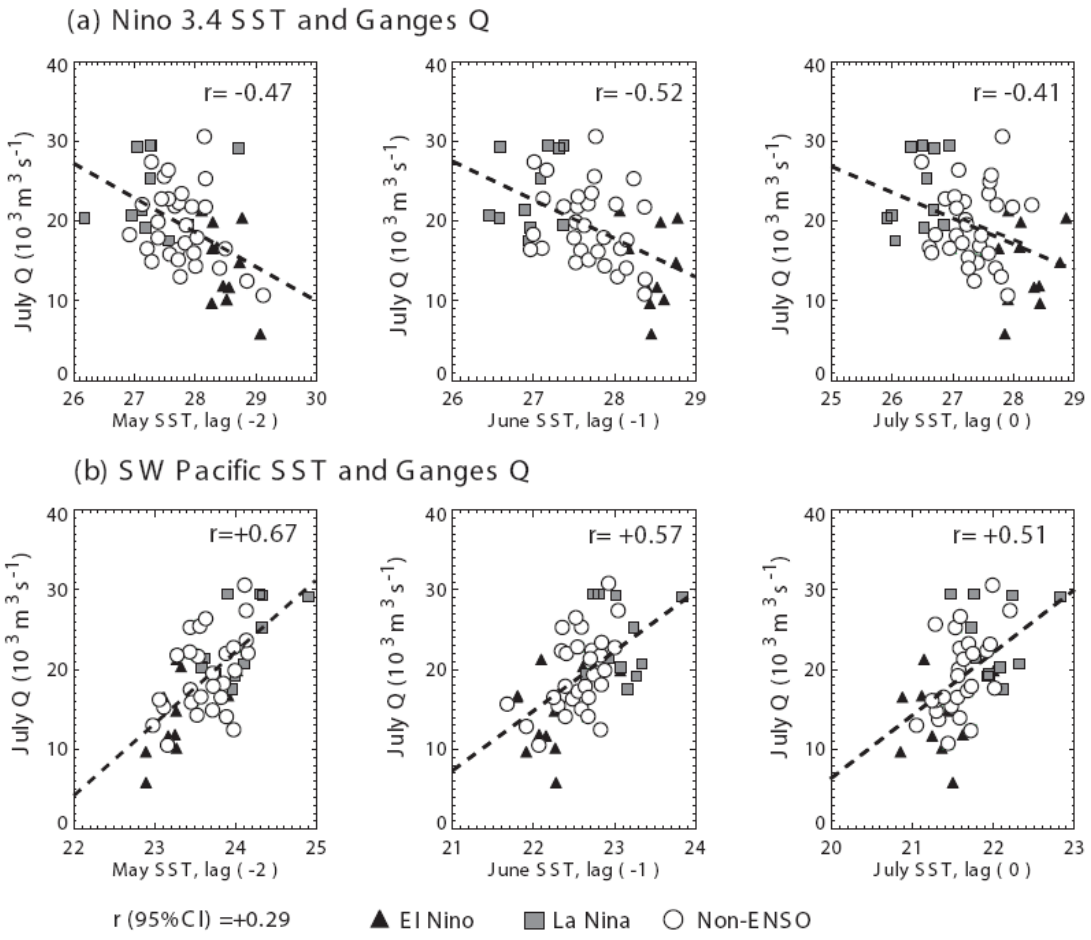

Figure 2.10 Regional scatter points of SST verses July Ganges discharge data with linear regression line and correlation coefficient marked.

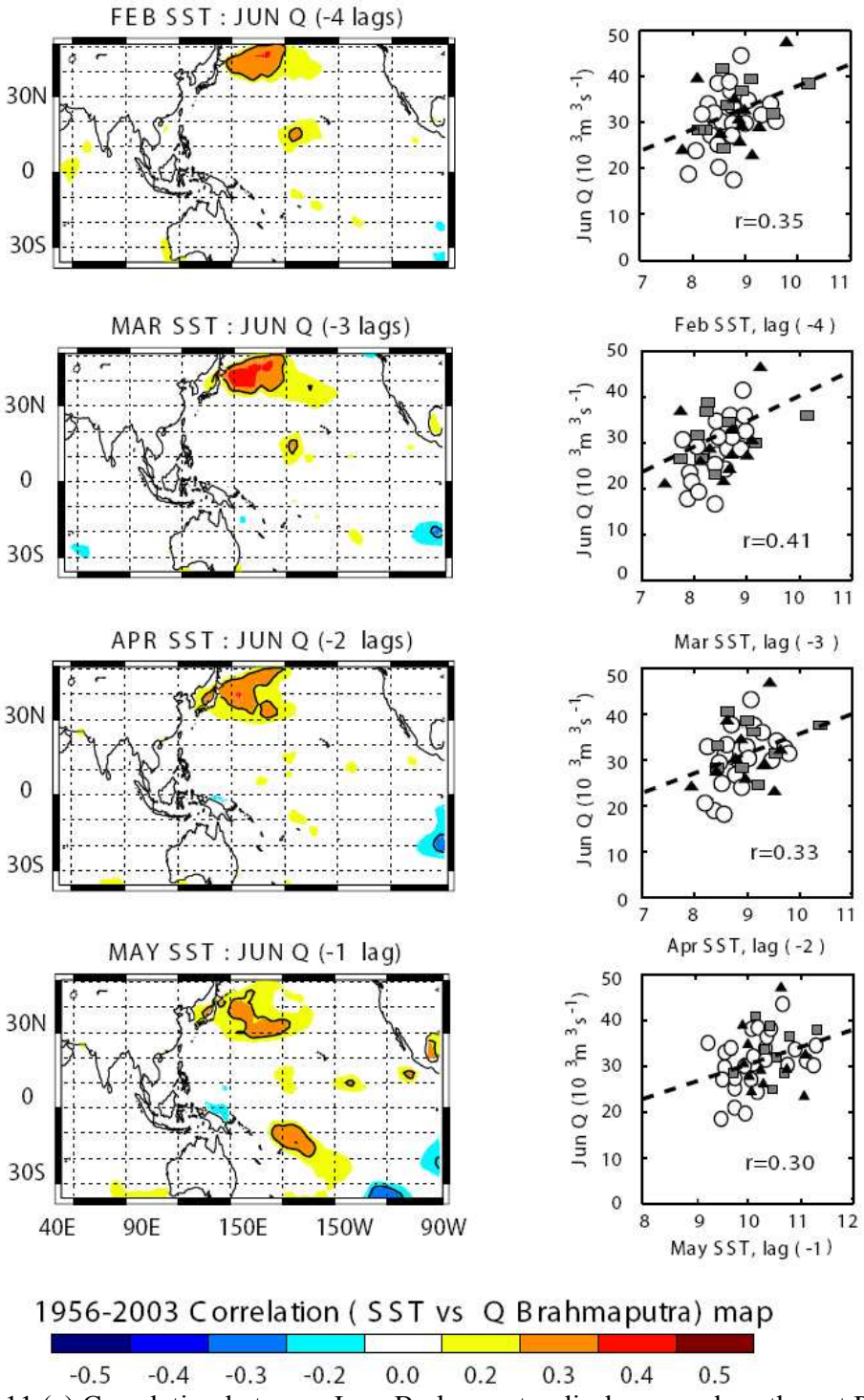

Figure 2.11 (a) Correlation between June Brahmaputra discharge and northwest Pacific SST. Left panel shows the correlation map between discharge and previous monthly SSTs of May, April, March, and February. Right panel shows the scatter plots between the two variables, respective to the left. (b) Same as (a) but between the July Brahmaputra discharge and previous monthly SSTs with the exclusion of 1998's value

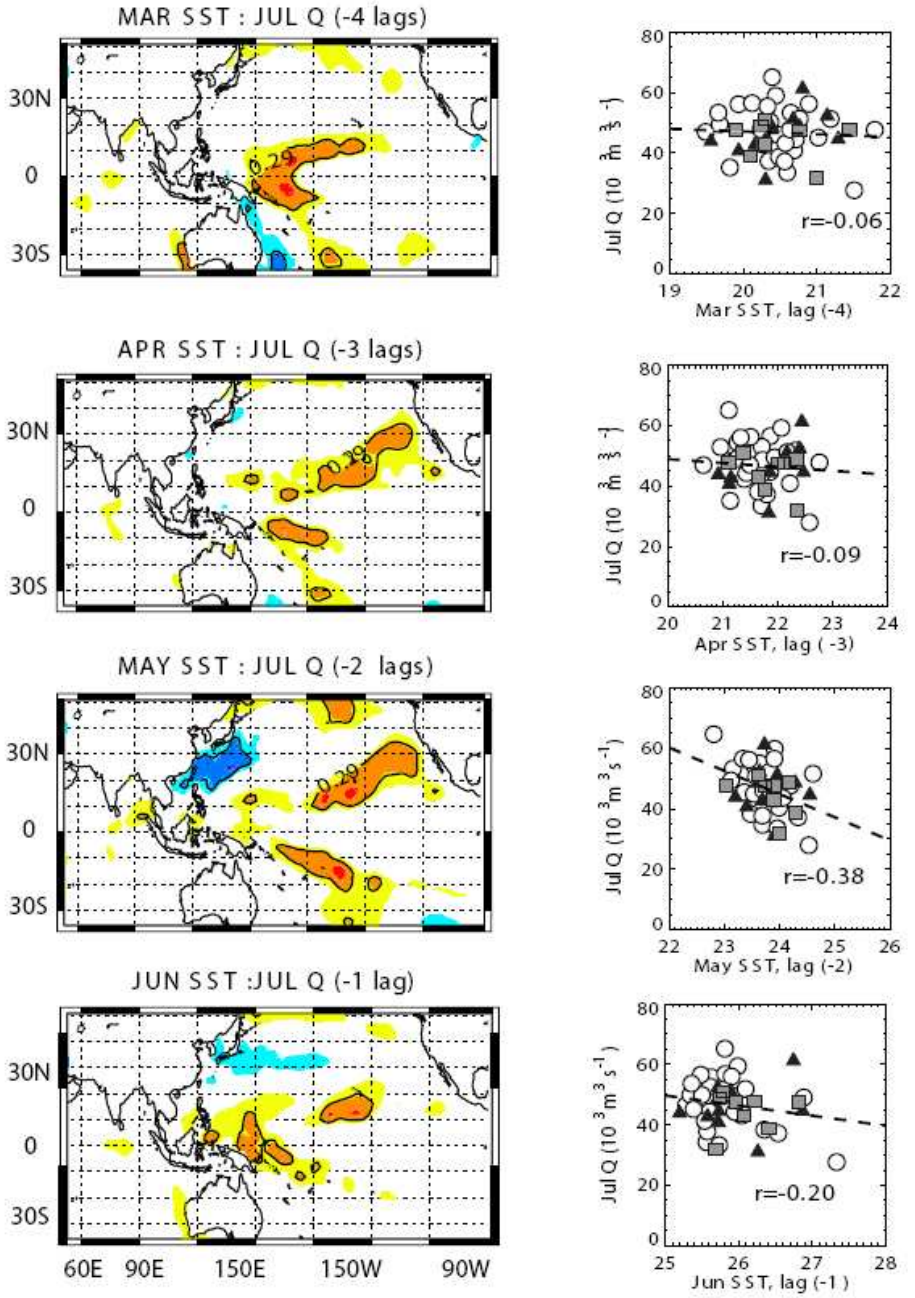

Figure 2.11 (continued)

We hypothesize that the changes in patterns is the result of two competing physical actions. Considering that a large proportion of the May and June Brahmaputra flow results from the melted snow pack over the Himalaya and the Tibetan Plateau (e.g., Shaman et al 2005), it is possible that the northwest Pacific SST is related to upstream winter storm activity that causes variations in snow pack. To some extent, this contention is corroborated by SST correlations for the July Brahmaputra discharge. The positive SST correlations in the northwest Pacific (Figure 2.11a) have changed to statistically significant negative correlations. In addition, there are persistent regions of positive SST anomalies in the central Pacific spanning the equator.

CHAPTER 3

SST-DISCHARGE RELATIONSHIP FOR THE YANGTZE, BLUE NILE, AND MURRAY-DARLING RIVERS

3.1 River features

All continents, with the exception of Antarctica, have major catchment areas that are the centers of agriculture and commerce. A selection of major river watersheds in African, South and East Asian, and Australian are illustrated in Figure 1.1 in addition to the Ganges and Brahmaputra rivers discussed earlier in Chapter 2. These are the Yangtze, Blue Nile, and Murray-Darling River systems. In each of these basins, precipitation is related to strong atmospheric circulations and modified by SST anomalies. The Yangtze River (region c, Figure 1.1), like the Brahmaputra and the Ganges rivers, rises in the Himalayas and the Tibetan Plateau. The Blue Nile River system (region d, Figure 1.1) which, together with the White Nile, provides water for the entire Nile system from Khartoum Sudan to the Mediterranean Sea. The Murray-Darling River system (region e, Figure 1.1) rises in northern Australia and flows southward to the west of the Australian coastal mountains to flow into the Great Australian Bight near Adelaide. These additional river basins were chosen because of their importance to regional societies, their relative differences and the availability of relatively long data records.

3.1.1 Dataset of monthly discharge

We used monthly streamflow datasets from Bodo (2001) and others archived at National Center for Atmospheric Research (NCAR, ds552.1 and ds556.0; available online at http://dss.ucar.edu/catalogs/ranges/range550.html) to get the gauge records of Yangtze and Nile streamflow rates. The gauges closest to the mouth are preferred to represent the integration of large-scale precipitations. However, here we cannot apply the station data located in the downstream of Nile River. It is because the Aswan Dam was completed in 1970 and after then it is used to regulate water flow to be constant throughout the year. We therefore concentrate on river flow above the Aswan Dam so that we can achieve a longer and homogeneous data record. The Blue Nile river discharge used in this study comes from Roseires Dam, 400 kilometers upstream of Khartoum because this station has a longer climatic record.

The Murray-Darling river discharge data are provided by Murray-Darling Basin Commission, Australia. For the same reason in Nile River case, the directly measured Murray-Darling discharge are not applicable as there are a number of irrigation and town water supply off takes and a storage (Lake Victoria) with a capacity of 677 Giga Liters before the Lock 1 where we have the data. Here we are going to use the natural discharge data modeled by scholars in the same organization.

Table 1.1 lists the basic features of the observational monthly discharge dataset adopted here for all five rivers. Most destructive flooding occurs in the downstream where the discharges are heavy; therefore, the overflow would cause more damage. In next chapter, we will compare the observational data with modeled precipitations most of which have a much coarse grid resolution (> 150 kilometers). Considering the above

factors, we determine to choose the observational data located much close to the mouth of the river to cover more catchment areas and better match the applied model precipitation area.

The Yangtze and Blue Nile River discharge data have some period missing. However, for the correlation and the following analysis procedures (Q-Q technique and Mann-Kendall analysis, etc.), the dataset continuity is not necessary. The missing data period is simply removed which does not affect the result.

3.1.2 Temporal analysis of the Yangtze, Blue Nile and Murray-Darling River discharges

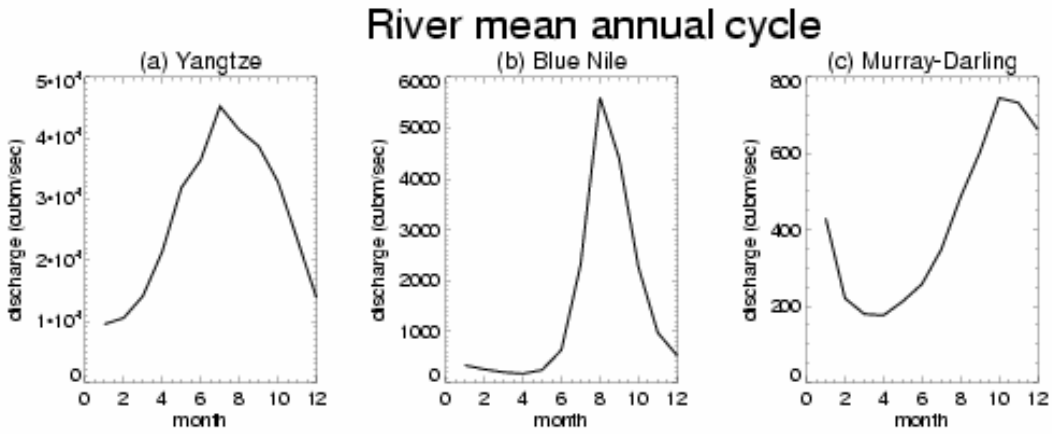

Figure 3.1 (a) Climatology annual cycle of the Yangtze River discharge averaged over period 1922-1937 and 1949-1988; (b) the Blue Nile discharge cycle averaged over 1912-1995 (c) the Murray-Darling discharge cycle averaged over 1891-2000. The Yangtze River wet season period is longer than the Blue Nile River.

In Figure 1.2, all five rivers' mean annual flows are observed to have large interannual variability. In Table 1.1, we know that Yangtze River has the largest mean annual flow of 2.87×10^4 $m^3 s^{-1}$, nearly three times of Ganges, 18 times of Blue Nile, and

68 times of the Murray-Darling River discharge. Figure 3.1 shows the climatological annual cycles of the Yangtze, the Blue Nile, and the Murray-Darling rivers. Similar to Figure 2.3, we know they all have a robust seasonal cycle. Heavily influenced by summer Asian Monsoon precipitation, the Yangtze, Ganges and Brahmaputra River stream flows are over ten times larger than the Blue Nile and Murray-Darling river stream flows.

Figure 3.2-3.4 illustrate the watershed areas of the Yangtze, Nile, and Murray-Darling rivers with land types. As a part of the Nile River system, the Blue Nile River catchment is circled by solid green line. The locations where the observation data were measured and the red boxes where the modeled output will be accessed are also marked. The locations and model accessing area of Ganges and Brahmaputra rivers are marked in Figure 2.1 a.

In the following paragraphs, we follow the same strategy as in last chapter by seeking causal factors that determine the interannual variability of the Blue Nile, the Yangtze, and the Murray-Darling River systems. We do this by seeking relationships with SST fields.

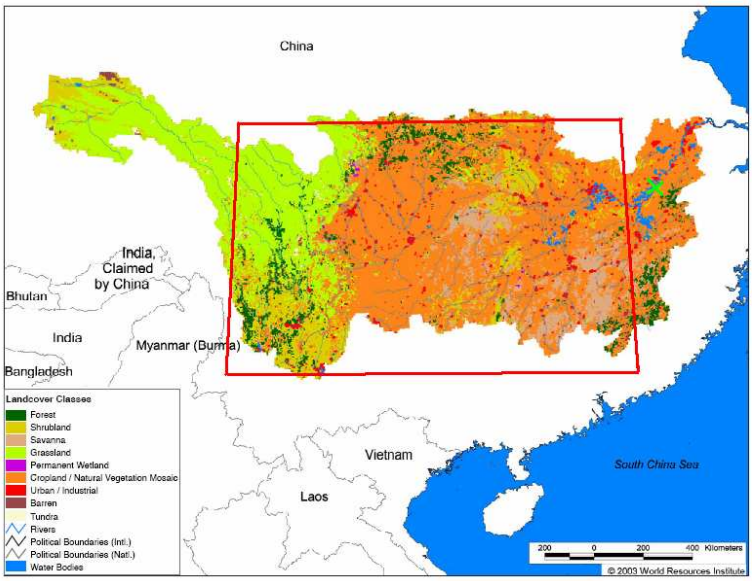

Figure 3.2 Map of the Yangtze River watershed with the land cover classes. The red box indicates the area used to retrieve IPCC model precipitation in Chapter 5 (adjusted from http://earthtrends.wri.org/pdf_library/maps/ watersheds/as32.pdf).

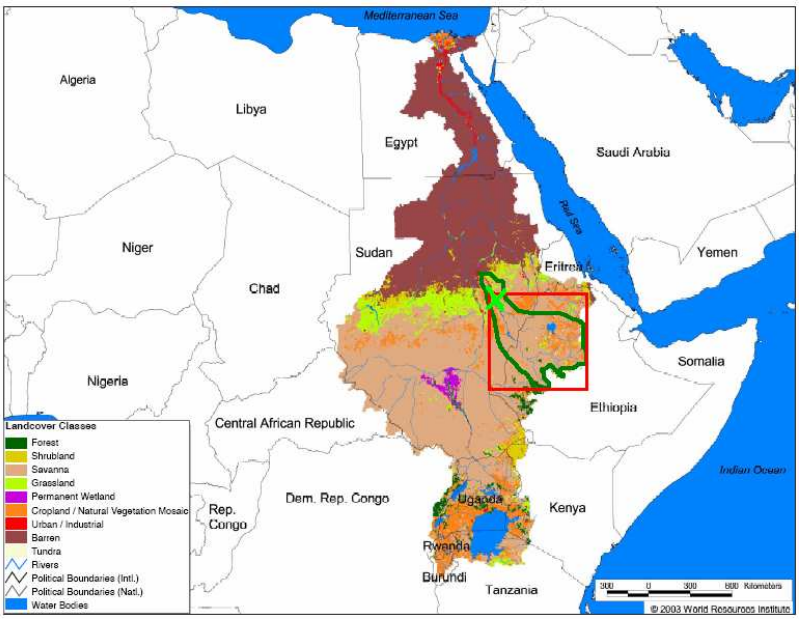

Figure 3.3 Same as Figure 3.2 but for the Nile River watershed. The Blue Nile catchment area discussed here is circled with dark green contour (adjusted from http://earthtrends.wri.org/pdf_library/maps/watersheds/af15.pdf).

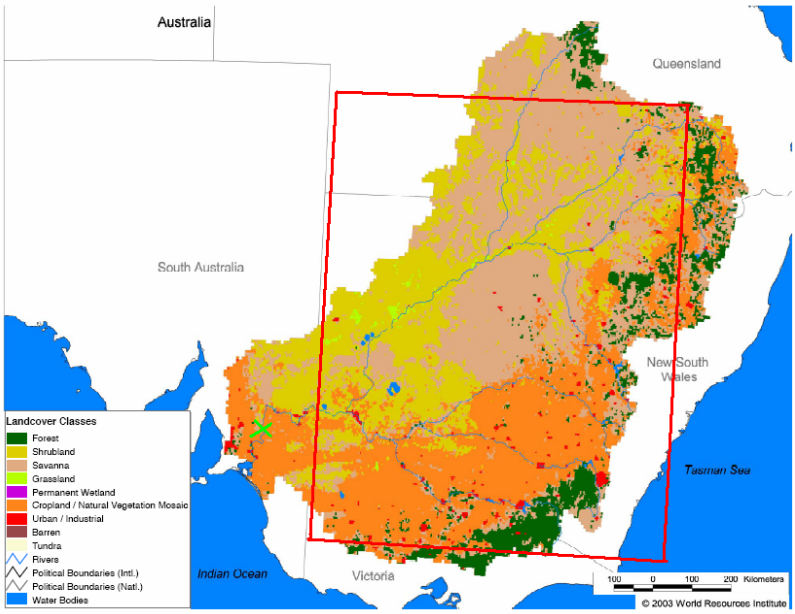

Figure 3.4 Same as Figure 3.2 but for the Murray-Darling River system (adjusted from http://earthtrends.wri.org/pdf_library/maps/watersheds/oc4.pdf)

3.2 Wet season river discharges –SST correlations

3.2.1 Yangtze River discharge-SST correlation

Yangtze River summer season discharges are the results of summer monsoon rainfall and connected with eastern equatorial Pacific SST (Zhang et al.2007, Chang et al. 2000a, 2000b) and western Pacific and Indian Ocean SST variations (Xue 2001). The total wet season (from June to August) mean Yangtze discharge is correlated with two seasons earlier (December-January-February, denote as DJF), one season earlier (March-April-May, MAM), simultaneous (June-July-August, JJA) and one season lag (September-October-November, SON) SSTs over the Pacific and Indian Ocean. In Figure 3.5, spatial distributions of the correlations between the wet season of the Yangtze River (June to September, denote as JJAS) discharge with the SST (a) one season later (September-

November), (b) simultaneous (June-August), (c) one seasonal earlier (March-May) and (d) two seasons earlier (December-February).

Areas with negative relationship are observed in eastern and middle equatorial Pacific SST during the simultaneous season (JJA) and one season (SON) later. The negative area position is similar to the Ganges River case. However, the correlations are marginally weak and do not pass the field significance test of Livezey and Chen (1982).

Located east of Tibetan Plateau and directly facing the Pacific Ocean, Yangtze River is not only influenced by the South Asian monsoon (Indian Monsoon), but also the East Asian monsoon southeasterlies from western Pacific Ocean and the warm pool (Bing et al. 2003). This multi-source climatic forcing makes the diagnostic of the Yangtze River complicated (Xu et al. 2007, Zhang et al. 2007, Fang et al. 2003)

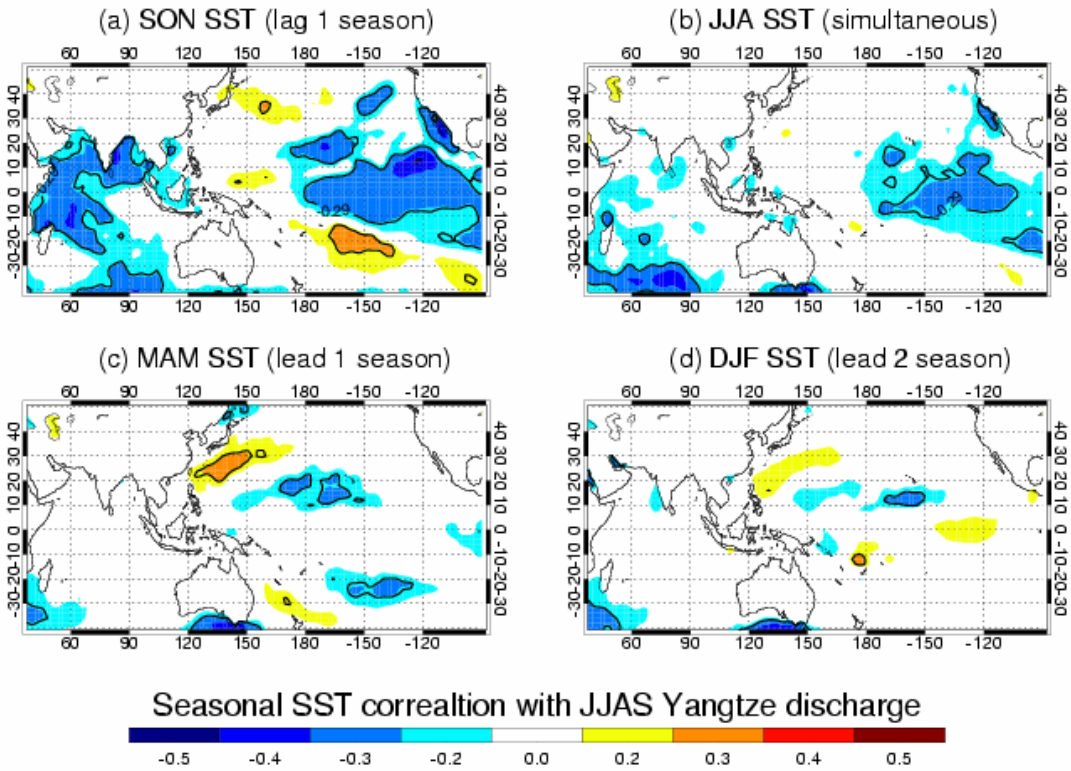

Figure 3.5 Spatial distributions of the correlations between the wet season Yangtze River (June to September, denoted as JJAS) discharge with the SST for (a) one season later (September-October-November, denoted as SON), (b) simultaneous (June-July-August, denoted as JJA), (c) one seasonal earlier (March-April-May, denoted as MAM) and (d) two seasons earlier (December-January-February, denoted as DJF). The equatorial Pacific Ocean SST has a relative weak negative correlation with wet season Yangtze River discharge. Correlations in other areas are marginal.

3.2.2 Blue Nile River discharge- SST correlation

As the longest river in the world, the Nile River streamflow has fed the civilization and peoples living along the delta region for over 5000 years. Eldaw et al. (2003) found that the "flood season" [July to October (JASO)] Blue Nile River flows are significantly correlated with the previous year August-November Guinea precipitation and with the leading SSTs identified in a number of ocean regions. The SST correlations develop through time in a manner that is coordinate with ENSO development. A model built on

multiple linear regression (MLR) and principal component analysis (PCA) successfully forecast the Blue Nile wet season flows with lead times of 4-16 months.

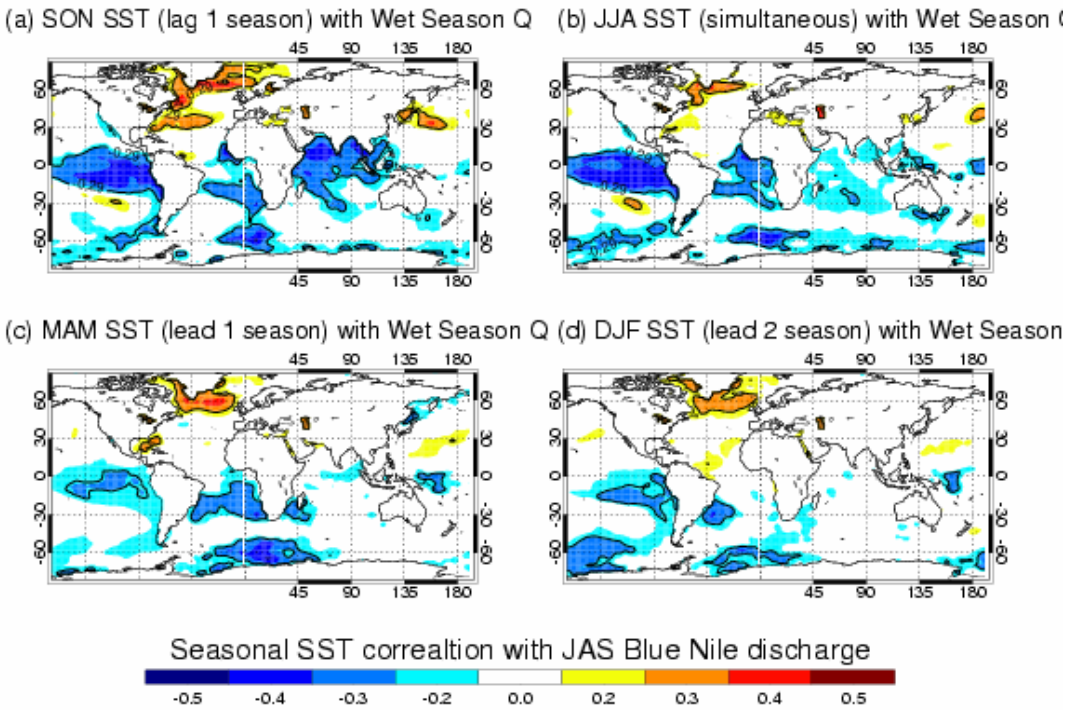

Figure 3.6 Same as Figure 3.5 but with the wet season (July to September, denoted as JAS) Blue Nile River discharge. In general, the Blue Nile discharge is correlated negatively with the equatorial eastern Pacific Ocean at all lags. The Indian Ocean, like the equatorial eastern Pacific Ocean, has the maximum negative correlation at a season lag.

The two main tributaries of the Nile are the Blue and the White Nile that join at Khatoum, Sudan. The Blue Nile River has a substantial annual cycle and contributes 70% of the stream flows in summer. In fact, 90% of Nile water originates in the Ethiopian Highlands. As a branch of the Nile River, the Blue Nile River is also correlated with equatorial SST variations.

Figure 3.6 shows the spatial distributions of the correlations between the wet season of the Blue Nile River (July-August-September, denote as JAS) discharge with the SST (a) one season later (September-November), (b) simultaneous (June-August), (c) one seasonal earlier (March-May) and (d) two seasons earlier (December-February).

The western Indian Ocean, South Atlantic Ocean and eastern equatorial Pacific Ocean SST have a strong negative correlation with wet season Blue Nile River flow on the same season and one season lead. However, the strong connection at lag time has little predictability to forecast discharge.

3.2.3 Murray-Darling River discharge- SST correlation

Murray-Darling River flow is the smallest among all five rivers. However, the water supply demand is large as the catchment area is well irrigated and developed. The water channel is full of dams and locks to put much of the flows in reservoir for agriculture usage and other water supply. Thus the direct flow reading is much less than the basin-wide integration of precipitation and cannot be used as a natural measure. The Murray-Darling water resource department in Australia has made a hydrological model to estimate the mouth flow that would exist in absence of dams. Here we use the model output as the effective discharge data.

Murray-Darling River is among the rivers that are closest to equatorial Pacific Ocean, where ENSO events occur. It is not surprising that Simpson et al. (1993a, 1993b) and Dutta et al. (2006) find strong correlations between the precipitation and runoff in the Murray-Darling basin and preceding ENSO or SST signals. The model built by the former can forecast the flows in up to one-year advance. Figure 3.7 shows the spatial

distributions of the correlations between the wet season of the Murray-Darling River (September-October-November, denote as SON) discharge with the SST (a) simultaneous (September-November), (b) one seasonal earlier (June-August), (c) two seasons earlier (March-May) and (d) three seasons earlier (December-February).

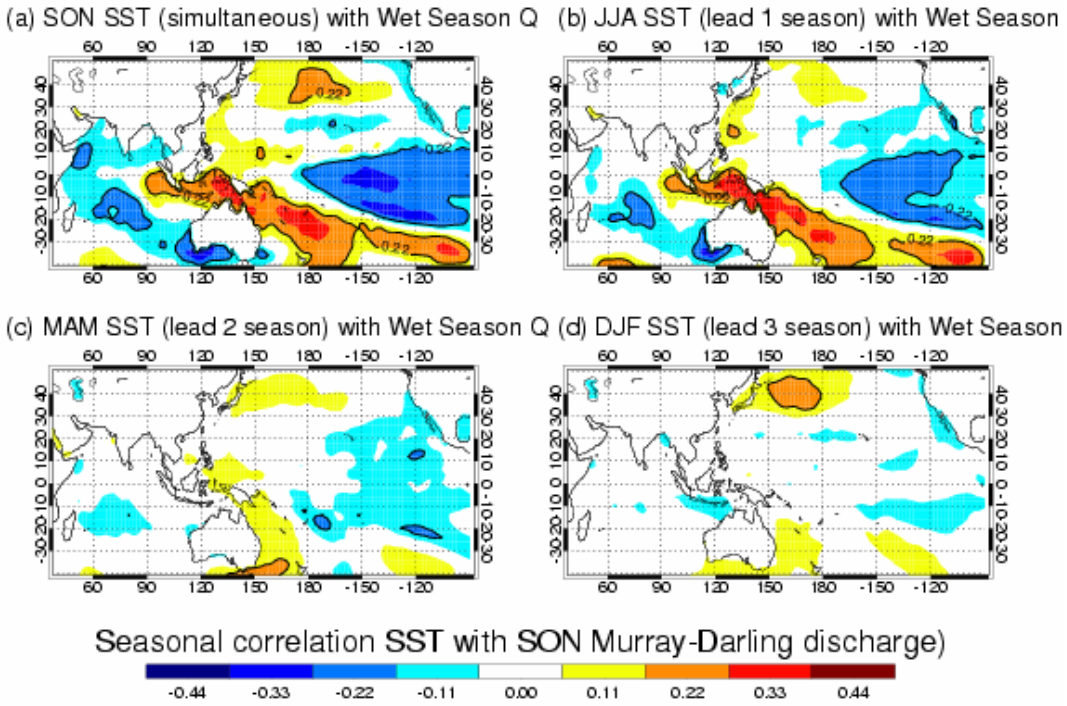

Figure 3.7 Spatial correlation between the wet season (from September to November, denoted as SON) Murray-Darling River discharge and seasonal SSTs at simultaneous (SON), one season earlier (June-July-August, denoted as JJA), two season earlier (March-April-May, denote as MAM) and three season earlier (December-January-February, denoted as DJF) in advance.

The equatorial Pacific Ocean SST has a relative weak negative correlation with total wet season Murray-Darling River discharge, the other area's correlations are marginal. Ocean areas directly adjacent to the north and northeast of Australian Continent have strong positive correlations with Murray-Darling discharge in one season earlier and

simultaneous. The seasonal SST-discharge correlation suggests that a lead time of one season forecast is possible.

3.3 Predictability of the three rivers

The new rivers introduced in this chapter have common characteristics: they are all strongly correlated with ENSO events or equatorial Pacific SST with the Murray-Darling River the possessing the strongest relationship and the Yangtze River the weakest. An accurate forecast of river flow has a substantial economical and social benefit.

There is some evidence of predictability for the Blue Nile with strong SST patterns occurring at significant levels a season ahead and simultaneously with the discharge measurements. Strong simultaneous relationship exist with the other two basins but little relationship between discharge and the SST the season before. Thus, there is limited predictability for both the Yangtze and the Murray-Darling rivers. Yet, there is considerable utility in the simultaneous relationships. One of the purposes of this study is to forecast the likely evolution of the flow in major rivers in the face of a changing climate and a warming world. These forecasts will be made on the basis of the IPCC climate model simulations discussed subsequently. Thus, if there are strong simultaneous relationships between SST and river discharge, and if the models can predict such major climate patterns as El Nino, then the models will possess the basis for a prediction of future river flow.

CHAPTER 4

PROCEDURES FOR FORECASTING FUTURE RIVER DISCHARGE IN THE 21ST CENTURY

One of the great challenges for humankind in a period of rapidly growing populations is the continued provision of adequate and safe water for consumption and agriculture. This challenge is exacerbated by the changes in precipitation patterns that might accompany global warming. For future water resource management it is extremely important that assessments are made of future water availability.

We have assessed the relationships between variations of SST patterns and volume flow for a number of rivers that, besides the Australian Murray-Darling, sustains very large percentages of the global population. The problem reduces to two issues: (i) What will the river flow be in these important river basins in the next hundred years? (ii) Will the water available in each basin be able to supply the water needs for the increasing population?

To assess the first issue, we use the Intergovernmental Panel on Climate Change (IPPC) model runs made for the recent 4th assessment report (AR4). The models were run for a variety of GHGs (including CO2) scenarios that take into account increases of population and various economical assumptions. The second issue will not be addressed here. However, its eventual resolution depends must be based on an understanding of the future state of river flow in different parts of the planet.

In this chapter, we establish a methodology that allows imperfect models to be used to determine the probability of changes (or lack of change) of river flow in the future. In Chapter 5, the projections for each of the river basins considered will be discussed.

4.1 Background of IPCC and AR4 assessments

In 1988, concerned about the possible anthropogenically induced effects on the environment, two United Nations organizations, the World Meteorological Organization (WMO) and the United Nations Environment Programme (UNEP), established IPCC to assess scientific, technical, and policy-economic information relevant to the understanding of climate change and their potential impacts and options for adaptation and mitigation. IPCC does not consider itself a research organization and is not involved in the measurement of relevant climate data or parameters. The IPCC bases its climate assessment mainly on peer reviewed and published scientific and technical literature. There have been three previous assessments: 1990 and its supplement 1992, a second in 1995, and a third in 2001, all of which consider the impact of the influence of humankind on climate.

On February 2, 2007, the IPCC issued a draft of its fourth Assessment Report (IPCC-AR4) on climate change. A major conclusion of the 4th assessment is "The anthropogenic warming of the climate system is widespread and can be detected in temperature observations taken at the surface," and furthermore, "*It is extremely unlikely (<5%) that the global pattern of warming observed during the past half century can be explained without external forcing*" Solomon et al. (2007, IPCC-AR4, WG1-TS, page 60). This assessment is the result of the cooperative work of more than 2,000 scientists. Drafts

were reviewed by scores of governments, industry, and environmental groups. The detailed assessment released in May 2007 states that *"the large-scale patterns of seasonal variation in several important atmospheric fields are now better simulated by AOCGMs than they were at the time of the TAR* (the third assessment report released in 2001)*"*. (Randall et al. 2007, IPCC-AR4, WG1 page 592)

4.2 Overview of CMIP3 models and the SRES scenarios

Global climate models or general circulation models (GCMs) are computer-driven models used for forecasting weather and for climate simulation. They are considered an effective tools and the best method we have so far to study changes of earth-atmosphere system. However, these models are imperfect (e.g. Karl et al., 2003, Trenberth et al. 2004，2005) and out of these flaws emerges uncertainty in the veracity of the model results. Many early models did not contain an interactive ocean. Noting that the ocean has an important and dynamic role in climate variability and change, more comprehensive atmosphere-ocean coupled global climate model (AOGCM) has been developed and have been used most recently to estimate the past and future state of climate.

Internally coordinated projects have persuaded various groups around the world, each with their own model version of the climate system to contribute to assessments of climate change with increasing greenhouse gases. Examples of these coordinated programs are the phase one and two of Paleoclimate Modeling Inter-comparison Project (PMIP1 and PMIP2, by CLIVAR). PMIP1 and PMIP2 study the role of climate feedbacks rising for the different climate subsystems (atmosphere, land surface, ocean,

sea ice and land ice) and evaluate the capability of state-of-the-art climate models to reproduce climate states that are radically different from those of today (Crucifix et al. 2005, PMIP special report 2000). In PMIP2, both coupled ocean-atmosphere models and ocean-atmosphere-vegetation models will be considered.

With respect to future climate, there has been phase one, two, and three of Coupled Model Inter-comparison Project (CMIP1, CMIP2, and CMIP3, by IPCC). In CMIP1, groups are soliciting contributions from global coupled general circulation models (GCMs) that operate over the complete global domain and include atmosphere, ocean and sea ice components. Any type of spin-up and/or flux adjustment is allowed. CMIP2 continues the effort started in CMIP1 to involve the international coupled modeling community to assess three objectives: 1) documenting the mean response of the coupled climate system to a transient increase of CO2 in the models near the time of CO2 doubling; 2) quantifying the effects of flux adjustment on climate sensitivity in the coupled simulations, and 3) documenting features of the simulated time-evolving climate system response to gradually increasing CO2 (Meehl CMIP2 announcement in 1997, Meehl et al. 2006). The analysis here is based on CMIP3 output that has been used to support IPCC-AR4 and is downloadable from https://esg.llnl.gov:8443/index.jsp. The main features (model ID number, sponsor institute and country, adopted atmosphere and ocean models, sea ice, coupling, and land schemes) of the IPCC-AR4 CMIP3 models are listed in Appendix A copied from Randall et al. (2007, IPCC-AR4, WG1 page 597-599).

Each CMIP3 model ensemble member can have up to 12 expanded designs relative to the different CO2 increase scenarios developed by IPCC. The first experimental step in all these sequenced or branched experiments is a stabilized climatology and

oceanography state, In this stabilized state, most climate variables such as temperature are kept in a uniform and small range by allowing no changes in atmospheric composition or changes in natural external forces (e.g., solar variability). In such pre-industrial spin-up (PIspup) runs, there is no forced long-term trend. Climate drift, whereby the model cannot find an equilibrium state, can occur but this is removed following the initial constant forcing case. Subsequently, the models have run for another 200 years simulating the pre-industrial climate (PIcntrl). This simulation is used for reference to the historical (20C3M) and continuous branching SRES experiments to consider the impacts of the different greenhouse gases and aerosols from natural and anthropogenic sources. The impacts of the various scenarios are gauged by comparison between the various runs.

In CMIP3 group, almost all the models run to 2100 under COMMIT and SRESA2 scenarios. Most of them have a longer run time till 2200 or 2300 under SRESA1B and SRESB1 to seek if the models can reach an equilibrium state. The entire SRES scenario is using the end of 20C3M as the initial state and I will work on either period.

Figure 4.1 shows the experimental timeline used by Meteorological Research Institute in Japan (MRI). The color scheme used to distinguish major scenarios will be retained for the rest part of this paper. Other modeling groups may have used different setups for the initial stabilizing run, but all of them have the same CO2, sulfur, and other GHGs concentration conditions provided by the IPCC Special Report on Emissions Scenarios (SRES, IPCC 2000). That is the reason why six SRES scenarios (A1B, A1T, A1F, A2, B1, and B2) and the fixed 2000-level GHG and aerosol concentration

experiment (under the commitment of Kyoto Protocol, denoted as COMMIT scenario) have been referred in many reports.

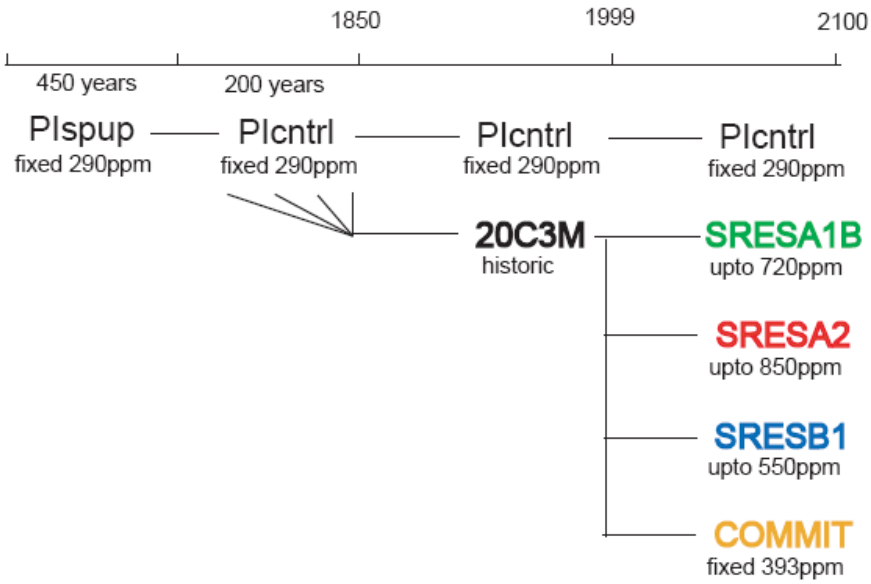

Figure 4.1 Timeline cutoff of the IPCC-MRI scenarios for last century and next centuries, and associated CO2 concentrations (ppm) in each of the scenarios.

Table 4.1Summary of the IPCC AR4 SRES family scenarios

Family Characters		A	B
		A world with rapid growth of both economical and technology level	A much-developed world in economical structures, emphasizing sustainability and diminish of cultures
1	Populations increase in the first half of the 21st century but decrease thereafter	A1B A1T A1F	B1
2	Continuous growth of populations, emphasizing the self-reliance and local effort to sustain the social development	A2	B2

The SRES scenarios can be divided into "letter" families A and B, and "number" families 1 and 2. The letter families depict the economic status of the future society and the number families focus on the development of the population, adaptation, and mitigation. Each individual SRES scenario is described with one letter family and one number family, as presented in Table 4.1. Here only four future scenarios namely SRESA2, SRESA1B, SRESB1, and COMMIT are analyzed. These are defined as:

COMMIT: assumed political policy adopted and anthropogenic forcing frozen at the year 2000 level.

SRESA1B: continued development with no change of current fuel usage strategy until an eventually establishment of a stabilized balance between fossil fuel and non-fossil fuel usage.

SRESB1 and SRESA2: represent the lowest limit of CO2 increase at the present economic and technical development and the high limit, respectively

Based on the development assumption of energy technology, economical levels and structures, and population distributions, the IPCC Data Distribution Centre has issued GHGs estimations for different scenarios. The full dataset can be fount at http://sres.ciesin.org/final_data.html. One example of time series of three major GHG (CO_2, CH_4, N_2O) concentrations and sulfate aerosol mass are shown in Figure 4.2. It is clear that the SRESA2 scenario has the most abundant GHG concentration among all of the scenarios. The COMMIT scenario assumes a fixing of GHG concentrations in the global mean 2000 levels, representing the adoption of the Kyoto Protocol. This scenario is used as a base level control experiment.

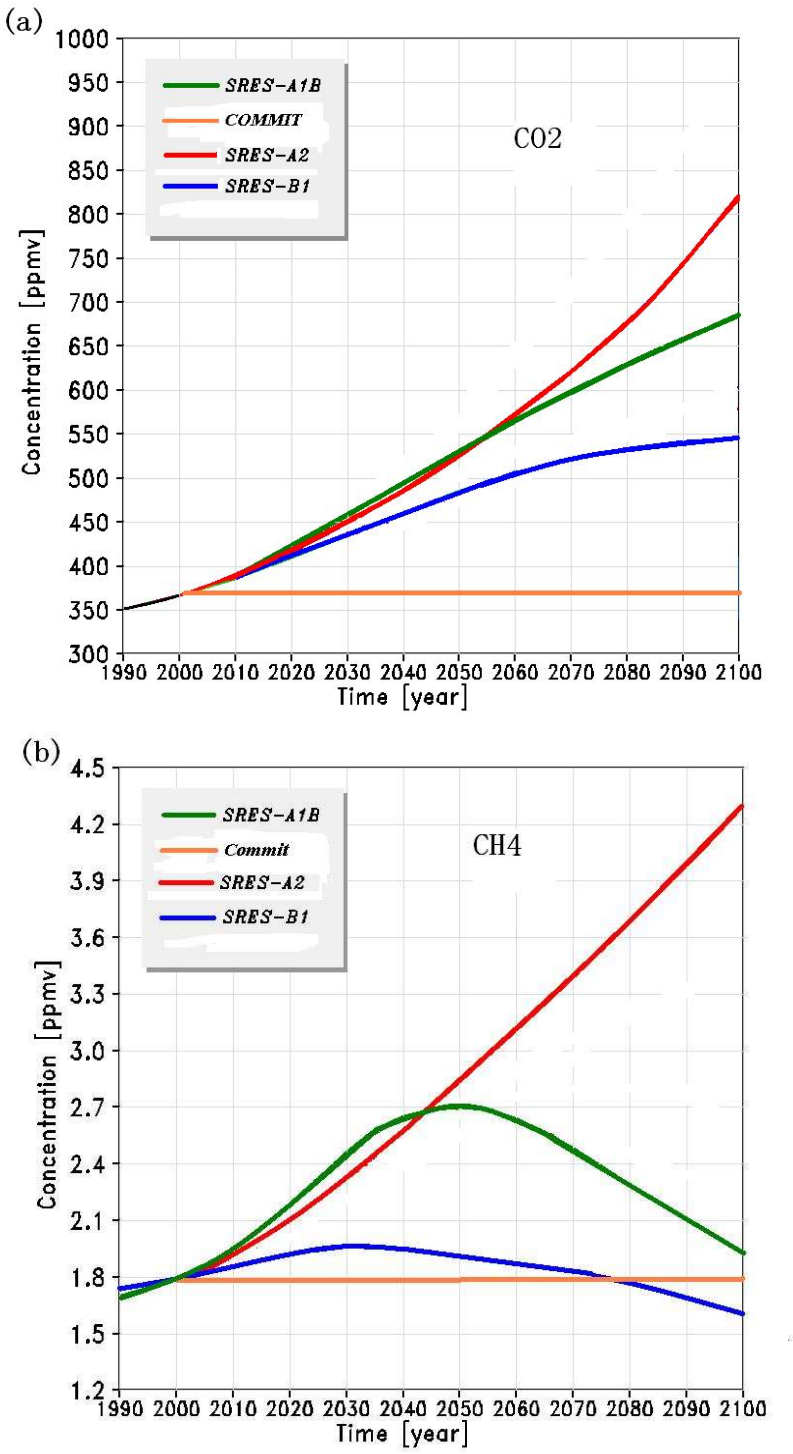

Figure 4.2 Time series of concentrations of the four scenarios for greenhouse gases (a) CO_2, (b) CH_4, (c) N_2O, and (d) sulfate aerosol (adjusted from http://www.mri-jma.go.jp/Dep/cl/cl4/IPCC-AR4/simulations2.html, Meteorological Research Institute, Japan climate modeling organization).

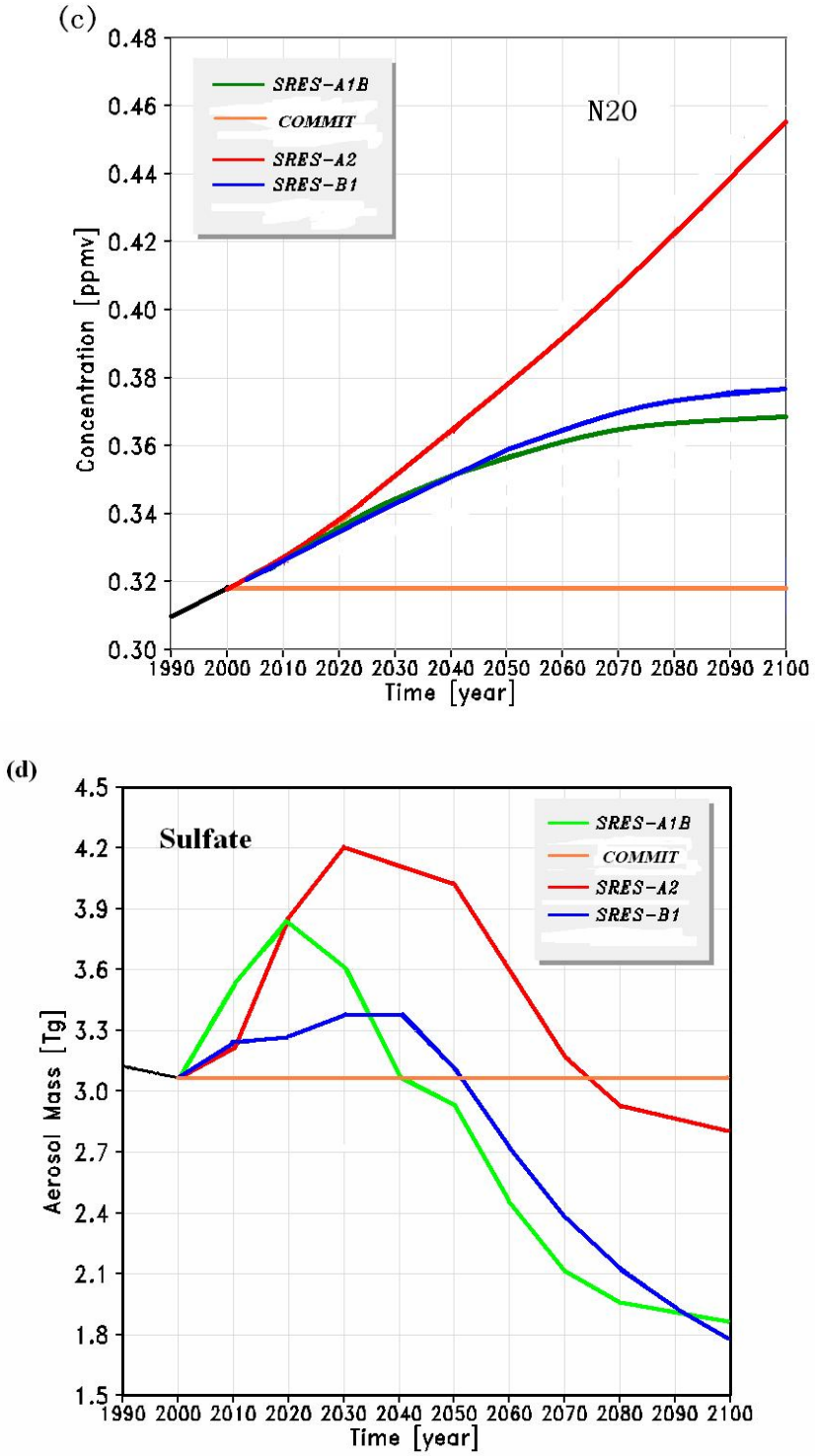

Figure 4.2 (continued)

4.3 Model biases

As with all climate models, there have been concerns about the uncertainties within IPCC forecasting ensemble models. These uncertainties arise from contradictory predictions, inability to reproduce similar results with the same forcing scenario and large variations of model fields from observations have raised concern about the model's ability to simulate climate change (Räisänen, 2007).

Climate models are evaluated mainly on their ability to predict temperatures and precipitation. The predicted increase of the global mean temperature during the 21st Century ranges 1-2°C in the first IPCC assessment report (IPCC, 1990), 1.0 to 3.5°C in the second (IPCC, 1995), 1.4 to 5.8°C in the third (IPCC-TAR, 2001), and 1.8 to 4.0°C in recent fourth assessment (IPCC-AR4, 2007). The IPCC-AR4 multi-model surface temperature predictions are illustrated in Figure 4.3. Note that the four temperature time series follow the CO2 concentration most closely than the other GHGs shown in Figure 4.3. The scenario with larger CO2 concentration is expected to have larger temperature increase.

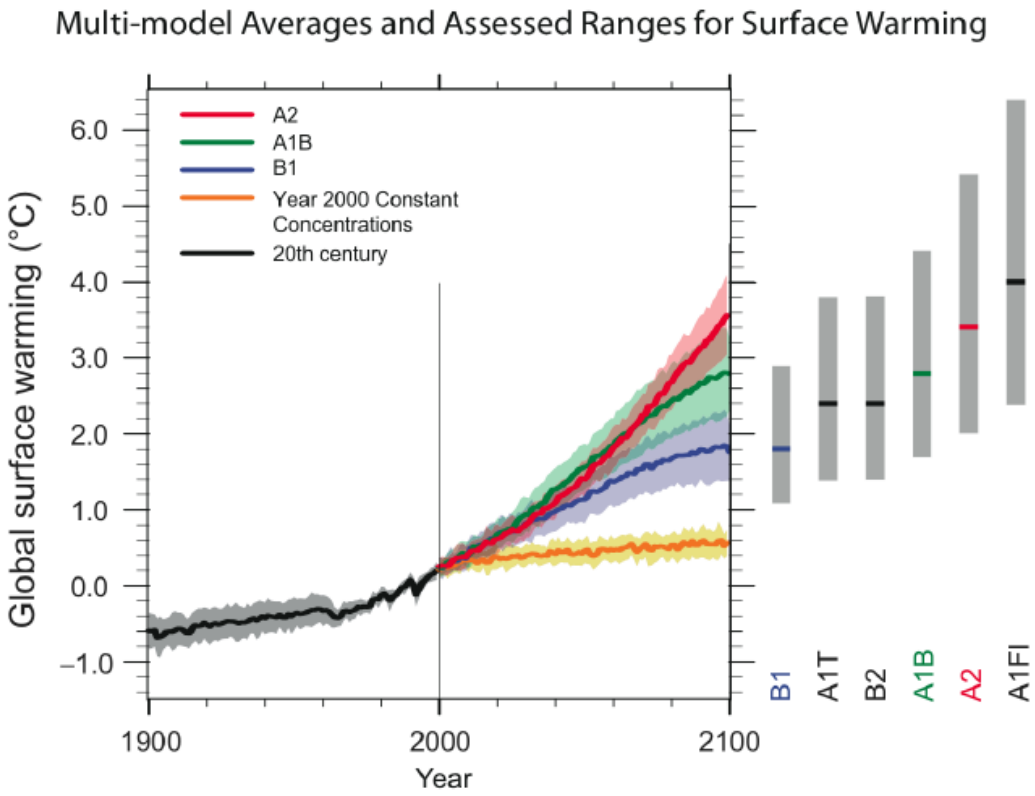

Figure 4.3 IPCC multi-model averages and assessed ranges from CMIP3. Solid lines are multi-model global averages of surface warming (relative to 1980-99) for the scenarios A2, A1B and B1, shown as continuations of the 20th century simulations. Shading denotes the ±1 standard deviation range of individual model annual averages. The orange line is for the experiment where concentrations were held constant at year 2000 values. The gray bars at right indicate the best estimate (solid line within each bar) and the *likely* range assessed for the six SRES marker scenarios (applied from IPCC report issued in Feb 2007).

The possible climatic and social influences due to the temperature change have gained attention in academic journals. The Web of Science search engine v2.0, between 1990 till present identifies 9930 articles referring to temperature changes found in climate models. Also, 5159 articles are found for the same period related to precipitation.

Precipitation studies have focused on two parameters: mean trend and extreme event probability. Räisänen et al. (2001) studied the possibility of global mean precipitation change over 10% under a combination of 17 CMIP2 models. Based on the same models, Palmer et al. (2002) and Räisänen (2002, 2005) applied different statistical methods to quantify the probability of extreme precipitation events and suggested they are increasing over large regions of the globe. Various studies (Senior et al. 2002, Benestad et al. 2006, Zhang et al. 2006, Barnett et al. 2006, Boroneant et al. 2006, Vavrus et al. 2006) suggest both mean and extreme precipitation events are increasing, statistically more likely in high latitudes. However, unlike the temperature trend, currently no global mean precipitation trend map with accurate quantities and confidence intervals have been accessed. As Räisänen (2007) remarks, "*Models do not agree on all aspects of future climate change, particularly not on small horizontal scales. Overall, the agreement on changes in precipitation and atmospheric circulation is worse than the agreement on temperature changes.*"

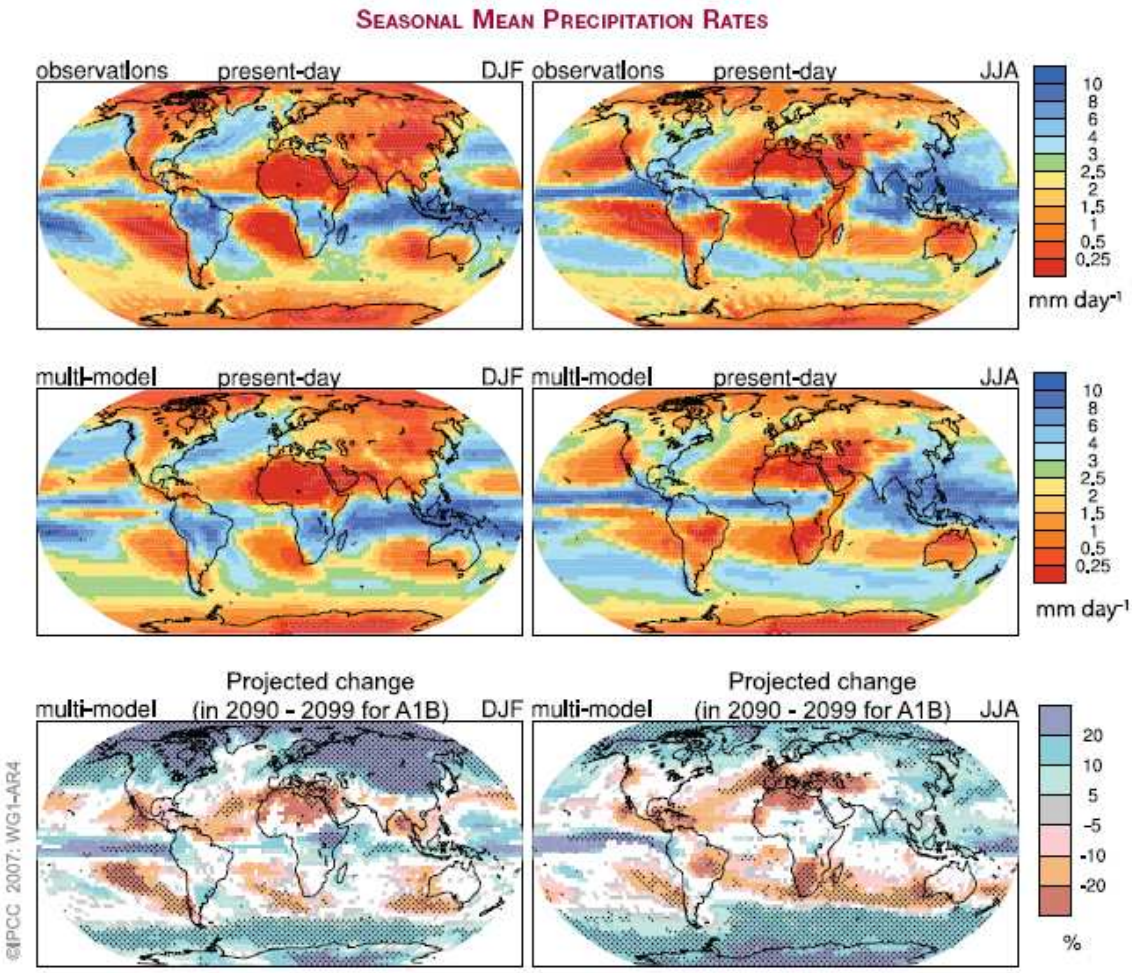

Figure 4.4 Observed spatial patterns (top row) and multi-model mean (middle row) of seasonal mean precipitation rate (mm/ day) for the period 1979 to 1993, and the multi-model mean for changes by the period 2090 to 2099 relative to 1980 to 1999 (% change) based on the SRES A1B scenario (bottom row). December to February means are in the left column, June to August means in the right column. In the bottom panel, changes are plotted only where more than 66% of the models agree on the sign of the change. The stippling indicates areas where more than 90% of the models agree on the sign of the change (from IPCC-AR4 Workgroup I, report TS, pp 76, Figure TS 30).

The panels in the top row and middle row of Figure 4.4 (from Soloman et al. 2007 IPCC-AR4 WG TS, page 76) compare the observed and multi-model mean (of 20C3M run) seasonal mean precipitation rate (mm/day) for the period 1979 to 1993. They are very similar in both spatial distribution and magnitude. However, later we will show that the inter-model deviations are very large. The bottom row compares the spatial distributions of the differences between mean precipitation observed in the 1980/1999 and the multi-model forecast of the 2090-2099. Differences for two periods are presented: December through February (DJF) and July through August (JJA). Changes are plotted in blue or red color only where more than 66% of the models agree on the sign of the change. Stippled area indicates unanimity model predictions. Large blank area located in the extra-tropics and equatorial Atlantic-Africa indicates large uncertainties. High latitudes in the polar regions and Siberia area are in stipple dark blue indicating a large percentage increase of precipitation. This result appears to be consistent with recent observation of Arctic ice sheet melting and retreat. That is because when the low temperature air is warmed, the saturation vapor pressure also increases in the atmospheric saturation vapor pressure and subsequently greater. Meehl et al. (2007 IPCC-AR4 WG1, page 767) also suggests that, with much good agreement of multi-model results, more precipitation is expected at high latitudes. However, the absolute change of total precipitation is relative small since the absolute values are small. On the other hand, a small percentage climate change in precipitation in an already heavy precipitation region (such as Ganges-Brahmaputra catchment) could be related to large net changes in precipitation and could have large economical and social consequences for the region.

4.4 Reducing uncertainty in model simulations: the Quantile-to-Quantile (Q-Q) technique

4.4.1 Basis of the Q-Q technique

In order to diminish the uncertainty by introduced large modeled precipitation variability between models, a new Q -Q technique is applied to reconstruct the future river discharges from modeled precipitation output is applied. This method, developed by Hopson (2005), aims to connect multi-model precipitation output and observational river discharge by mapping a one-to-one index between model-space and observational-space. Here the "space" refers to the sorted dataset (model or observation) over the period considered, regardless of their original time sequences. This method is built under the assumption that the full climate models in IPCC CMIP3 have skill in simulating long-term climate change, which is likely influenced by the external non-natural forces (e.g., GHG increases) or through natural variability (such as produced by ENSO). However, it also assumes that the model possess biases. The Q-Q is intended to remove these biases.

To ensure that the technique does not lose information during the mapping stage, cumulative density functions (CDF) of both discharge-space and ensemble member-space are calculated. Common overlap periods are chosen for both the observed discharge and the simulated rainfall from the models to ensure that the same GHG domain is sampled. The method is very simple. The observed discharge from a particular basin is separated into N equally spaced intervals from lowest to highest. Similarly, the model rainfall output for the particular basin is also divided into the same number of intervals. N may be any number. Here we choose N=500.

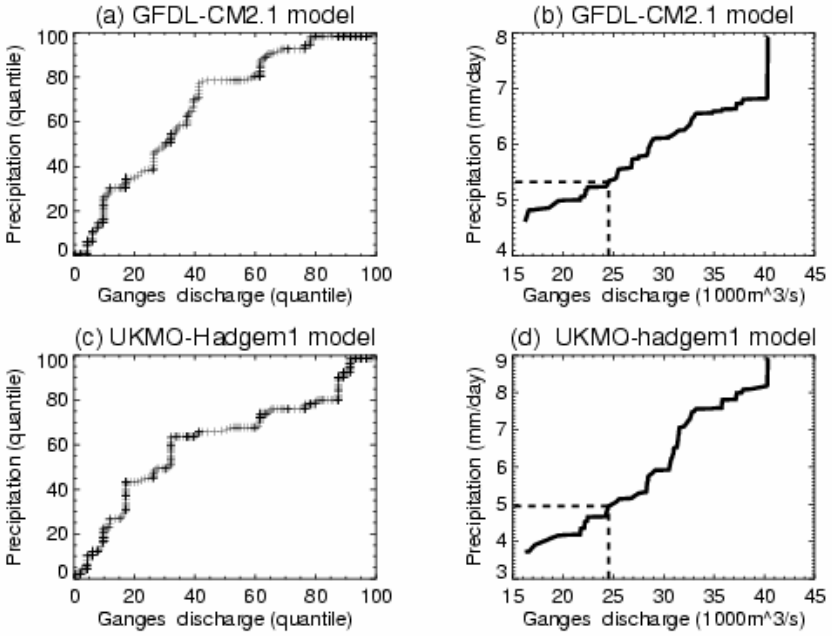

Figure 4.5 Quantile plots (a) and (c) and constructed mapping indices (b) and (d) between wet season mean Ganges River observational discharge and the modeled precipitation (in mm/day). The two models are GFDL CM2.0 (ID=11 in Appendix A) and UKMO Hadgem1 model (ID=23). The 24th members in model spaces and observational space are linked in (b) and (d).

After interpolation, at each interval point, the accumulated quantile value (CDF, from 0 to 100) is calculated based on the information that how many percentages of the data points are less or greater than this point. Then we link the quantile points in model-space to the same quantile point in the observational-space. Thus, the observed 24th discharge quantile of Yangtze River discharge is related to the 24th modeled precipitation quantile generation for the period. For example, two CDF series of observed Ganges River discharge and one ensemble of Geophysical Fluid Dynamics Laboratory climate model version 2.0 (GFDL-CM2.0) simulated average Ganges River basin precipitation are shown in Figure 4.5 (a). Each cross symbol (totally 500) represents the quantile positions at the same order number of equally-space intervals for both data series. The x

ordinate in Figure 4.5 (a) represents the quantile values of Ganges River discharge series. The y ordinate is for modeled precipitation. Both x and y axes range from 0 to 100, representing the data quantile position in the entire data space. Overall, this diagram illustrates the non-linearity of both data series. A perfect model would have a straight line directly from quantiles (0, 0) to (100, 100). The place where the profile slope less than one indicates that data points are denser in the corresponding observational discharge (X) interval than the modeled precipitation (Y). As an example, the profile is close to flat line when x interval value is between 80 and 100. This means that more data points were observed in the high tail of the observational discharge interval than those (maybe only one) in the high tail of the modeled precipitation. The correspondence index between two dataset is plotted in Figure 4.5 (b). As a consequence of these one or two extreme high values (maybe outliers) in modeled results, in this ensemble output of the model GFDL-CM2.0, any wet season precipitation averaged over Ganges basin with values between 6.8mm/day and 8 mm/day would be converted into a discharge value close to 40,300 $m^3 s^{-1}$ as indicated in the top-right of panel (b). Whenever this ensemble of model is applied, the same relationship should keep valid.

Figure 4.5 (c) and (d) show the quantile profile and correspondence index with ensemble one of United Kingdom Met Office Hadley Centre Global Environmental model version 1 (UKMO-Hadgem1). The profiles look different with (a) and (b), indicating the different spans of the modeled precipitation. For each ensemble of the 23 models, we have made individual quantile profile and index. The non-linear monotonic lines in (b), (d) and other ensembles build up the mapping index between modeled precipitation and observed discharge, which can be used further.

4.4.2 Advantages and disadvantage of the Q-Q technique

There are advantages in using the Q-Q technique. First, the constructed mapping index (such as Figure 4.5 b and d) is made between the 20C3M experiment precipitation and observational river discharge, both of them under the same influence of the 20th century GHG radiative forcing. In addition, all four future SRES scenario experiments are initialized directly from the ending state of the climate of the same 20C3M experiment as defined separately by each model. As no other dynamic or thermal adjustments or forcings are modified (other than the assumed growth of GHG concentrations under the various scenarios), it is reasonable to apply the same ensemble-specific index to the four SRES scenarios precipitation output to construct the future river discharges. The variability of the mean river discharges is then most likely due to the different SRES scenario GHGs concentration hypotheses.

A second positive point about the Q-Q technique is that the mapping index profile is monotonic with a non-negative slope, which means that a larger discharge always corresponds to a larger precipitation. This index is also non-linear, so that the excessive data crowding at one side of the interval will not cause twist after the mapping. One additional point is that the index is independent for each ensemble of each model, so that the variability and mean value of the reconstructed discharge are also independent. The index can be extended with interpolation on the ending points. If the future modeled precipitation output lies outside of the current model space, we can estimate the discharge through the extension line.

The Q-Q technique also has disadvantages. As in binning the observations and model output, we did not use the information that some observational data and model output

were occurring simultaneously. That is, the frequency coordination between the climate models and the observations are not considered. However, this drawback is probably less important in climate models because we are more interested in long-term climate change and less with high frequency variability. In addition, in most cases the ability to retrieve low frequency trend from the observational data is limited.

4.5 A strategy to pick up the best performing models

The IPCC-AR4 CMIP3 project provides a large number of models. The question is how does one choose the best model to calculate future river discharges? Or does one average the results of all the models and their families of ensembles and use a multi-model mean? The virtue of the latter method is that random error will tend to be eliminated by the averaging process. But there is a downside too. Different models have systematic errors that are regional so that not all models will produce realistic fields of precipitation in all river basins. Even with the use of the Q-Q technique does not guarantee that a particular model will be successful in all river basins. Krishnamurti et al. (1999, 2002, and 2006) and Chaves et al. (2005) recognized this fact and developed a "super-ensemble" technique that used the weighting factor regressed from a suite of weather prediction models to come up with a composite forecast. We do not follow this approach but do note that some models will do better regionally than others. The key is to develop a methodology that screens the models and chooses the best model or group of models for a particular basin.

A number of efforts have been made to identify the uncertainties within the complex of CMIP3 models. Allen and Tett (1999) applied an optimal fingerprinting algorithm,

which is based on standard linear regression, to detect an individual model's consistency and uncertainty via parametric test on the regression residuals or, in another words, the climate noise. Palmer (2000) applied chaos theory and Brier score to estimate the uncertainty of the non-linear weather and climate model predictions. Based on this theory, Räisänen et al. (2001) attempted to score the CMIP2 models and identify the outliers. Referring to the CMIP3 model simulations as a computer produced multi-scheme complex, Craig et al. (2001) analyzed the uncertainties of the forecasting outcomes from such systems, using a Bayesian approach. However, these efforts are usually based on purely statistical theory, independent of the model's climatic dynamic properties.

Given that IPCC models are the predictors for future climates under anthropogenic influence, we would like to analyze their performance from a climate viewpoint. One basic idea is to test the model's ability to produce a realistic annual cycle as a filter. In the full-band spectra map of most weather variables, the maximum power frequency is associated with the diurnal cycle. The next oscillation peak after the diurnal cycle is the annual cycle followed by synoptic variability, intraseasonal 20-80 day variability in parts of the tropics and interannual variability. Both the diurnal and annual cycles are related directly with the Earth's rotation and solar radiation and should be simulated by state-of-the-art climate models (e.g. Dai et al, 1999, 2004). The verification of the annual cycle of precipitation output from CMIP3 climate models would be a good method to test the model validity.

The flows in all the five rivers studied in this paper have a strong seasonal cycle since the majority total annual rainfall occurs in only a few months which is generally reflected in enhanced river discharge after taking usage and storage into account.

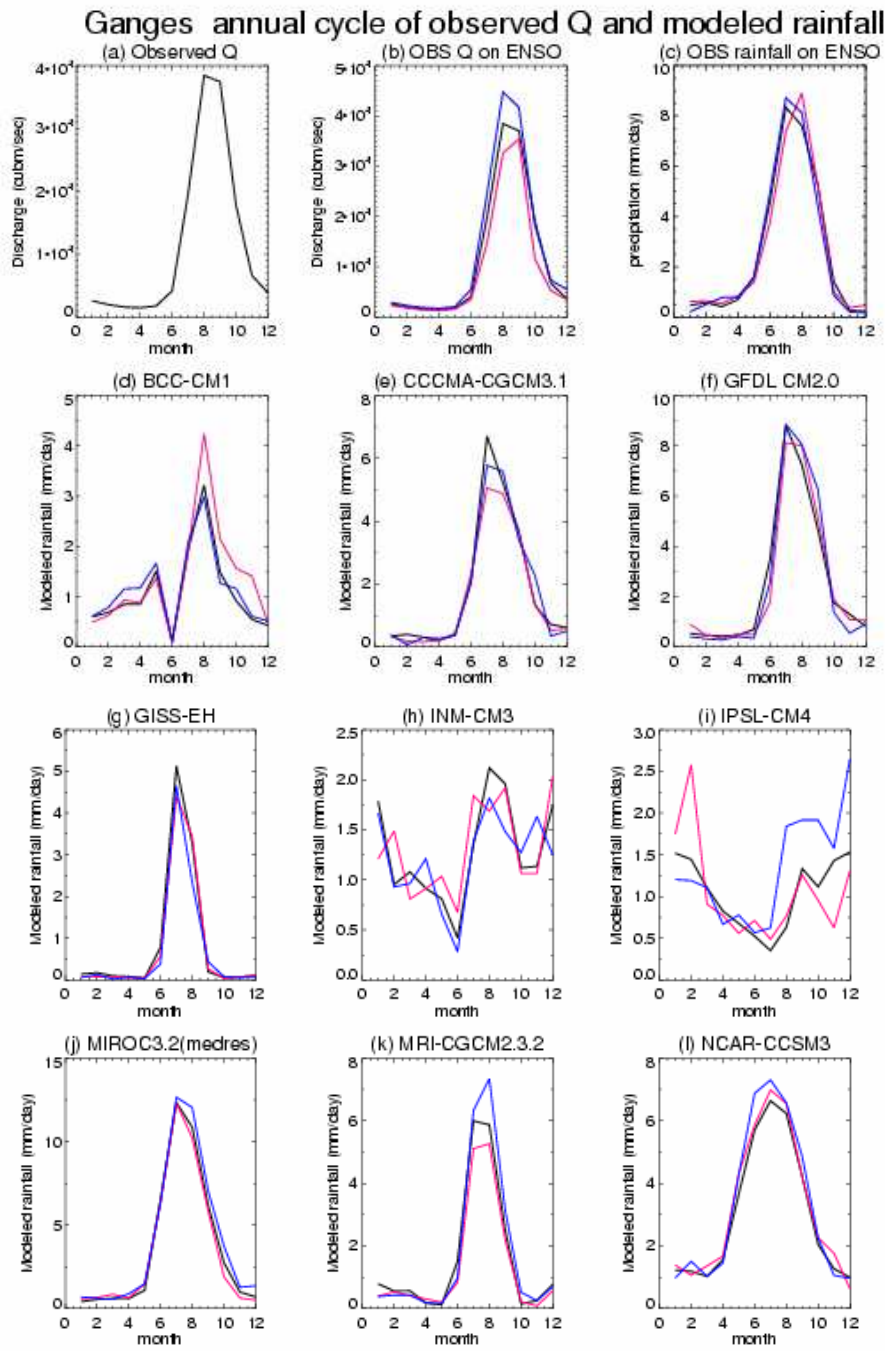

Figure 4.6 Climatological mean annual cycle of

(a) observed Ganges River discharge averaged from 1950-2004,

(b) observed Ganges River discharge categorized by ENSO events,

(c) satellite imaged GPCP rainfall averaged from 1979-2004 over Ganges River basin and categorized by ENSO events,

(d)-(i) Same as (c) but from selected IPCC-AR4 CMIP3 modeled 20th century precipitation, respectively, indicating the different models' ability to reproduce annual cycle.

Figure 4.6(a) is similar to Figure 3.3, illustrate the annual precipitation cycle over the Ganges River catchment. As discussed earlier, all the five rivers are strongly influenced by ENSO events, especially the Blue Nile, Ganges, and Murray-Darling rivers. In Figure 4.6(b), the annual cycles averaged from El Nino years, La Nina years and non-ENSO years are plotted with red, blue and black. It is observed Ganges River usually has more discharges during the La Nina year, and less on El Nino year. In Figure 4.6(c), the satellite-measured GPCP observed precipitation annual cycle confirms this ENSO influence but with less deviation. That is probably due to the available GPCP precipitation dataset cover a period of 26 years, much less than the 56 years in observation. In addition, we did not take the effect that the precipitation is not equal to discharge even though they are highly connected. We observed there is a one-month lead-time for the high-level precipitation to be turned into high-level discharge.

The panels in Figure 4.6 (d)-(i) show nine CMIP models selected from 23 models representing the "good" or "bad" ability to reproduce climatological cycle and ENSO effect. Here the ENSO year related categories are defined directly from respective model SST output. The model El Nino (La Nina) year is defined as the year which mean winter SST (from November to next February) temperature greater (less) than one standard deviation of the total winter SST time series. The other years are defined as a "normal year" or a non-ENSO year. We see most models can simulate quite well both annual cycle and the influence of ENSO onto river basin averaged rainfall. Exceptions are discussed below. Similar to the observations in (c), La Nina year has more rainfall than El Nino year. However, the ENSO year's deviation to the normal year is not as many as in the observation discharge.

In Figure 4.6 (d) and (g), the Beijing Climate Center Climate Model version 1 by China (BCC-CM1) and National Aeronautics and Space Administration (NASA)-Goddard Institute for Space Studies EH model by USA (GISS-EH) are observed to have a single extreme precipitation value on August and July, respectively, which is 40% larger than the maximum of the other months. Comparing with the observations in the first row, we know this is not true in the real world where we observe at least two closely monthly values during wet season. In Figure 4.6 (h) and (i), Institute for Numerical Mathematics Climate Model version 3.0 by Russia (INM-CM3) and Institute Pierre Simon Laplace Climate Model version 4.0 by France (IPSL-CM4) are unable to reproduce the seasonal cycle of the Ganges Valley precipitation shown in (c). Most other models have a good agreement with observations. Now we can manually mark those "bad" models" and do not use them as contributes to the predictions.

Another equivalent way of evaluating models is to look at the spatial distribution, by compare the seasonal accumulated precipitation between model ensemble output and reanalysis dataset. As an example, Figure 4.7(a) and (b) illustrates the long-term seasonal mean precipitation over March-April-May (MAM) and June-July-August (JJA) averaged over the 20th century (20C3M) run from IPCC-AR4 CMIP3 GFDL-CM2.1 model. The same seasonal averaged precipitation in the East Asia region from NCEP/CDC reanalysis dataset is shown in Figure 4.7(c) and (d). Comparing spatial MAM precipitation distribution between model result (a) and reanalysis dataset (c), we observe the spring Baiu-Mai-Yu rainfall in the lower Yangtze River valley and the Indian monsoon introduced rainfall north of Bay of Bengal. The modeled centers of the two rainfall areas are around 5 degrees north of reanalysis data. Besides that, the horizontal coverage and

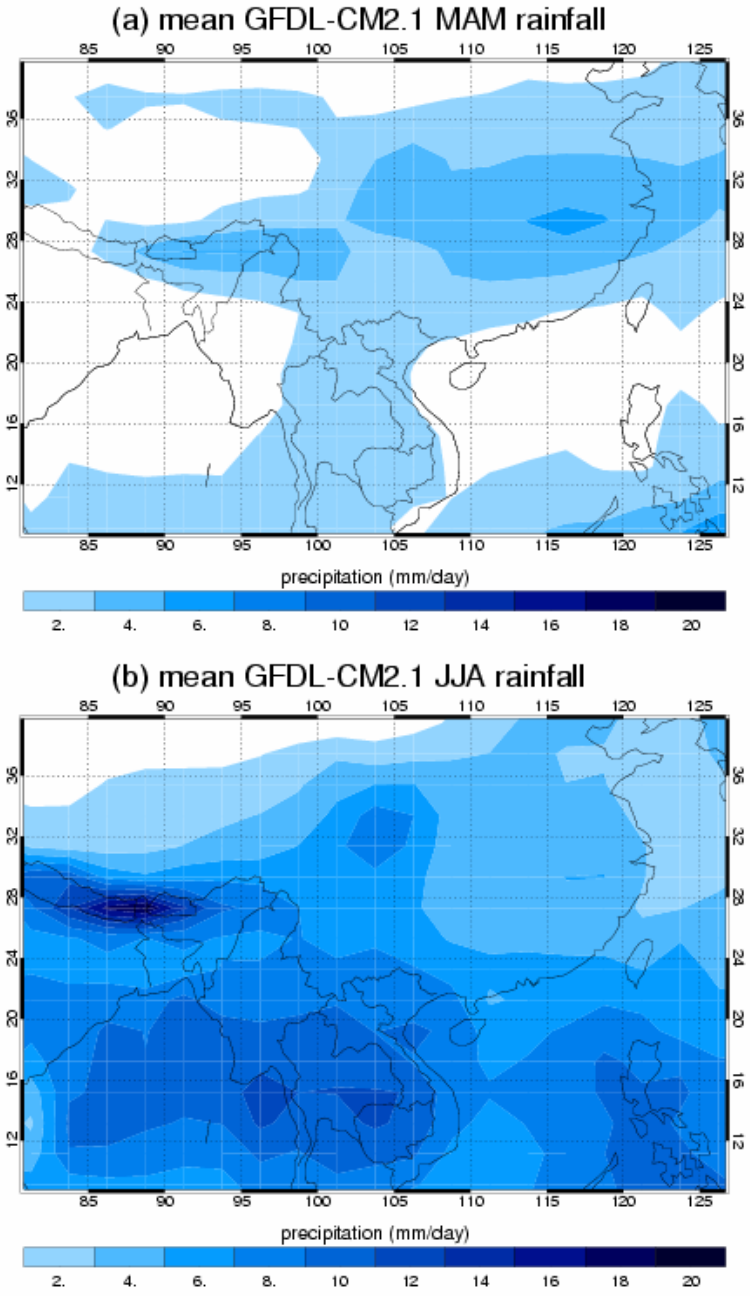

Figure 4.7 GFDL-CM2.1 modeled seasonal mean precipitation during (a) March-April-May (MAM) and (b) June-July-August (JJA) averaged over whole 20th century run experiment (20C3M). NCEP/CDC reanalysis of long-time mean precipitation in (c) MAM and (d) JJA (the reanalysis maps in (c) and (d) are provided by the NOAA-CIRES Climate Diagnostics Center, Boulder, Colorado, from the Web site at http://www.cdc.noaa.gov/).

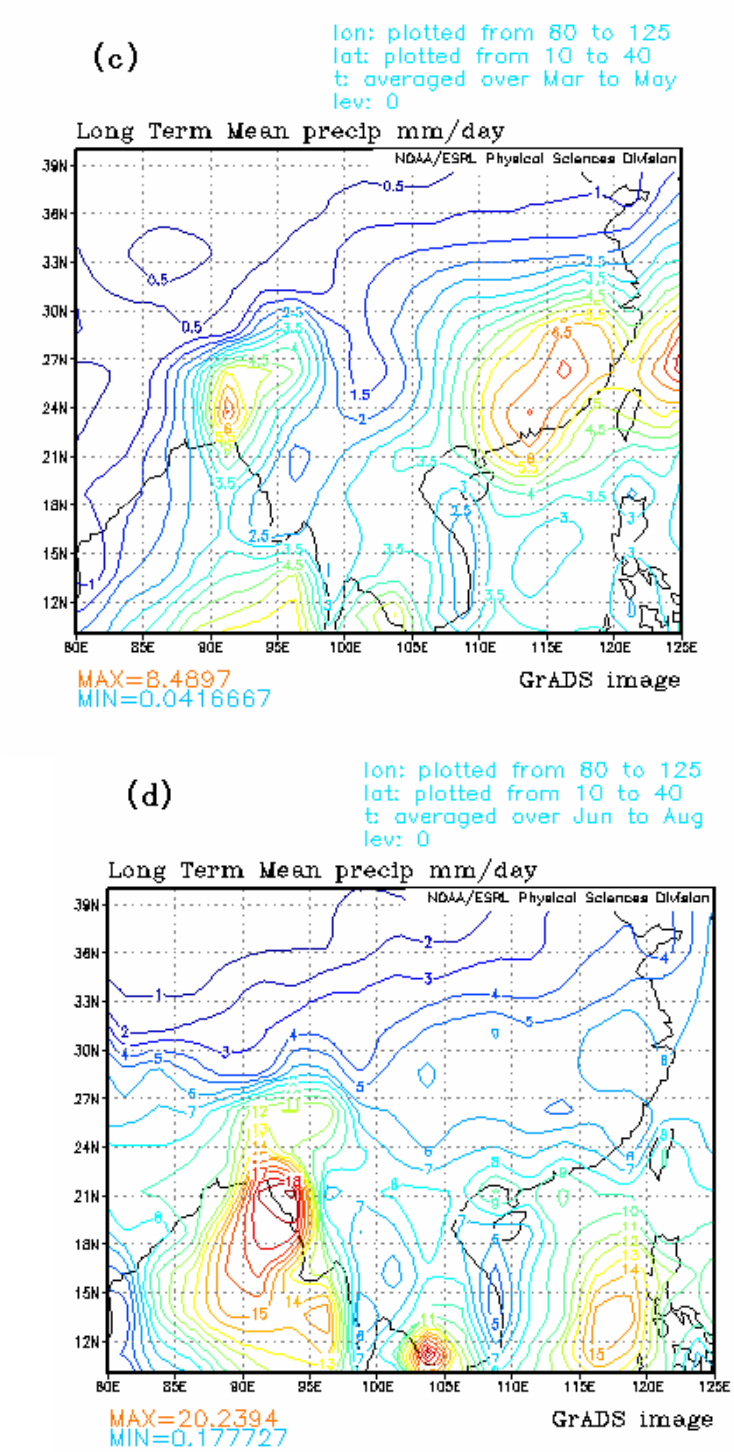

Figure 4.7 (continued)

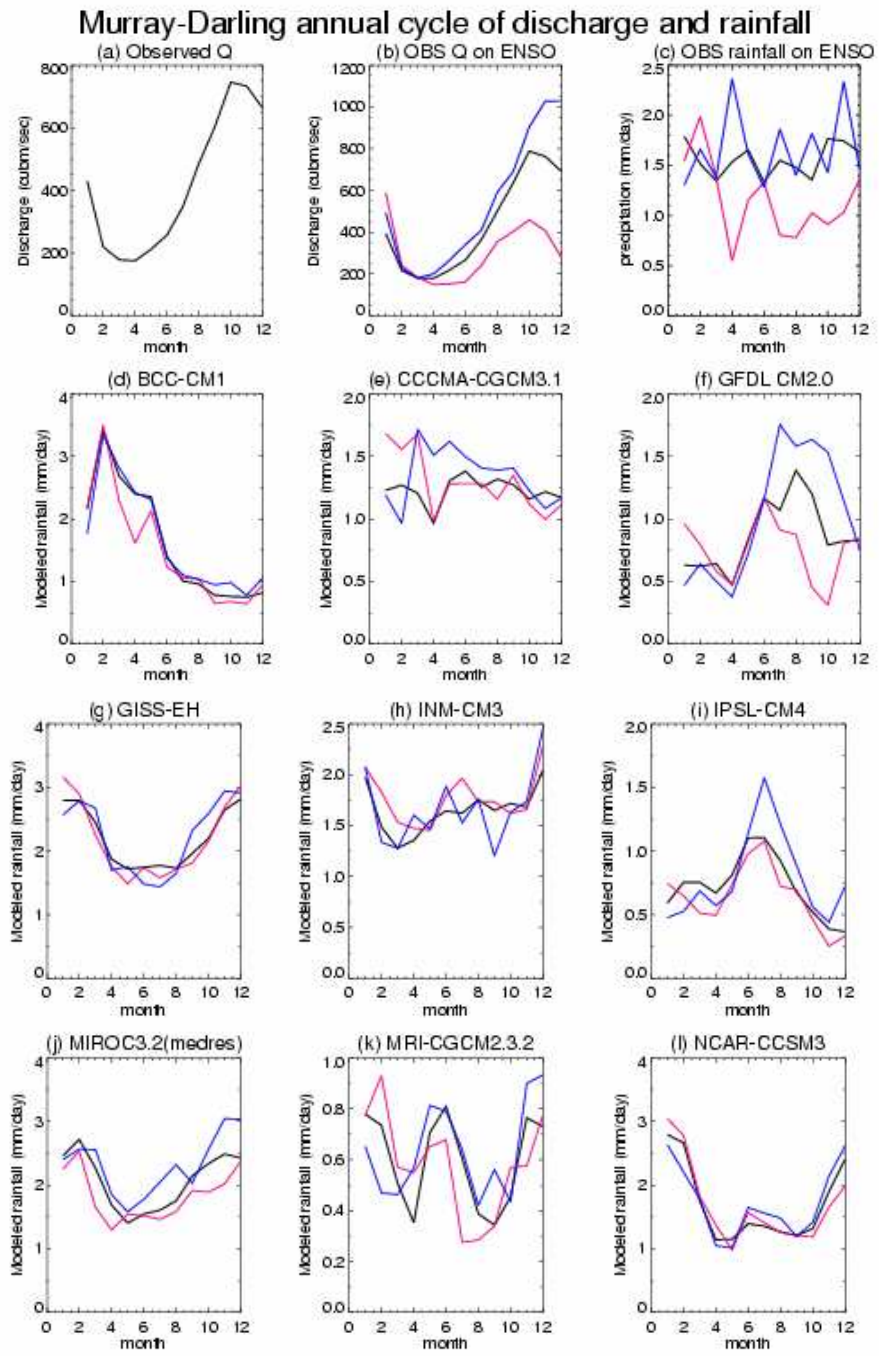

Figure 4.8 Same as Figure 4.6 but for the Murray-Darling River basin

relative magnitude are in apparent agreement. In summer time (b)(d), heavy rainfalls are observed in real time of Bay of Bengal while in the model it extends to the southwest of China. Overall, we may conclude that the GFDL-CM2.1 model is good at reproducing the spring and summer rainfalls in east and southeast Asian continent. For all the ensemble of all the models, the same diagrams and comparisons (not shown) are made. Other models do not do so well and many unsuccessfully simulate the East Asian climate. These are marked as "bad" models.

Similar filtering diagrams and procedures are applied for the Brahmaputra, Yangtze, and Blue Nile rivers (not shown). The final list of "good models" for above rivers is marked in Table 4.2. As we can see, most models appear to simulate the annual rainfall cycle well over the Brahmaputra River catchment area.

The Murray-Darling River catchment is different from the other river basins. In Figure 4.8, observations and modeled results are placed in the same way as Figure 4.6. In panels (d) to (i), few of the CMIP3 models have an exaggerated increase in Southern Hemisphere summer as in (a) discharge annual cycle estimated from the hydrological model. The inter-model deviation is large too. It is very possible that the numerous lakes, dams, and heavy irrigations along the Murray-Darling River substantially trap the precipitation and reduce the ground runoff at the river mouth. In fact, during times of drought during El Nino, there would be a greater use of irrigation because there would be less direct moistening of the soil from precipitation. The satellite-measured GPCP precipitation mean annual cycle is referenced in Figure 4.8 (c). It fits the modeled precipitation better than monthly discharge but still get many models invalid or "bad". The adopted "good" models for future analysis are marked as "O" in the last column of

Table 4.2. In addition, as the seasonality in most models are relative low or drifted, I will analyze the precipitation over the whole calendar year, instead of the wet seasons in other rivers.

Table 4.2 Overview of the CMIP3 models adopted for each river. "X" indicates that the model is "good" for precipitation simulation over the river basin, i.e. modeled precipitation well matched with observational discharge, "O" indicates that the modeled precipitation is "good" compared with GPCP satellite imaged precipitation.

ID	Model sponsor, model name, version	Yangtze	Ganges	Blue Nile	Brahma-putra	Murray-Darling
1	BCC cm1					
2	BCCR bcm2.0	X	X	X	X	
3	NCAR CCSM3.0	X	X		X	XO
4	CCCMA cgcm3.1(T47)	X	X	X	X	O
5	CCCMA cgcm3.1(T63)	X	X	X	X	O
6	CNRM cm3	X	X	X		X
7	CSIRO mk3.0	X	X		X	XO
8	MPI echam5	X	X	X	X	XO
9	MIUB echo_g	X			X	XO
10	IAP fgoals1.0	X	X		X	XO
11	GFDL cm2.0	X	X		X	XO
12	GFDL cm2.1	X	X		X	XO
13	GISS aom model	X	X	X	X	O
14	GISS EH model			X	X	XO
15	GISS ER model		X	X	X	X
16	INM CM3.0			X	X	O
17	IPSL cm4			X		
18	MIROC3.2 hires	X	X	X	X	XO
19	MIROC3.2 medres	X	X	X	X	XO
20	MRI cgcm2_3.2a	X	X	X	X	O
21	NCAR pcm1				X	XO
22	UKMO hadcm3	X	X		X	XO
23	UKMO hadgem1	X	X	X	X	XO

4.6 Inter-model and inter-ensemble precipitation simulations

Figure 4.9-4.13 represents the changes in precipitation in the various river basins using the models listed in Table 4.2. The Ganges results are summarized in Figure 4.9, which shows model estimations of precipitation changes for various scenarios. Arrows illustrate the changes of modeled precipitation over the next 100-year period. Each arrow represents the change in the precipitation of an ensemble member of the top wet four-month precipitation from 1980-1999 to 2080-2099 (the arrowhead). Ensemble members of the same model (identified by the model ID defined in Appendix A) appear to cluster. In contrast, the absolute values of the clusters differ a lot. The "good" and "bad" models defined earlier are marked red and blue. We observe that the blue arrows locating in both high and low part of the entire precipitation interval, indicating that the simulated precipitation magnitude is irrelevant to the model's ability on reproducing the climatological annual cycle. These four months are derived from the observed climatological annual cycle illustrated in Figure 3.1 and sub-diagram of Figure 2.2a. Note that not all the scenario experiments provide the full ensemble members as listed in Table A.1, which complicates data analysis and the arrow is shown only when both the 20C3M and the continuous SRES scenario experiment output are available.

In the high GHG scenarios (SRESA1B and SRESA2), the Yangtze, Ganges, and Brahmaputra River catchment rainfalls are very likely (>90% probability) to have an increasing trend. Modeled rainfalls in the Blue Nile and Murray-Darling River valleys have large uncertainties with diverse upward and downward possibilities, making it hard to make a confident prediction.

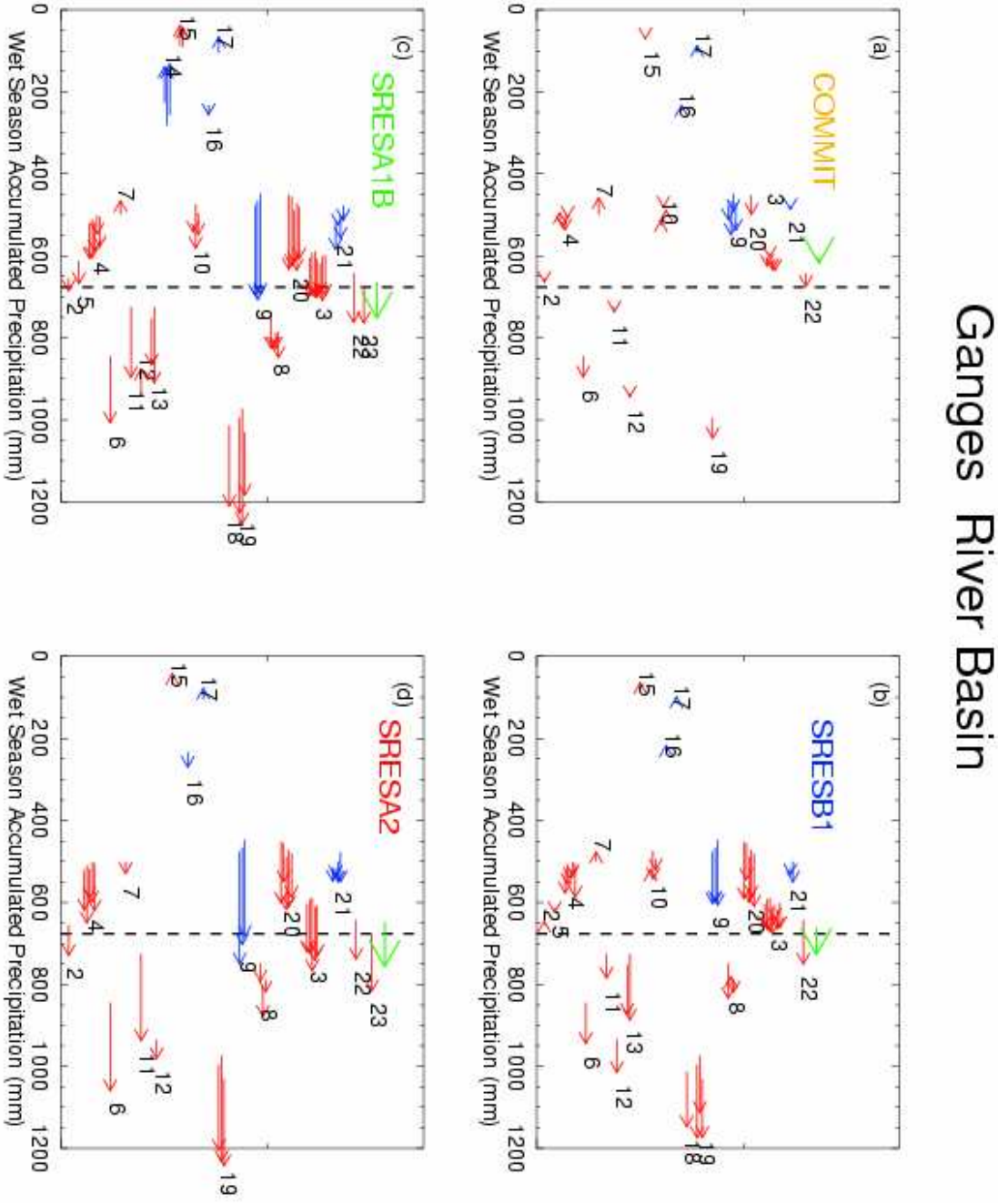

Figure 4.9 The changes of accumulated wet season (July to October) mean precipitation over Ganges River basin from 1980-1999 averaged in 20C3M toward 2080-2099 (arrow head) in (a) COMMIT, (b) SRESB1, (c) SRESA1B, and (d) SRESA2 scenario. "Good" or "bad" models are marked in red and blue. The large green arrows on the top of each panel mark the multi-model mean from all "good" model results. The ensemble members from the same model appear a cluster. The dash line marks the observation level averaged from 1979-2004 GPCP precipitation data. The numbers beside the clusters mark the model ID in Table 4.1 and Table A.1.

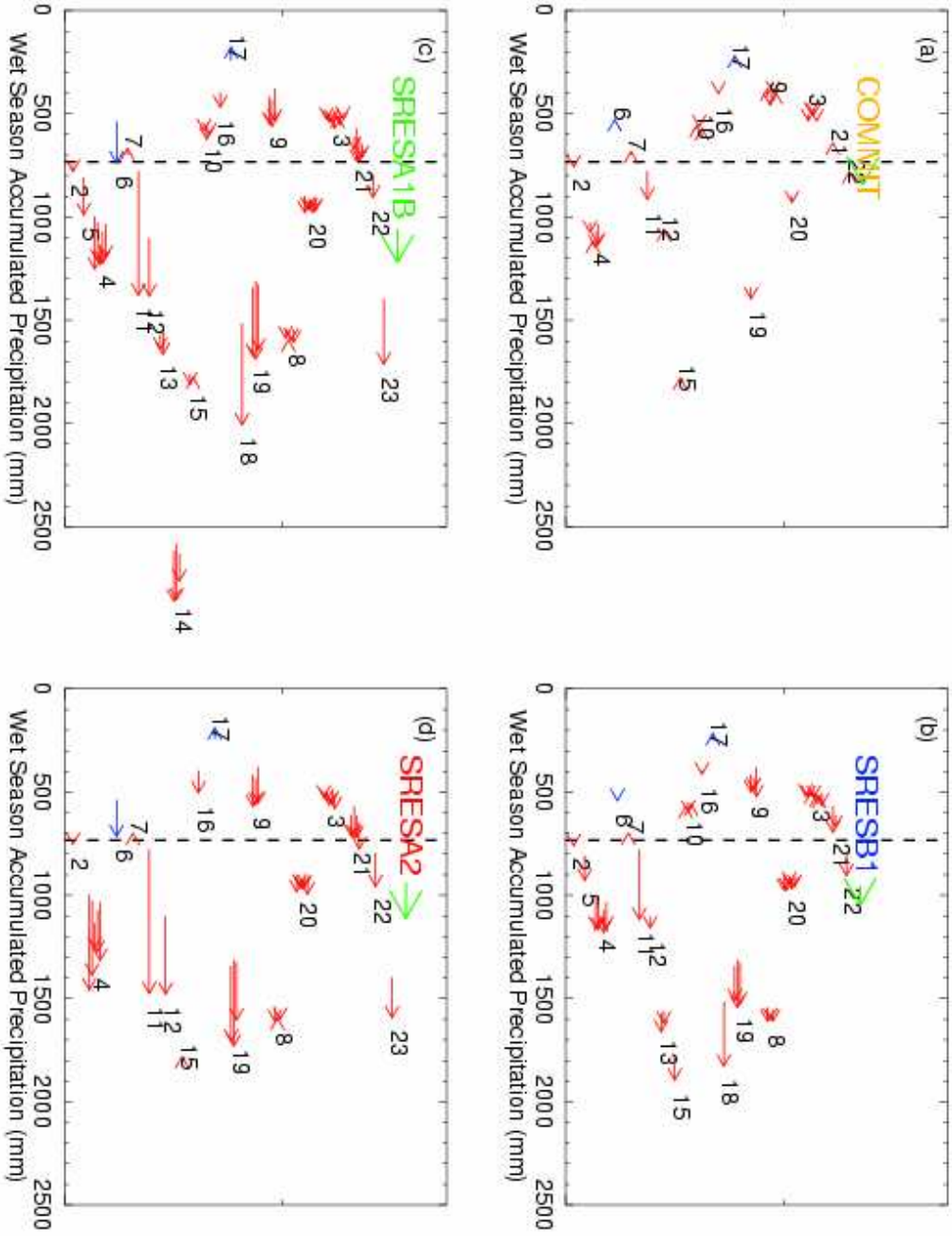

Figure 4.10 Same as Figure 4.9 but for the Brahmaputra River basin. The wet season is from June to September

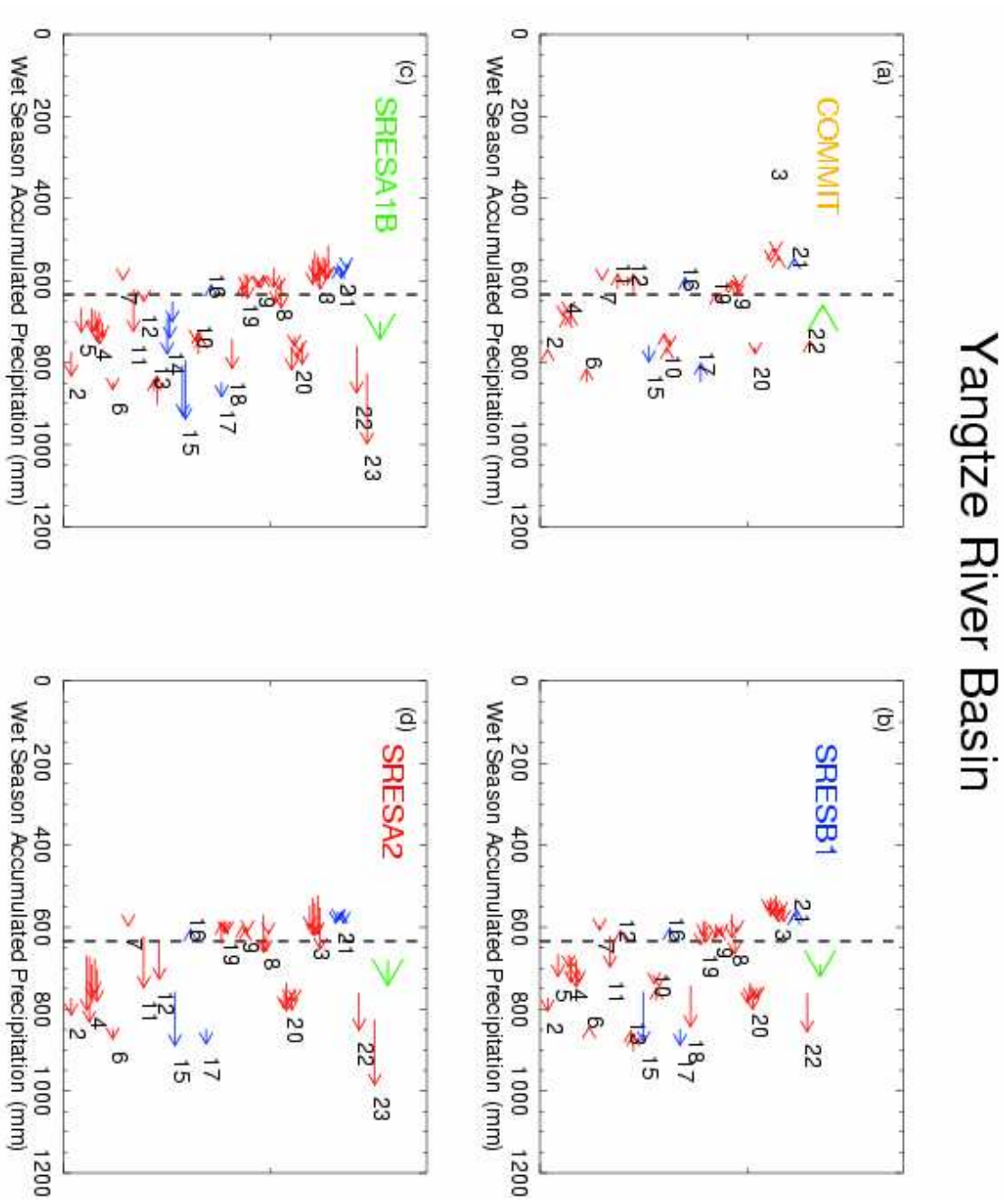

Figure 4.11 Same as Figure 4.9 but for the Yangtze River basin. The wet season is from June to September.

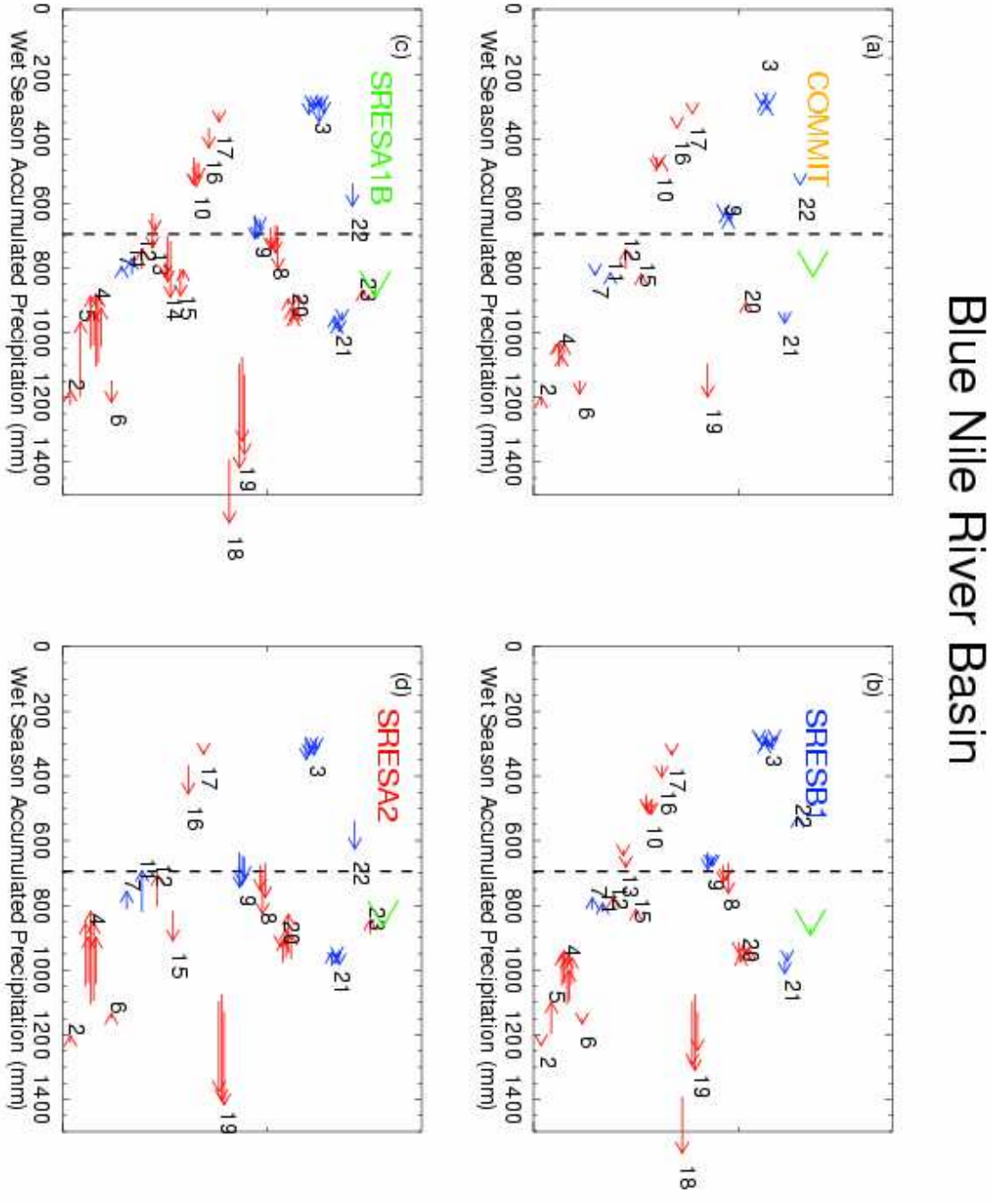

Figure 4.12 Same as Figure 4.9 but for the Blue Nile River basin, the wet season is from July to October.

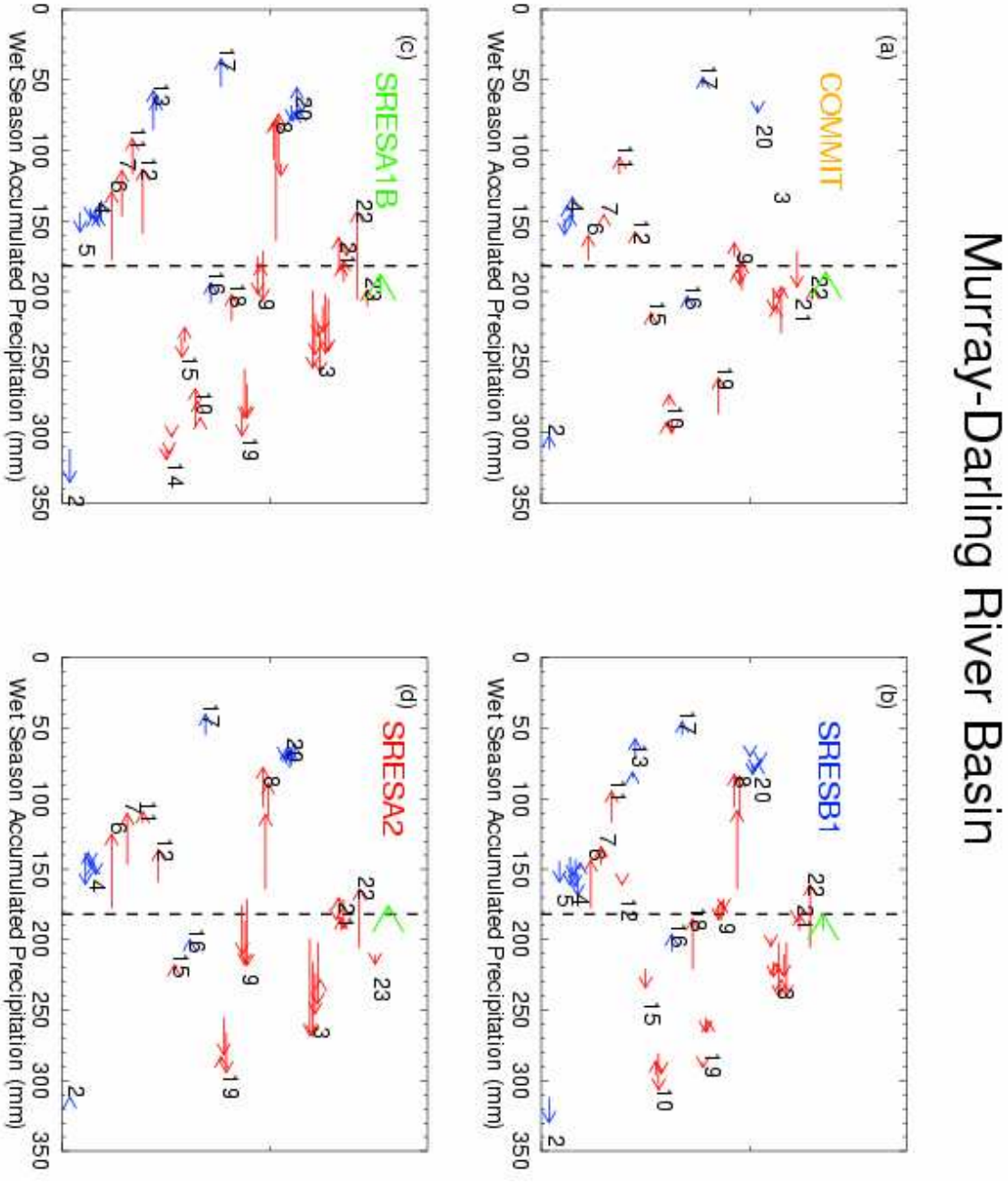

Figure 4.13 The changes of accumulated annual precipitation over the Murray-Darling River basin from 1980-1999 (arrow body) in 20C3M toward 2080-2099 (arrow head) in (a) COMMIT scenario, (b) SRESB1, (c) SRESA1B, and (d) SRESA2 scenarios. Here "Good" or "bad" models are determined by whether it has a similar annual cycle with satellite imaged precipitation (indicated by "O" in Table 5.2) and marked in red and blue.

Over all, the Yangtze River has less inter-model deviation while the Murray-Darling River has the largest deviation among estimates. In Figure 4.10, the Brahmaputra River has the biggest increasing trend. Even though the embedded ocean/atmosphere/land/ice models, grid resolutions, dynamic schemes, and parameters setup are quite different among these multi-country and multi-institute coupled climate models, the differences between these model output are still too large considering the value here are retrieved directly from the model output. In Figure 4.9, the Ganges River basin has a similar trend with Brahmaputra, but the absolute flow value is less. The "good" and "bad" models are marked red and blue.

It should also note that making the ensemble mean will reduce the climate variability making such a metric useless for studying extreme events. In any event, the large green arrow at the top of each panel of Figure 4.7 represents the mean change of the entire red colored ensemble mean (each model version equally weighted). That is, the green arrow is the multi-model mean of the ensemble mean of all of the "good" models.

With an assessment of the future precipitation in the various river basins, as established by the "good" models, we can now make projections of future river flow.

CHAPTER 5

RIVER DISHCARGE PROJECTION AND ANALYSIS

5.1 Time series of projected river discharges

The Q-Q technique developed in last chapter provides a new mapping index linking the observational discharge and precipitation simulation. We can apply each index to future modeled precipitation predictions as long as the model internal dynamic and thermal schemes remain unchanged with the external radiative forcing factors only influenced by GHG changes.

The total ensemble number of all available precipitation projections is large (40-50 per scenario and per river basin). Without losing generosity, we are going to illustrate one example of the simulated river discharge from the Community Climate System Model version 3 (CCSM3). The multi-model analysis results will be shown in the next section. CCSM is a project within the Climate & Global Dynamics Division (CGD) at the National Center for Atmospheric Research (NCAR). The CCSM3.0 model (Collins et al. 2006) is one of the best of the state-of-the-art models, widely adopted for climate simulation or large-scale external climate forcing to mesoscale models. It has a good ability to reproduce both spatial and temporal scale of atmosphere activities. We observe in the earlier study that this model is among the "good" models that have the simulation much close to the trend.

5.1.1 Wet season mean river discharges and their interannual variabilities

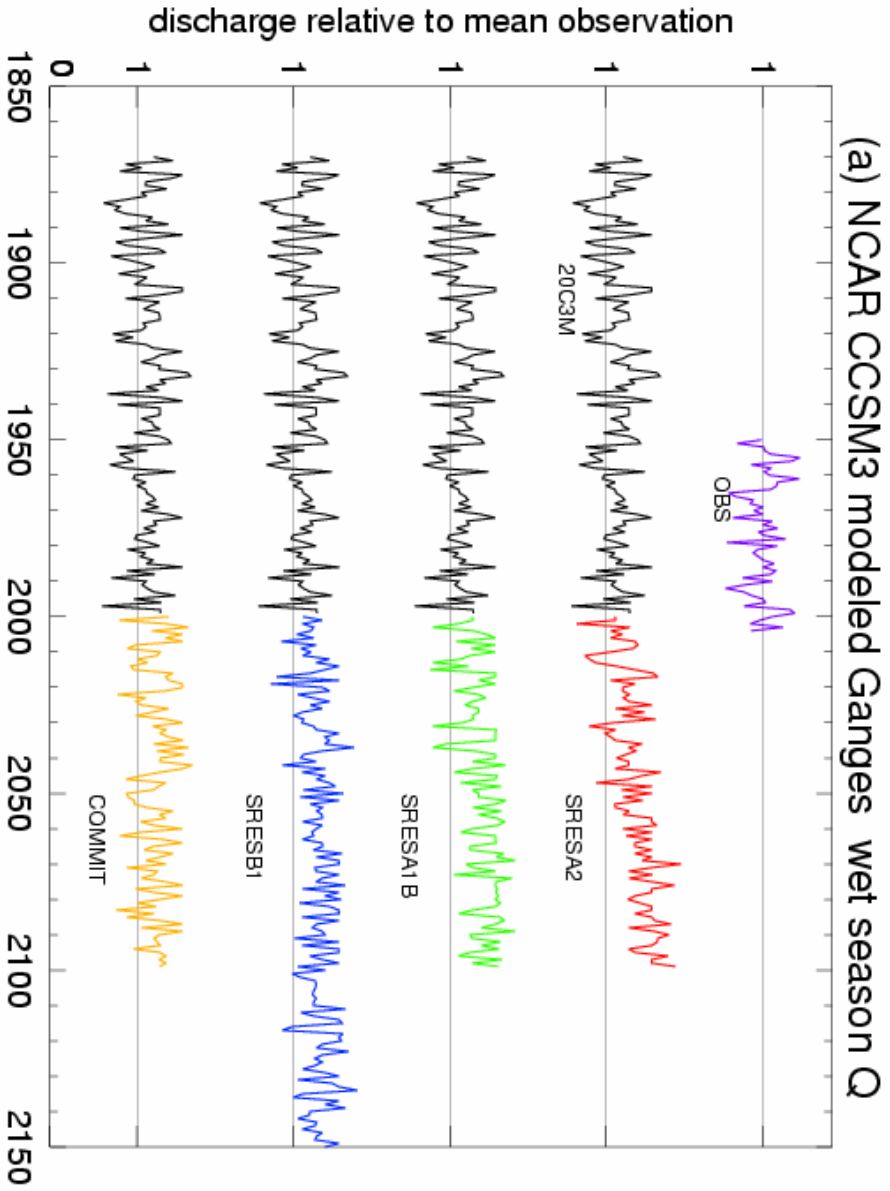

Figure 5.1 Time series of normalized NCAR-CCSM3 modeled (a) Ganges (b) Brahmaputra, and (c) Yangtze River mean wet season discharge under different SRES scenarios as the continuation of the 20C3M experiment. (d) Same as (a) but for the Blue Nile River and from Marc Plank Institute ECHAM5 model (MPI-ECHAM5). (e) Same as (a) but for the annual mean precipitation over the Murray-Darling River Basin. All river discharge data are divided by the climatology mean value of the available observations. The color scheme is the same as in Figure 4 .1, 4.2, 4.3.

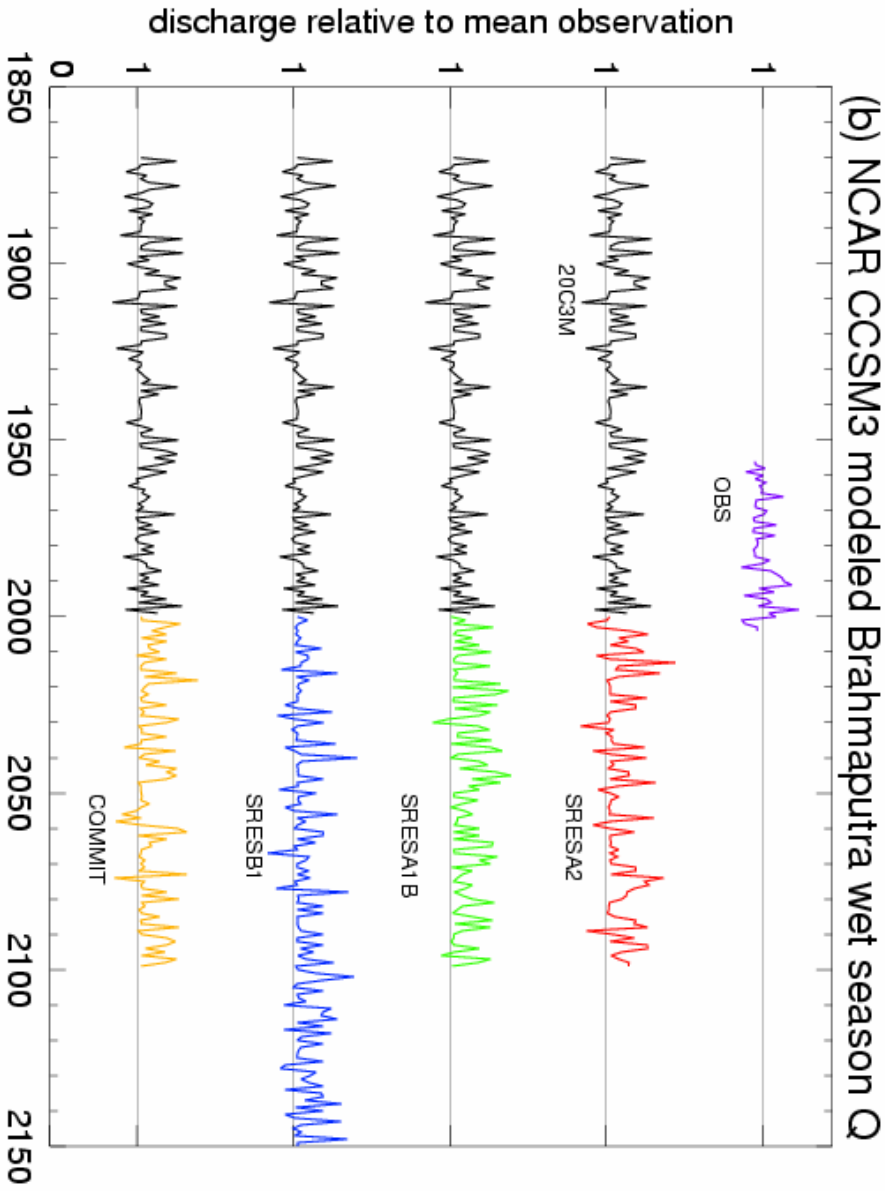

Figure 5.1 (continued)

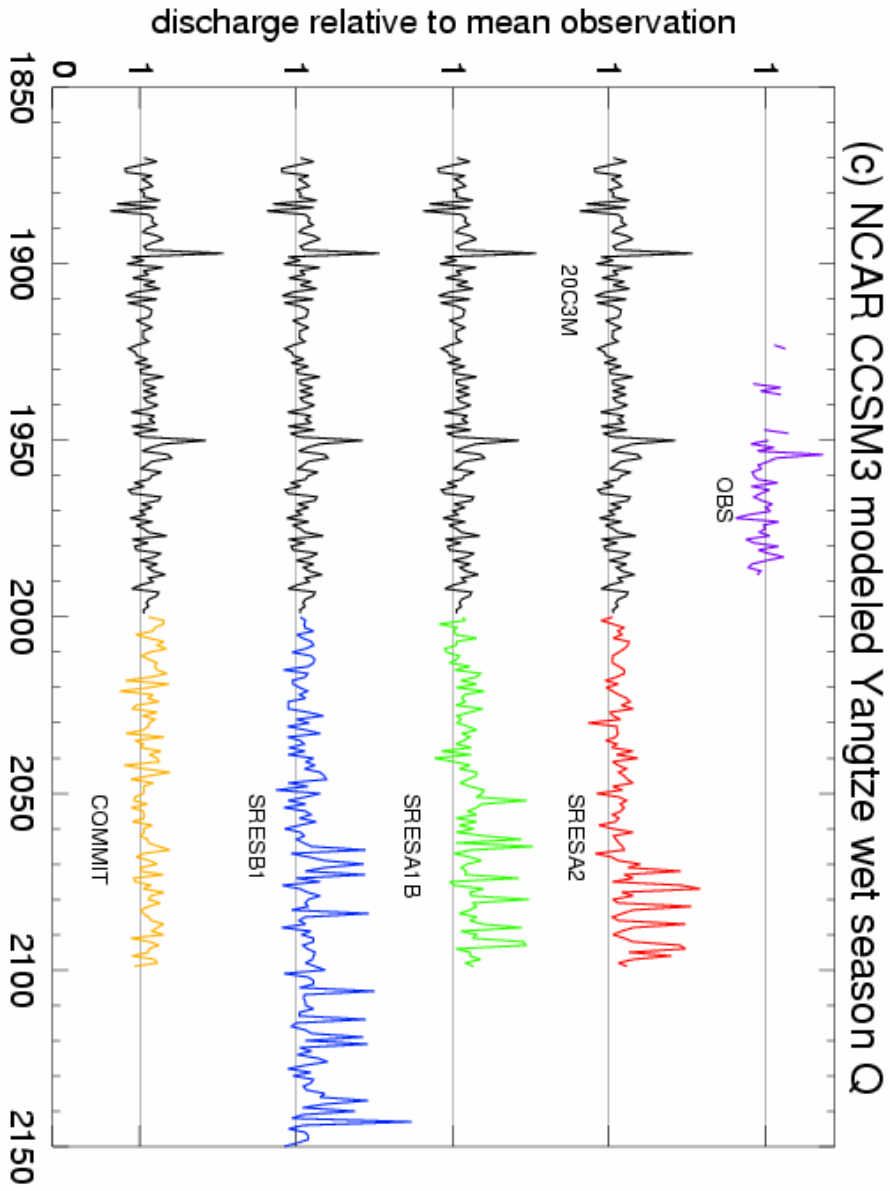

Figure 5.1 (continued)

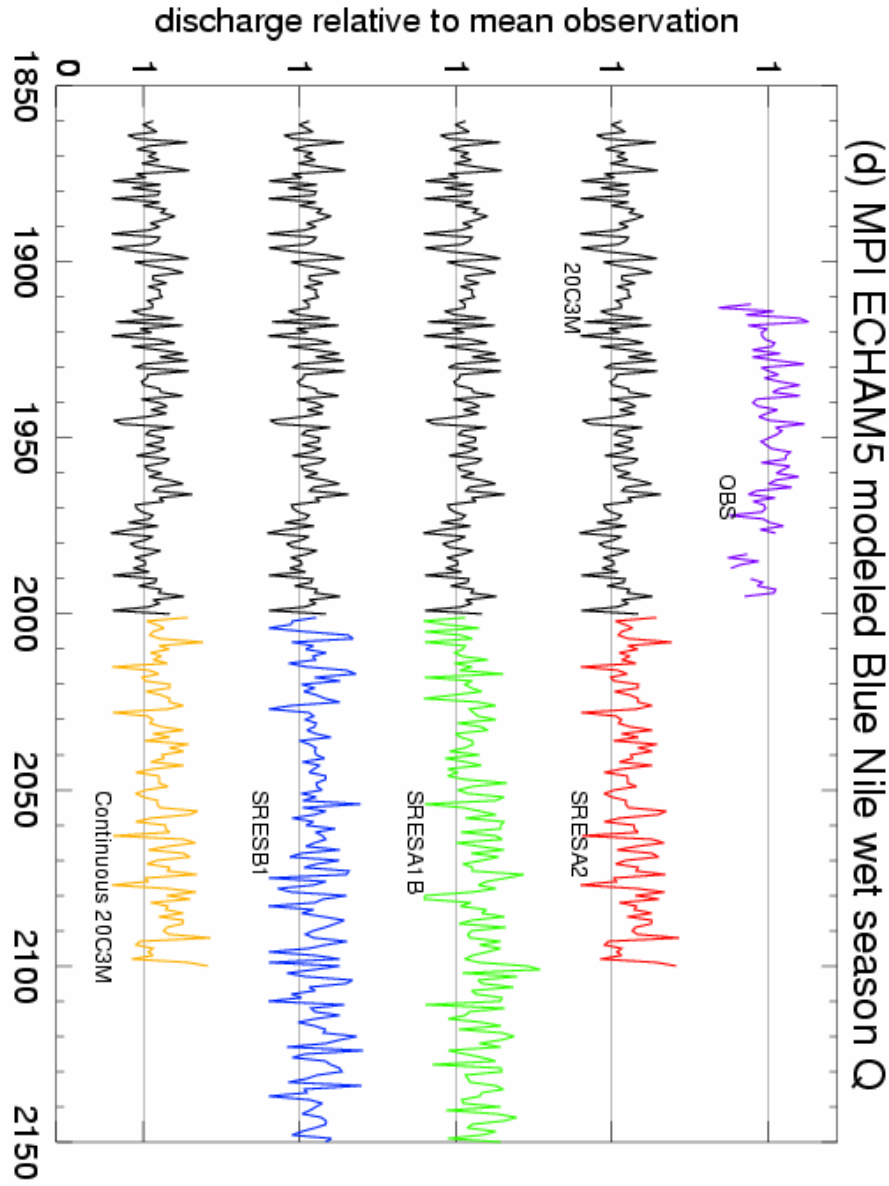

Figure 5.1 (continued)

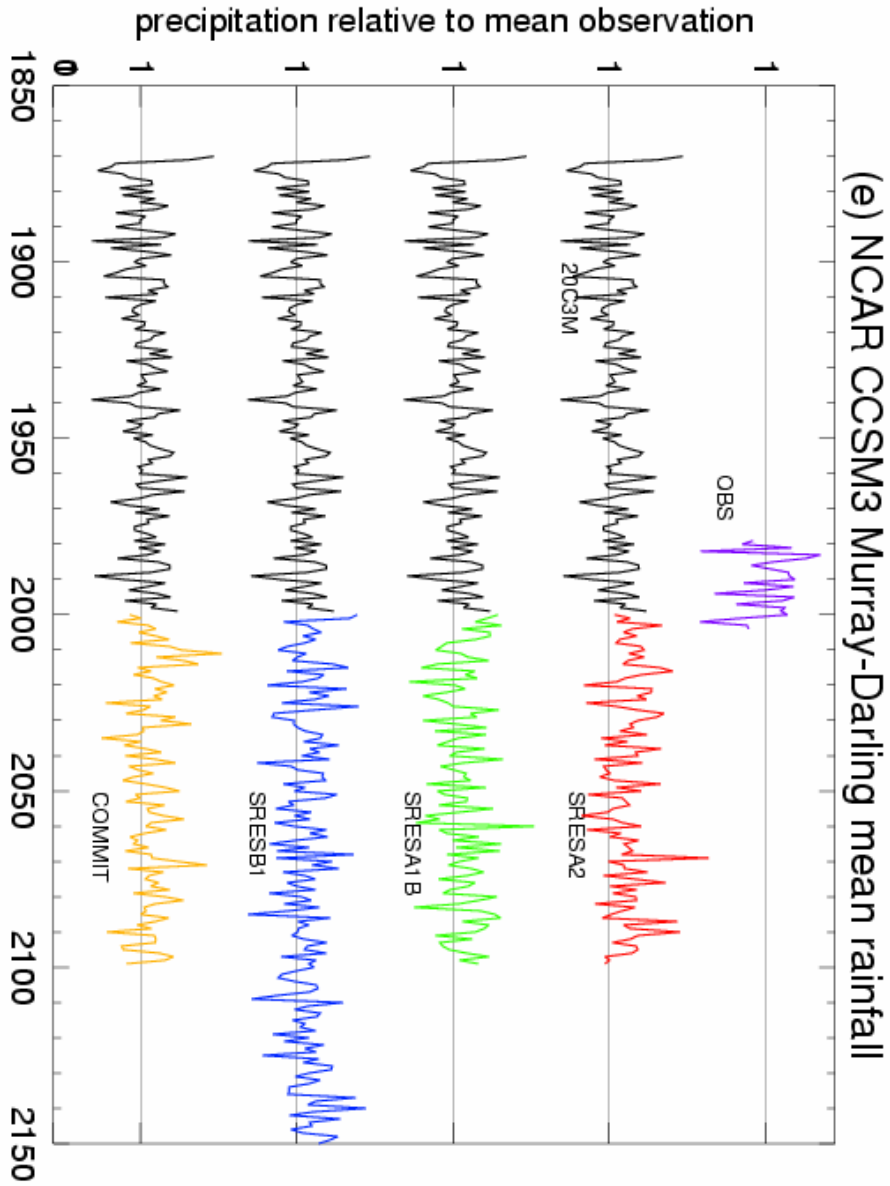

Figure 5.1 (continued)

Figure 5.1 (a) illustrates series of the Gangs River wet season mean discharge simulated under four IPCC SRES scenarios from the first ensemble experiment. They are all continuation of the precursor 20C3M run experiment. The observational wet season discharge is also shown in purple in the top of the panel. Annual values of wet season

discharge (June through September) are plotted. Starting from the same initial point (the end of the 20th century), the Gangs River discharges for the four scenarios differ a lot. Except for the SRESA2 case, this model suggests little change is discharge during the next 100-year period. The SRESA2 scenario shows increment in both variance and magnitude during the second half of the 21st century.

Figure 5.1 (b)-(e) shows time series of the Brahmaputra, the Yangtze, the Blue Nile River discharges, and the Murray-Darling River basin precipitation. As NCAR-CCSM is not considered as a "good" model in Blue Nile discharge simulation, Marc Plank Institution by Germany (MPI) ECHAM5 is considered in this case. The interannual variability is well reproduced.

We calculate the multi-model mean and average standard deviation of respective river discharges for quantitatively study purpose. The results are listed in Table 5.1. The differences between observational and reconstructed discharges during the same period are less than 1% in mean value and less than 5% in standard deviation for each basin. The first and second half of the 21st century is calculated separately to present the variability changes under the increasing GHGs concentrations. In the Ganges, Yangtze, and Brahmaputra rivers, the mean and standard deviation of the discharge series increase as the scenario GHGs concentrations increase, either from scenario to scenario or from earlier time to later. For all the scenarios and all periods, the Blue Nile and Murray-Darling rivers keep the same mean value as 20C3M run while the variations increase less than 10%. These characteristics are the same as the COMMIT scenario case in Ganges, Yangtze, and Brahmaputra rivers, which are heavily affected by Asian monsoon.

Table 5.1 Overview of mean and standard deviation of the interannual series of river discharges from different SRES scenarios, the 20C3M experiment run, and the observations. Wet season river discharges (m^3s^{-1}) and annual mean Murray-Darling Basin precipitation (mm day^{-1}) are retrieved from multi-model mean of the ensemble member mean.

		Ganges	Brahmaputra	Yangtze	Blue Nile	Murray-Darling
Observations		28307 ±5706	40027±5704	43695 ±7153	3777±785	1.478±0.269
20C3M (within OBS period)		28311 ±5900	40186±5939	43755 ±7027	3778±775	1.483±0.257
Whole 20C3M (from 19th century to 1999)		28672 ±5913	40148±6071	43965 ±7257	3819±782	1.485±0.263
COMMIT	2000-2049	29149 ±6384	40580±6365	42859 ±6657	3783±893	1.488±0.250
	2050-2099	28894 ±6793	40378±6276	43183 ±7167	3693±793	1.482±0.266
SRESB1	2000-2049	29745 ±6548	41740±6651	43662 ±7955	3800±808	1.498±0.276
	2050-2099	31507 ±6653	44429±7519	45844 ±9030	3874±880	1.481±0.282
SRESA1B	2000-2049	29452 ±6327	42460±7202	42984 ±7314	3805±803	1.500±0.275
	2050-2099	32306 ±6434	47764±8515	47023 ±9720	3916±852	1.494±0.283
SRESA2	2000-2049	29078 ±6381	41203±6927	42087 ±6430	3802±799	1.493±0.268
	2050-2099	32675 ±7243	47055±8921	46965 ±10159	3842±821	1.499±0.302

5.1.2 Decadal variability

To illustrate decadal variability and long-term trends, a 10-year moving average window smoother is applied to all series. Each sub-diagram in Figure 5.2 shows available smoothed series of Yangtze River wet discharge for all scenarios plus observation from one ensemble experiment (marked as "ens" plus number) of NCAR-CCSM model. The color scheme is following the one using in Figure 5.1. In (a)-(e), the discharges under SRESA2 and SRESA1B scenarios have similar trends, both increasing about 40-50% (>20,000cum/s) at the end of the 21st century. The COMMIT scenario suggests no obvious sign of long-term change. In all sub-diagrams where SRESB1 is available, the Yangtze River discharge is also supposed to increase at a speed between the SREA1B and COMMIT. All these increasing trends are very close to the CO2 increased trend in Figure 4.2 and surface warming trend in Figure 4.3. From discussion in section 4.4, we know that the diagrams are independent to each other.

Up to 49 ensemble members are simulated for Yangtze River. Among them there are at least 23-39 members (depends on different scenario) can be marked as "good" according through the annual cycle-fitting strategy. It looks like the CCSM is good at simulating the decadal variability of Yangtze River. However, in Figure 5.3 we know this may not be true for other models such as Commonwealth Scientific and Industrial Research Organization (CSIRO, Australia) and MPI- ECHAM5 model.

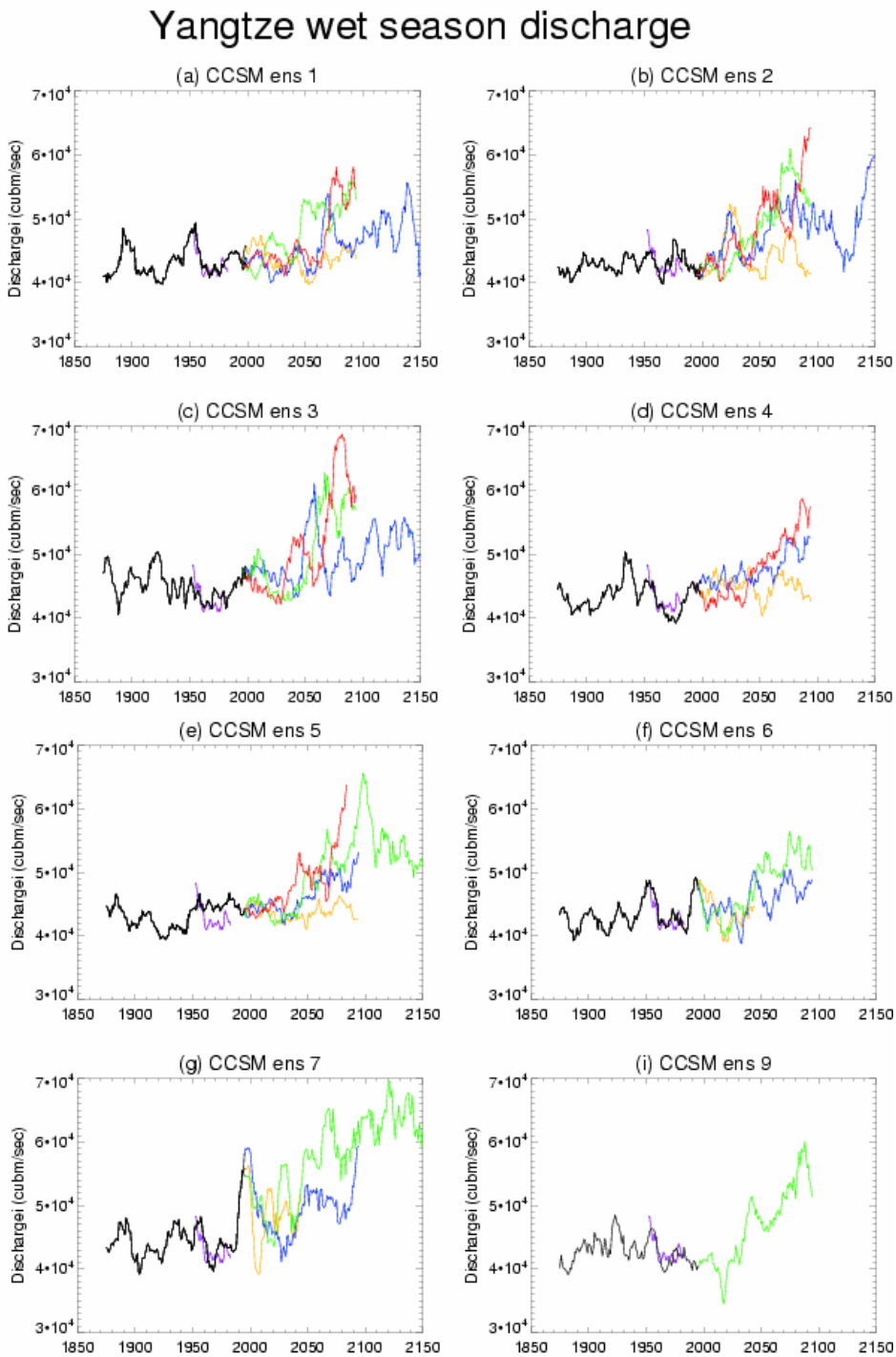

Figure 5.2 10-year moving average of the modeled Yangtze River wet season discharge retrieved from all ensemble experiments of NCAR CCSM3. The color scheme is the same as in Figure 5.1. SRESA2 (red) outputs are only available in the first five ensemble experiments but are observed to have a large increase in the second half of the 21st century. 10-year running mean of observation (purple) is well simulated by 20C3M experiment (black)

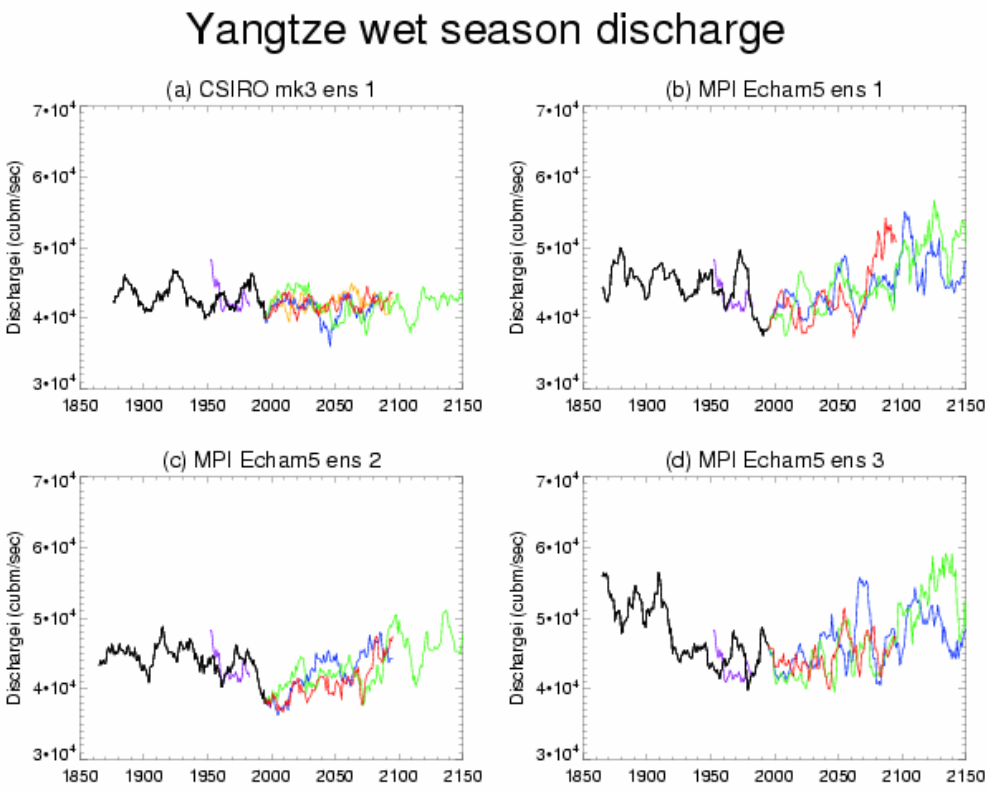

Figure 5.3 Same as Figure 5.2 but with (a) one ensemble of CSIRO model, and (b)-(d) ensembles No.1- No.3 of MPI ECHAM5 model. Observations are well simulated in magnitude but not in frequency. The projected 21st century mean discharges are less than in CCSM.

The 10-year running mean Yangtze River discharge series from all "good" ensemble simulations are shown in Figure 5.4 (a)-(d). In panel (a) the COMMIT (orange) and 20C3M (black) appear to be similar. In panel (b) (c) (d) most ensembles suggest an increasing trend. Note that the SRESA1B begins to rise before 2050 and SRESA2 in a much later time, which is close to the CO2 concentration trend rather than other GHGs. In particular, this diagram is an extended reconstruction of the arrow map in Figure 4.11. A non-parametric statistical (Kendall trend) analysis will be performed in section 5.4.

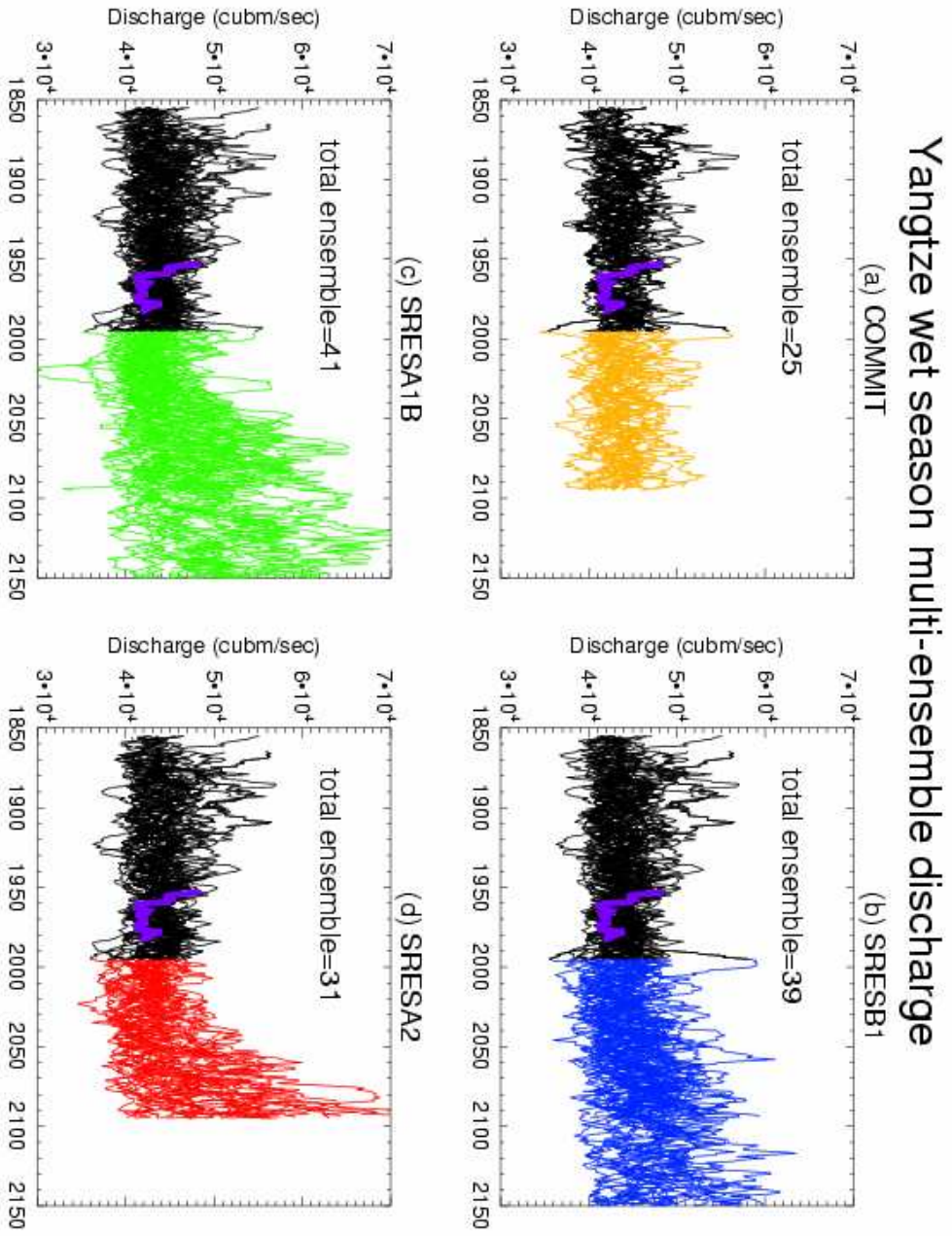

Figure 5.4 Multi-ensemble reconstructed 10-year running mean Yangtze River wet season discharges for (a) COMMIT, (b) SRESB1, (c) SRESA1B, and (d) SRESA2 scenarios continued from the 20C3M experiment (black). In each panel, there are 25-41 ensemble members from a total of 17 "good" models.

The Ganges River and Brahmaputra River simulated discharge are shown in Figure 5.5 and Figure 5.6. Overall, they verified the founding in Table 5.1. Both river discharges

show very similar long-term trend with the Yangtze River discharge under the same SRES scenario. As all three rivers are located closely and influenced strongly by Asian summer monsoon, it may indicate that the monsoon precipitation will vary heavily on GHGs concentration change, especially on the second half of the 21st century

In Figure 5.7, Blue Nile River modeled discharges act very different with the above three rivers. With different ensemble member numbers, the future SRES scenario simulations are largely distributed, while in the 20th century run (20C3M) the ensemble experiments have much closely results.

For all five river discharge projections, the fixed-GHG-concentration (COMMIT) scenario has the most similarity to the 20th century run.

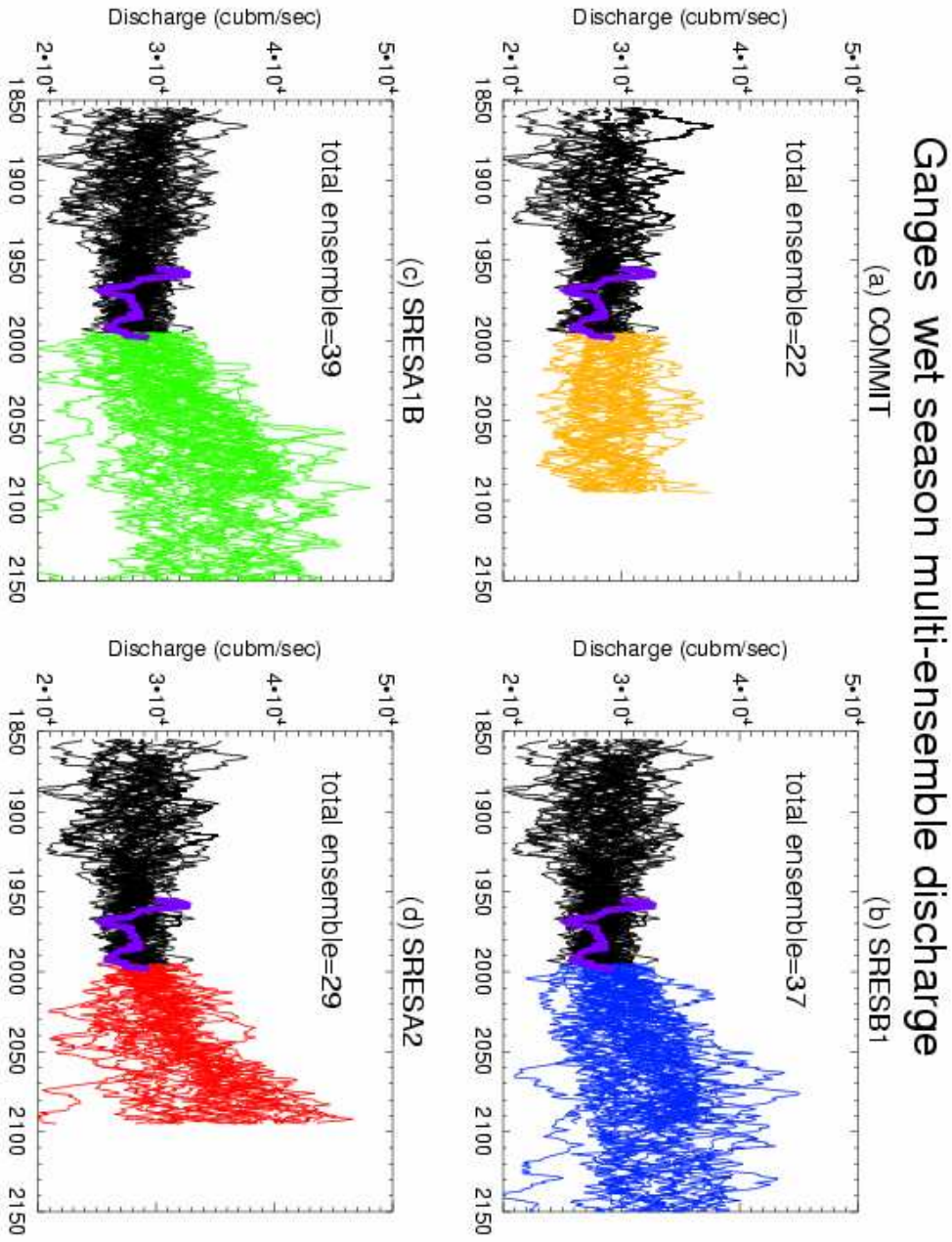

Figure 5.5 Same as Figure5.4 but with the Ganges River. In each panel, there are 34-51 ensemble members from a total of 17 "good" models.

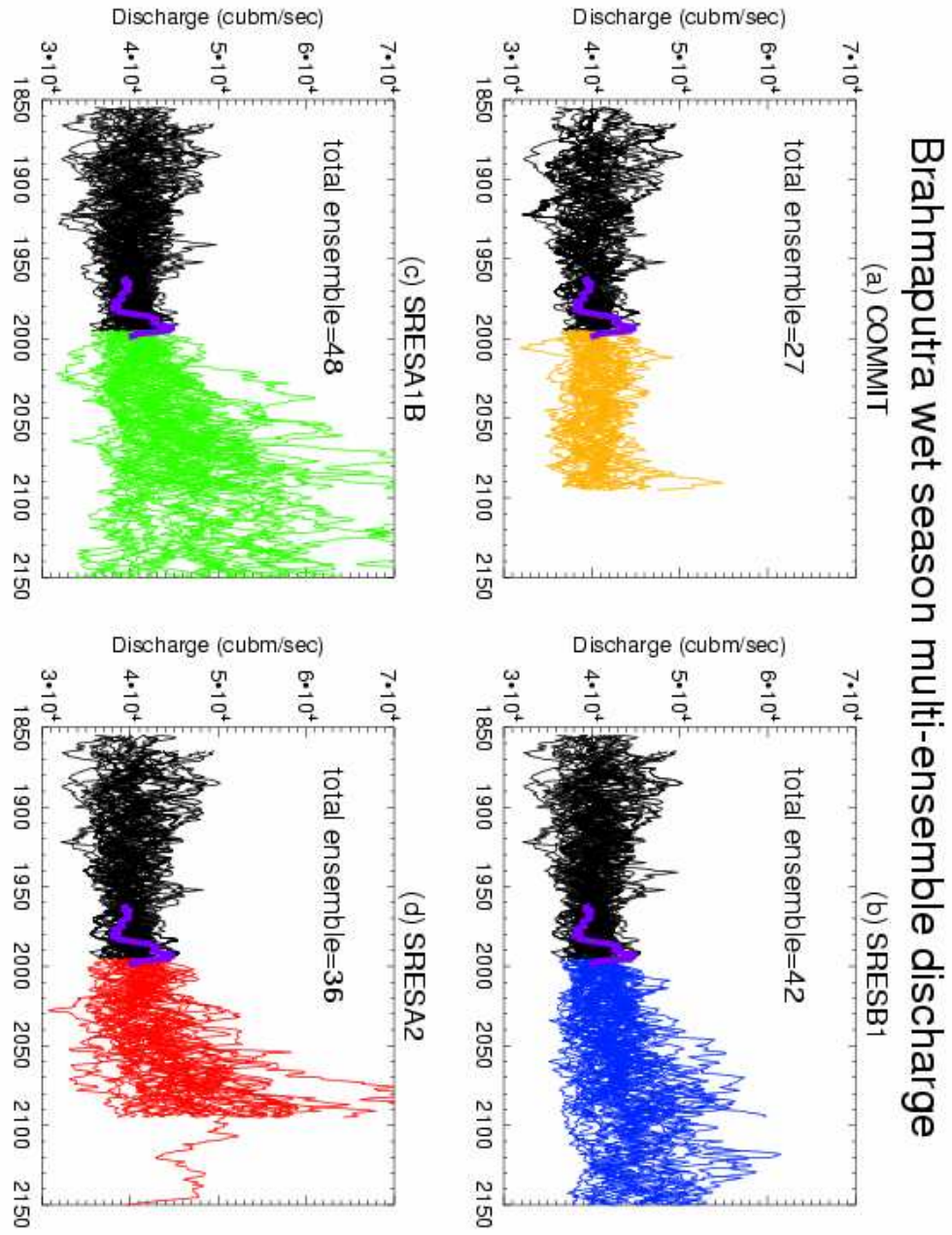

Figure 5.6 Same as Figure5.4 but with the Brahmaputra River. In each panel, there are 27-48 ensemble members from a total of 20 "good" models.

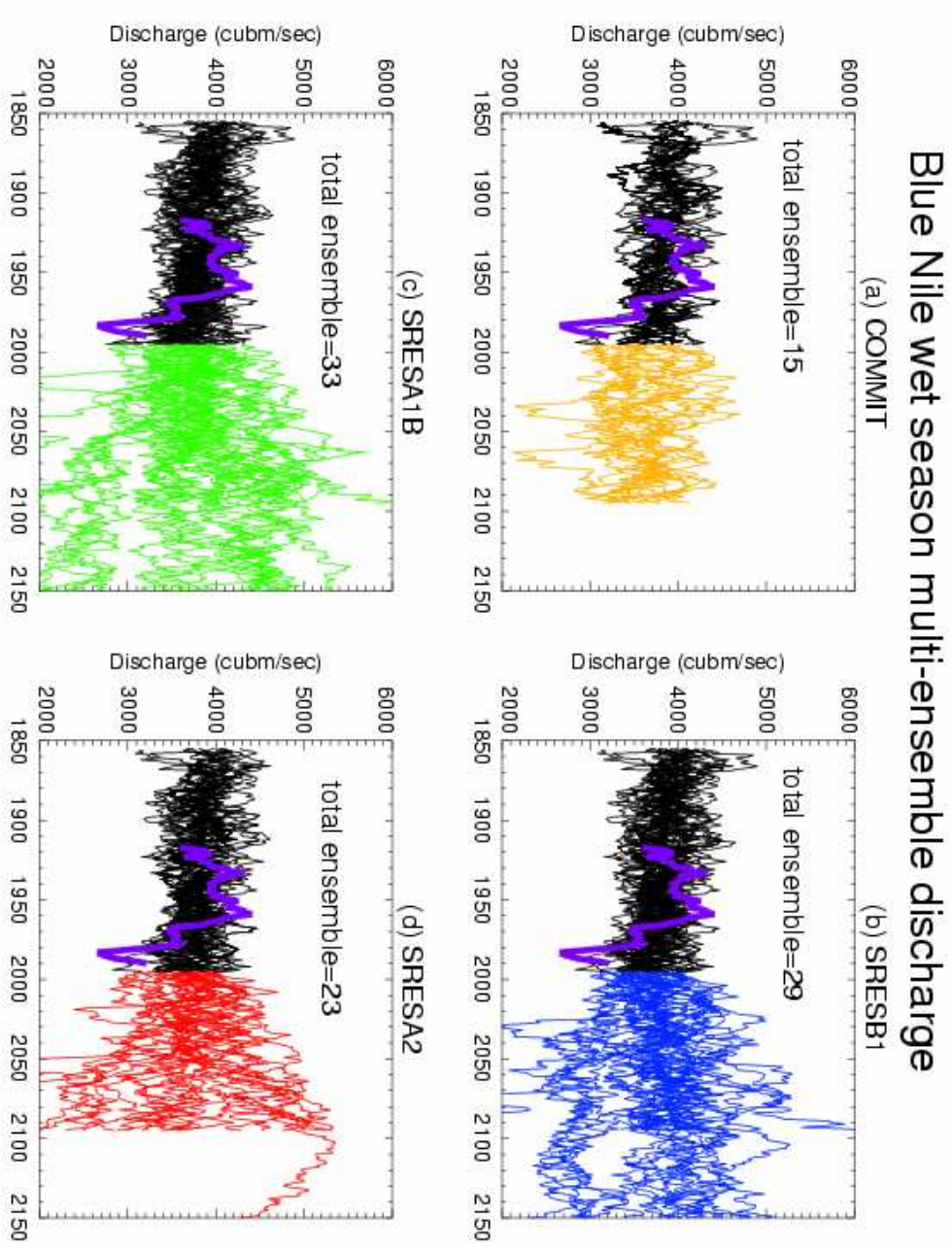

Figure 5.7 Same as Figure5.4 but with the Blue Nile River. In each panel, there are 15-33 ensemble members from a total of 14 "good" models. Other than COMMIT, large uncertainty is observed as the SRES scenarios begin at year 2000.

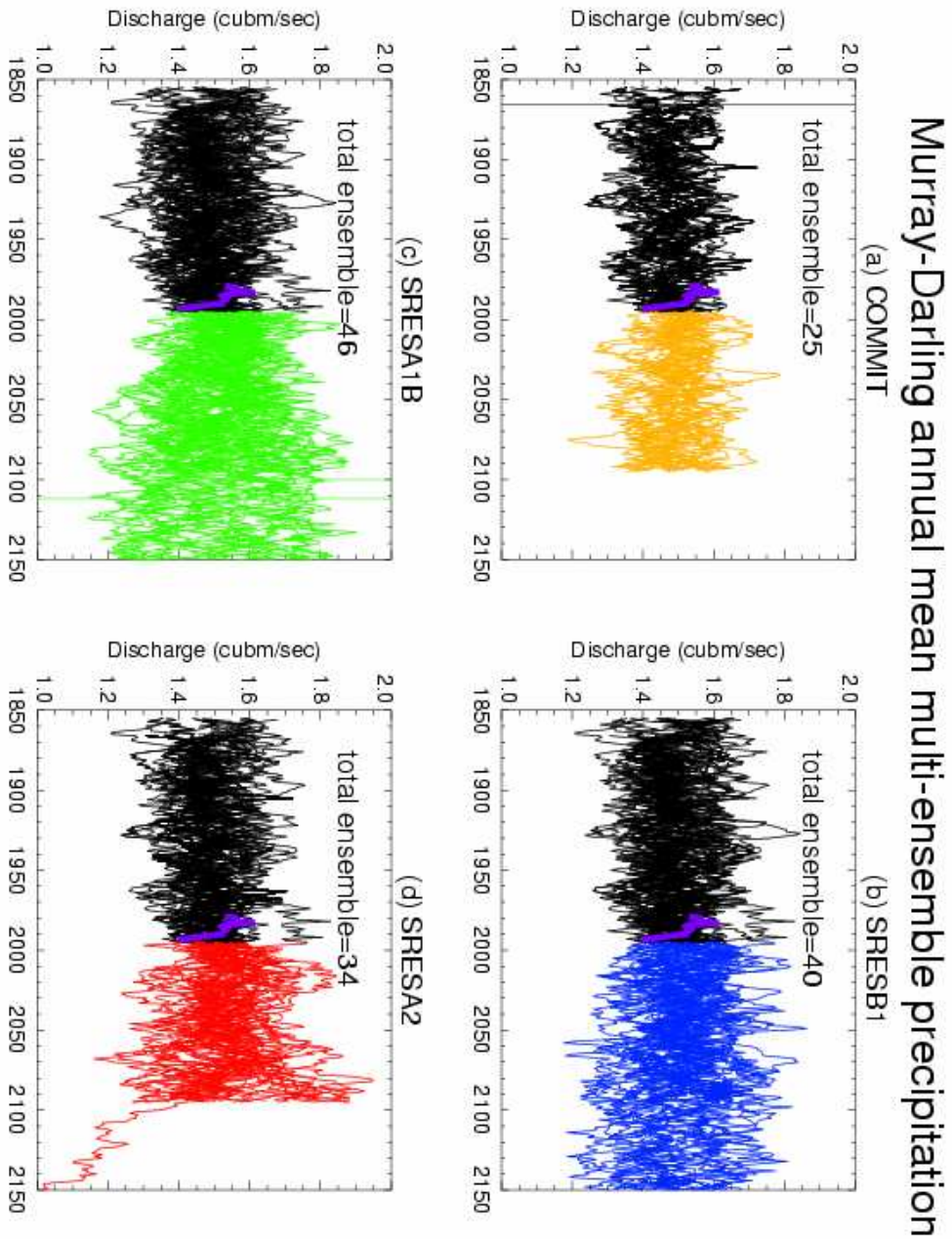

Figure 5.8 Same as Figure5.4 but with the Murray-Darling River Basin averaged GPCP rainfall. In each panel, there are 34-40 ensemble members from a total of 17 "good" models.

Like Blue Nile River, Murray-Darling River modeled precipitations also have large distributions. In Figure 5.8 we do see large oscillations present but no obvious long term

trend observed. We do not know if these oscillations, which increase the model projection uncertainties, are caused by their low-level flow rates which are one order of magnitude than the other three rivers. Overall, the future estimation does not support any significant change.

5.2 Multi-model assessments of the simulated river discharges: uncertainties

As discussed in last chapter, the surface temperature simulated by IPCC-AR4 has better agreement between different models than precipitation. The similar illustration on precipitation is limited because of large inter-model deviation. IPCC AR4 assessment applies percentage trend (Figure 4.4) to illustrate the change of regional rainfalls.

With the Q-Q technique, we are able to make the similar multi-model assessment of future discharge for each river. The 300-year modeled Ganges River discharge is illustrated in Figure 5.9 (a) for the period 1850 to 2150. The mean value of the ensemble means of the "good" models' chosen in Chapter 4 are shown and ensemble mean is plotted with solid lines. At each time step, the upper and lower limit of the shading is calculated from one standard deviation of the individual "good" model output. All scenarios are marked with the same color scheme applied in IPCC-AR4 report.

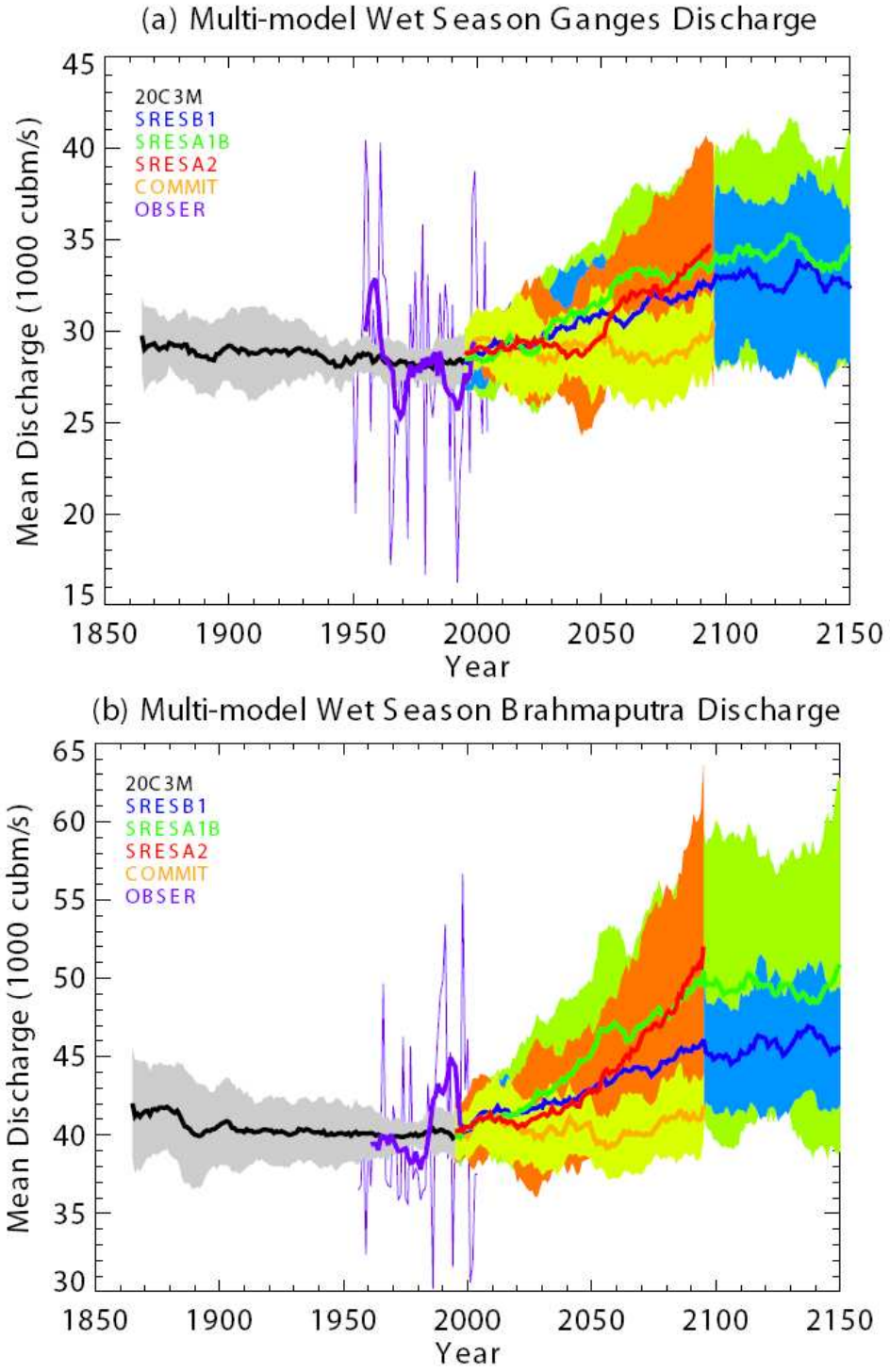

Figure 5.9 Simulated IPCC-AR4 multi-model wet season averaged discharges and accessed ranges of (a) the Ganges, (b) the Brahmaputra River, (c) the Yangtze, (d) the Blue Nile River, and (e) annual mean precipitation over the Murray-Darling River basin. The observation interannual (purple thin solid) and 10-year average (purple thick solid) are also presented. The solid lines denote the mean of the ensemble mean, the shaded areas one standard deviation of the multi-model output for each scenario.

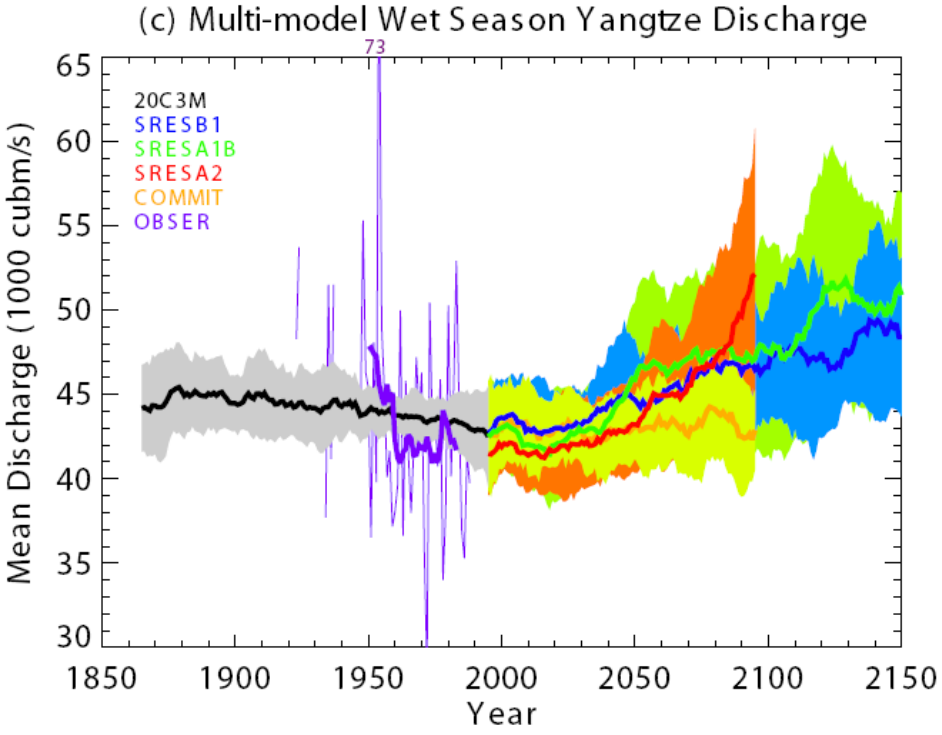

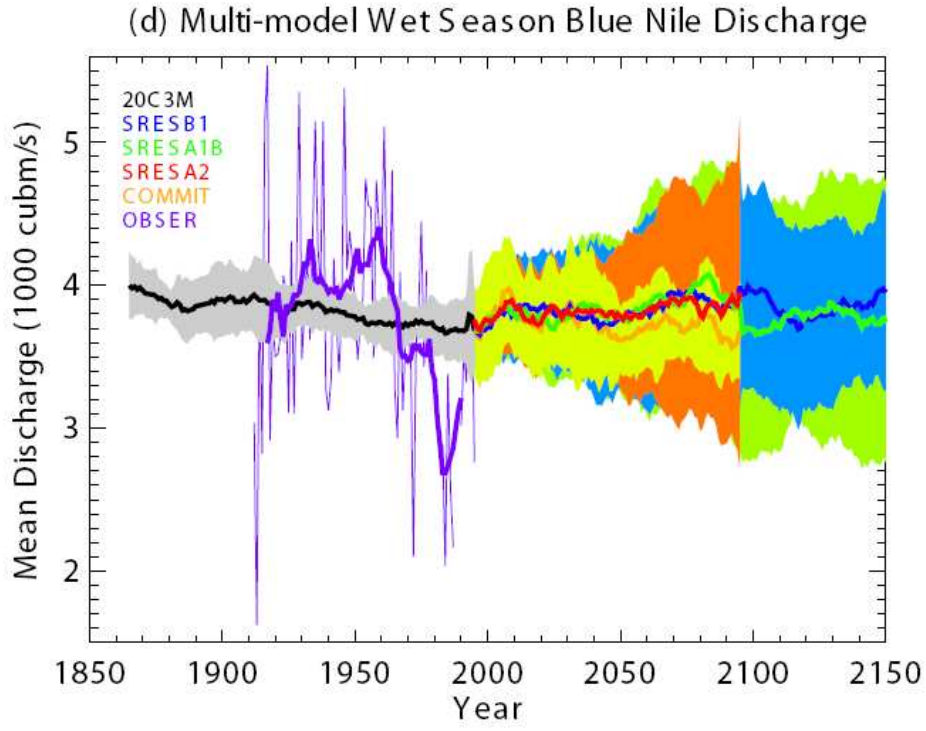

Figure 5.9 (continued)

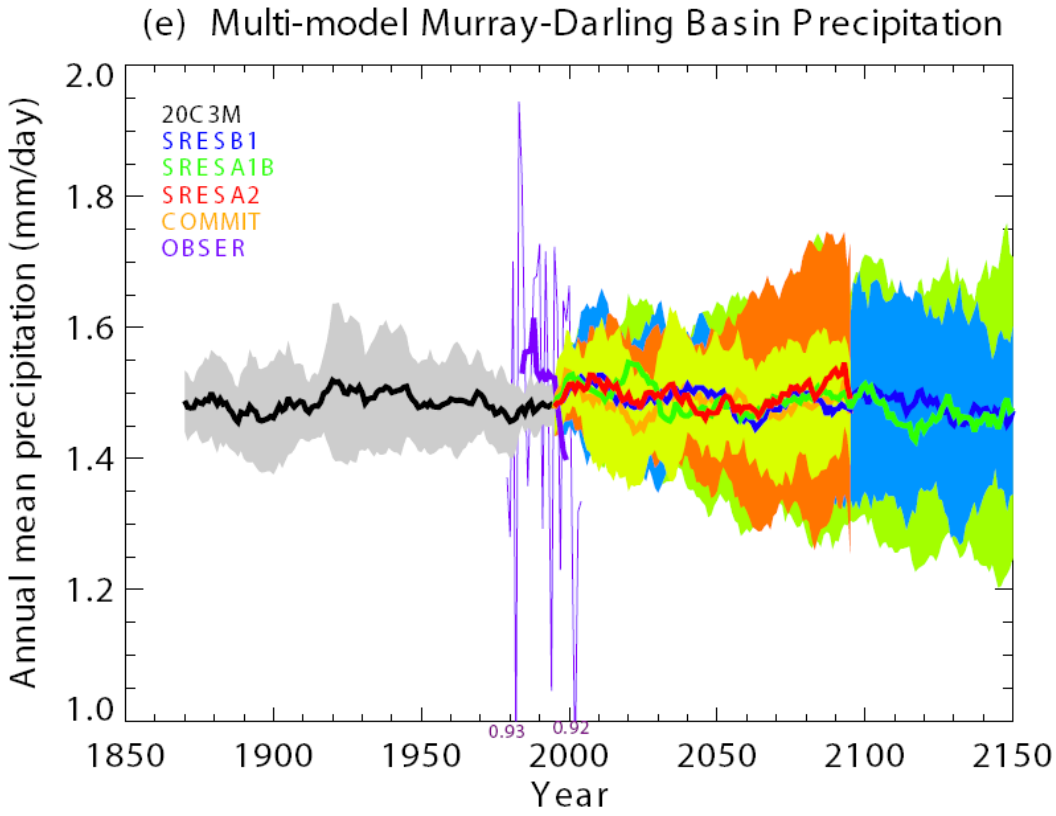

Figure 5.9 (continued)

In the left part, the black line and grey shade denote a slightly downtrend and good model agreement (shallow model span) in 20c3m experiment. The scenario continuations of the 20th century simulation keep close until 2020 and then have different development. The Ganges River discharge under SRESA1B has a larger value than the other scenarios from 2020 to 2080 and then overridden by SRESA2, who would experience a rapid increase in the second half of the 21st century. The COMMIT scenario suggests a steady and good multi-model-agreed Brahmaputra River discharge in the next 100 years.

In temperature trend diagram Figure 4.3, the same models under COMMIT suggest a steady and relative small (<0.5°C) warm-up. That is probably because the GHGs emitted at this level already contain the anthropogenic forcing component over last 50 years.

Those non-natural green house gases would retain in the atmosphere and continue to absorb the outgoing longwave radiation and warm the surface additionally. However, the mean and model span of river discharge under COMMIT scenarios are Besides, all four scenarios have the characteristics close to the global surface warm-up trend in Figure 4.3.

Meehl et al. (2007, IPCC-AR4, WG1 page 762) pointed out that, the numbers of models that are running during particular periods and under particular scenarios differ with each other. Thus, the mean value discontinuity between different periods does not have any physical meaning. Also the shaded area coverage among difference scenarios can not be directly used to present uncertainty. For the same reason, we did not count on the results before 1880 while the available model numbers are limited. However, within a specific period (1900-2000 or 2000-2100) and a specific scenario (20C3M and all SRES based) while the model number keeping constant, we can estimate long time trend and associated uncertainty of projected precipitation.

The Brahmaputra and Yangtze River discharges are plotted in Figure 5.9 b and c. Note that not only the rivers are having closely model simulations but also the decadal variability in observations is close too. The Brahmaputra River, having a lower flow rate than the Yangtze River, is located between Yangtze and Ganges River catchment. Besides that, its variability seems out of phase with the other two rivers. The three rivers simulations share the similar characteristics: large SRESA2 flow rising after 2080, shallow and keep-still COMMIT flows, huge model coverage of SRESA1B, relative shallow and slow increase under SRESB2, etc. The final multi-model discharges around

2100 have the scenario orders of SRESA2> SRESA1B>SRESB1>COMMIT. The relative increase ranking of the three rivers are Brahmaputra>Yangtze>Ganges.

Figure 5.9 d and e show the Blue Nile River wet season discharge and annual mean Murray-Darling River basin precipitation. As we observe from the 10-year averaged ensemble diagram Figure 5.7 and Figure 5.8, large uncertainties are observed for both rivers and exceeding 10% (COMMIT) to 40% (SRESA2) of the mean value. Note that even though the 20C3M models miss the 1980s excessive drought in the Horn of Africa (Mattsson et al. 1991), they estimate that the overall Blue Nile River discharge is downward during the whole 20th century. For all scenarios of the Blue Nile and Murray-Darling rivers, the future discharges do not change relative to the averages over the 20th century.

In each diagram, the multi-decadal variability of the modeled mean value series is less than the variability observed. As we discussed in section 4.6, the multi-model combination would diminish some properties of the time series such as the multi-decadal variability. However, it would not ruin the climate trend inside the diagram and we know that the reproduction of the interannual variability is good.

It should note that the lowest uncertainty of multi-modes, i.e. the shallowest shading ranges over 1970-1990. Considering the plotting after 1995 are affected by 10-year moving average of different SRES experiments, we could conclude that the discharge projection has the more model agreements on the last few decades of the 20th century, just as the temperature projection in Figure 4.3.

5.3 Probability of extreme flow

Most times extreme events such as excessive precipitation get more interest since majority of the heavy economical and social lost are due to the severe weather or climate conditions. Barnett et al. (2005), Benestad (2006), Senior et al (2005), and Zhang et al.(2006) have discussed the possibility of future extreme precipitation events. Palmer (2001) and Räisänen (2001, 2003, 2006, 2007) have applied the probability that during a specific period a single event occurs over two standard deviation of the past. All of them agree that extreme event would occur much and much more frequently.

We apply the same definition on discharge with Palmer and Räisänen's. An extreme event N1, N2, or N3 is defined to occur when its value has exceeded one, two, or three standard deviation of the observational series. The probability of the total population of N1, N2, and N3 relative to the total numbers is calculated per SRES scenario each 50 years period and listed in Table 5.2.

Table 5.2 Flood risk is calculated as the probability (in percentage) of excessive river discharge events under different IPCC-AR4 scenarios for (a) the Ganges, (b) the Brahmaputra, (c) the Yangtze, (d) the Blue Nile River wet season discharges, and (e) annual precipitation over the Murray-Darling River basin. Extreme events are defined as an event exceeding the observational mean plus one, two, and three standard deviations. The SRES scenarios during the 21st century are divided into two periods (2000-2049, 2050-2099) to study the long time trend.

(a) Ganges River discharge		P(occurrence > mean + 1 STD)	P(occurrence > mean + 2 STD)	P(occurrence > mean + 3 STD)
Observations		12.7	3.64	0
20C3M (in observation period)		13.35	3.89	0
Whole 20C3M period		13.44	2.82	0.08
COMMIT	2000-2049	18.33	5.21	0.58
	2050-2099	18.66	5.21	0.33
SRESB1	2000-2049	21.07	7.04	1.21
	2050-2099	30.97	12.57	2.44
SRESA1B	2000-2049	20.00	7.47	0.68
	2050-2099	36.97	17.80	3.25
SRESA2	2000-2049	18.62	6.78	0.40
	2050-2099	39.45	20.01	5.07

(b) Brahmaputra River discharge		P(occurrence > mean + 1 STD)	P(occurrence > mean + 2 STD)	P(occurrence > mean + 3 STD)
Observations		16.33	4.08	0
20C3M (in observation period)		16.72	4.47	0
Whole 20C3M period		15.74	4.01	0.74
COMMIT	2000-2049	20.98	7.32	2.55
	2050-2099	20.65	7.19	2.29
SRESB1	2000-2049	26.25	10.17	2.72
	2050-2099	35.05	18.12	7.51
SRESA1B	2000-2049	29.37	14.45	4.84
	2050-2099	48.63	28.59	14.21
SRESA2	2000-2049	24.82	11.65	3.57
	2050-2099	47.17	28.08	14.36

Table 5.2 (continued)

(c) Yangtze River discharge		P(occurrence > mean + 1 STD)	P(occurrence > mean + 2 STD)	P(occurrence > mean + 3 STD)
Observations		12.5	2.08	2.08
20C3M (in observation period)		14.05	2.18	1.74
Whole 20C3M period		13.09	2.63	2.00
COMMIT	2000-2049	11.10	2.10	1.44
	2050-2099	14.96	2.44	1.97
SRESB1	2000-2049	14.37	3.75	3.05
	2050-2099	22.14	7.39	5.32
SRESA1B	2000-2049	12.46	3.43	2.10
	2050-2099	25.64	10.21	8.02
SRESA2	2000-2049	10.99	1.47	0.72
	2050-2099	25.19	10.92	8.54

(d) Blue Nile River discharge		P(occurrence > mean + 1 STD)	P(occurrence > mean + 2 STD)	P(occurrence > mean + 3 STD)
Observations		12.82	3.85	0
20C3M (in observation period)		14.15	3.24	0
Whole 20C3M period		14.93	2.32	0.098
COMMIT	2000-2049	14.38	3.65	1.00
	2050-2099	12.3	1.67	0.20
SRESB1	2000-2049	15.40	2.82	0.60
	2050-2099	21.28	6.82	1.51
SRESA1B	2000-2049	16.30	3.63	0.43
	2050-2099	25.52	8.47	1.41
SRESA2	2000-2049	14.68	2.98	0.22
	2050-2099	22.76	8.36	1.21

Table 5.2 (continued)

(e) Murray-Darling Basin Precipitation		P(occurrence > mean + 1 STD)	P(occurrence > mean + 2 STD)	P(occurrence > mean + 3 STD)
Observations		13.76	2.75	0.92
20C3M (in observation period)		10.51	4.91	2.49
Whole 20C3M period		10.34	4.84	2.56
COMMIT	2000-2049	9.85	4.36	2.74
	2050-2099	10.49	4.04	1.61
SRESB1	2000-2049	10.52	5.46	2.77
	2050-2099	11.75	5.71	2.54
SRESA1B	2000-2049	10.55	5.89	3.44
	2050-2099	11.38	6.06	2.89
SRESA2	2000-2049	9.39	4.95	2.83
	2050-2099	11.02	7.25	4.65

We observe that, even though the other GHGs other than CO2 take a large contribution on greenhouse effect, the occurrence of the Gangs, Brahmaputra, and Yangtze River extreme discharges seems highly correlated with the CO2 concentration that increases monotonically with time or possesses different values with SRES scenarios.

The SRESA2 Brahmaputra River discharge, with the multi-model mean value increasing about 20%, has much more extreme events in the 21st century. The frequency of N1 event occurrence increases from one per eight year (p=0.16) to one per two years (p=0.47). The N3 event, which is equivalent to one per 100 years or less, has increased to one per seven years (p=0.14). The other scenarios also have some increases, more or less. Note that the frequency under COMMIT scenario keeps steady throughout the time, indicating that the models are stable under a fixed GHGs concentration assumption.

As expected, extreme event occurrence is highly related with the trend of mean value and variability. The Yangtze River discharge has much less probability on flooding than

Brahmaputra. In SRESA1B and SRESA2 scenarios, the second half of the 21st century, the Yangtze River has the frequency of N3 events at one per 12 years (p=0.085, 0.080) relative to one per 50 years in observations (p=0.02). It is verified in Figure 5.9 c where we observed a rapit increase over the last few decades.

The Ganges River would have most extreme events occurred at a probability between the Yangtze River case and Brahmaputra River case. For example, the same events N1, which have occurred one per 8 years in the 20th century, are projected to occur one per 3 years for Ganges, one per 2 years for Brahmaputra, and one per 4 years for Yangtze River in the second half of the 21st century.

The Blue Nile and Murray-Darling River discharges are not going to have much extreme flooding events as in the above three rivers. The increased N1, N2, N3 events are high likely due to the inter-model deviations in those regions so that they should not be taken as risk of flooding.

5.4 Non-parametric Mann-Kendall trend analysis

Initiated by Mann (1945) and Kendall (1938) and described by Hirch et al. (1982) and Kendall et al. (1990), the Mann-Kendall seasonal trend analysis is often used to determine whether there are increasing or decreasing trends of a hydrological constituent over a particular period. As a non-parametric seasonal test, it is based on a ranking procedure. Thus, it does not need to presume a distribution type of the objective variable. Recently it is used to analyze and compare the SST trend in different reanalysis dataset (Agudelo and Curry 2004, Hoyos et al. 2006). As discussed in last chapter, in most GCMs, precipitation or discharge often possesses a larger variability and contains more

outliers than surface temperature. Without any presumed parameter, Mann-Kendall trend test is more reliable to solve the questions that whether a trend is significant and estimate the trend slope. We apply the seasonal Mann-Kendall analysis here because these variables are seasonal.

According to Mann, the null hypothesis H_0 states that a dataset of {xi} are retrieved from a set of independent and identically distributed random variables. The alternative hypothesis H_1 states that the distribution of $\{x_k\}$ and $\{x_j\}$ are not identical for all k,j <n with $k \neq j$. Hirsch et al. (1982) developed a trend test statistics S defined as

$$S = \sum_{k=1}^{n-1} \sum_{j=k+1}^{n} \mathrm{sgn}(x_j - x_k) \tag{1}$$

$$\text{where} \quad \mathrm{sgn}(x) = \begin{cases} 1 & x > 0 \\ 0 & \text{if } x = 0 \\ -1 & x < 0 \end{cases} \tag{2}$$

As to the definition, the mean and variance of S under H_0 are given by

$$E[S] = 0$$
$$Var[S] = \frac{n(n-1)(2n+5) - \sum_t t(t-1)(2t+5)}{18} \tag{3}$$

where t is the extent of any given tie (a pair of identical values) and $\sum_t$ denotes the summation over all ties.

Given that both Mann (1945) and Kendall (1938) noted that the normality approximation for S is excellent even for small n, the standard normal variate Z used for hypothesis H_0 and H_1 is

$$Z = \begin{cases} \dfrac{S-1}{\sqrt{Var[S]}} & S > 0 \\ 0 & \text{if} \quad S = 0 \\ \dfrac{S-1}{\sqrt{Var[S]}} & S < 0 \end{cases} \qquad (4)$$

In a two-sided test for trend analysis, H_0 is rejected at significance level α if $|Z| > z_{1-\alpha/2}$, where $z_{1-\alpha/2}$ is the Z value from standard normal distribution (mean=0; variance=1) with probability of α/2. A positive value of Z indicates an upward trend and a Z negative indicates a downward trend.

Hirsch et al. (1982) also introduced a seasonal Kendall test, which account for the existence of seasonality. As our discharge data (observational or modeled) are retrieved for the wet season and the hypothesis H_0 assumes that monthly flow independent and random variables, the seasonal Kendall test would retreat to the original Kendall test.

The calculated Z values for all scenarios and all rivers are listed in Table 5.3. The values exceeding 95% and 99% significance level are marked separately in bold and with "*". The Kendall test suggests that the Yangtze, Ganges, and Brahmaputra River discharges are going to have a deterministic increase if the GHGs concentration increases dramatically. The Blue Nile and Murray-Darling River's modeled data are not sufficient to draw a conclusion. The fixed-GHG-level scenario does not support any increasing or decreasing trend.

The Z values from the observation and the 20th century run sharing the common period are listed in the first two rows. In general, Z values from multi-model mean are less strong than from observation. However, the models successfully reproduce the sign of the Z values.

Table 5.3 Z value of Mann-Kendall trend test of the IPCC-AR4 CMIP3 modeled river discharge. Larger absolute Z values indicate the likelihood of the time series increasing (positive value) or decreasing (negative). The symbol "*" indicates that the values are above the 95% significance level to reject the hypothesis H_0 that the data are randomly distributed. The dual symbol "**" marks the 99% significance level.

	Blue Nile	Ganges	Brahmaputra	Yangtze	Murray-Darling
Observation	-2.403**	-0.580	1.077	-2.060*	-0.317
20C3M	-0.707	-0.268	0.162	-0.026	-0.129
COMMIT	-0.398	-0.253	0.348	0.059	-0.324
SRESB1	-0.055	1.748*	2.109*	1.949*	-0.332
SRESA1B	0.688	3.564**	3.106**	3.529**	-0.635
SRESA2	0.845	2.848**	3.029**	2.604**	-0.403

Given the strong certainty that the Yangtze, Ganges, and Brahmaputra River discharges are going to increase next century, we want to quantify their discharge ascending rate, i.e., change per unit time. The seasonal Kendall slope estimator K is provided by Hirsch et al. (1982). The computing process is simple. While the seasonal Kendall trend test is being performed, record the slopes for each (x_{ij}, x_{ik}) pair where slope is defined as $E_{ijk} = \frac{(x_{ij} - x_{ik})}{j-k}$, with $1 \le k < j \le n_i$, where x_{ab} is the variable for month a and year b. Then K is defined as the median number (interpolate if needed) of these E(i, j, k) values, which makes it non-parametric and robust against the effect of outliers.

Table 5.4 lists the Kendall slopes for the Yangtze, Ganges, and Brahmaputra rivers, which are statistically significant to have their discharges increased under the increasing-GHGs-concentration scenarios. The scenario with the highest slope is SRESA2, which predict decadal discharge increments of 332, 350, and 571 $m^3 s^{-1}$ for respective rivers in the 21st century. These results are in good agreement with Figure 5.2 (a-c). Of course, this increased water not only introduces more flooding, but also would provide more water supplies toward those river basins whereas the populations are increasing too. With this water, we can accommodate more people in the corresponding area under the assumption that flooding would be well controlled and the external water can be collected and applied well.

Table 5.4 Mann-Kendall slope estimator K on modeled river discharge, the symbol "*" indicates the values are significantly different from zero at the 95% confidence level. The unit is cubic meters per second per decade.

	Yangtze	Ganges	Brahmaputra
COMMIT	-22.23	-3.32	6.10
SRESB1	142.68	102.80	144.35
SRESA1B	390.03	204.62	323.54
SRESA2	539.25	707.01	717.17

5.5 Discussions: seasonal cycle effect, uncertainties, and reversed SST-monsoon rainfall relationship

The three Asian monsoon-affected rivers, the Yangtze, the Brahmaputra, and the Ganges River are expected to have wet season mean discharge increased up to 12.3%, 17.9%, 25% in SRESA2 scenario. During the same time, the occurrence of extreme flooding events is nearly doubled.

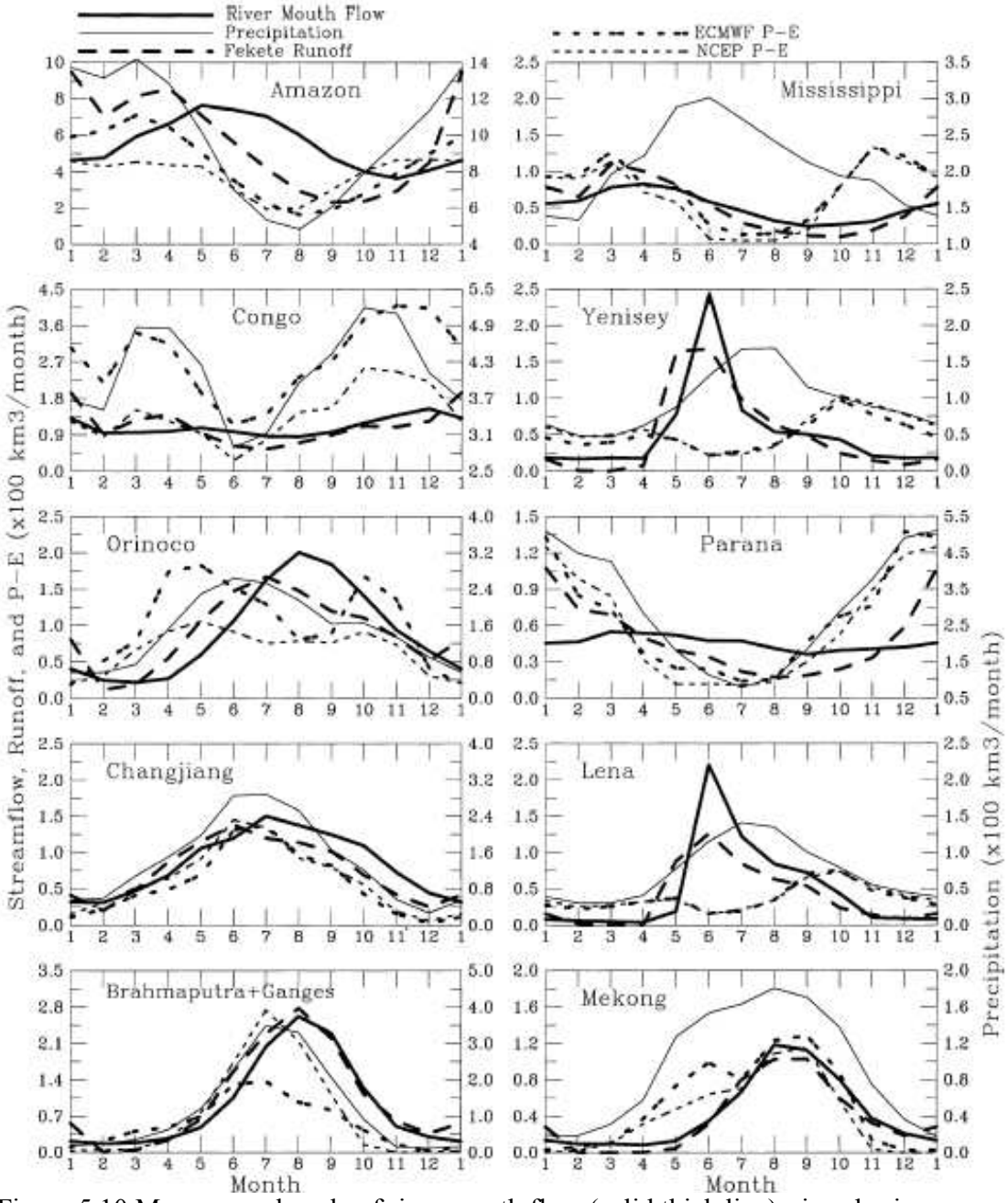

Figure 5.10 Mean annual cycle of river mouth flow (solid thick line), river-basin-integrated precipitation (thin solid line, read on the right ordinate), runoff, and reanalysis *P–E* for world largest 10 rivers (from Dai and Trenberth, 2002).

It is important to note that not all the rivers can use this "good" model selection strategy and related discharge reconstruction. Only those seasonal cycled rivers are suitable for estimation. The Figure 5.10 (from Dai et al. 2001) compared the rainfall, runoff model, reanalysis precipitation, and observational station data at the mouth of the flow for the 10 largest rivers in the world. The rivers with large lags between peaks of discharge and precipitation (such as Amazon River) or the rivers with a missing seasonal cycle (such as Congo River) are not suitable for the current Q-Q technique and, thus, we do not have a best river selection strategy. It is comforting to see that the Yangtze River and Ganges-Brahmaputra River's monthly mean discharge profiles are well fitted with their monthly catchment accumulated precipitation with less than one-month lag. These rivers are all located at Asian monsoon areas and probably the increases in discharges are the result of future enhancement of the Asian monsoon.

In CMIP3 project, most models share the same prescribed GHGs and aerosols concentration. However, several biogeochemistry processes, including carbon cycle and sulfate cycle feedbacks, are not considered by those climate models. Those processes, as well as the inter-model and regional deviations, contribute to the model uncertainties. The detailed discussion of the biogeochemistry processes can be found in Meehl et al. (2007, IPCC-AR4 WG1, page 753-754, 789-796)

In Chapter 3, the Yangtze, Blue Nile, and Ganges River wet season discharges are observed negatively correlated with equatorial SST variation. This is in agreement with the statistical non-stationary negative relationship between Asian monsoon and NINO SST (e.g. Webster et al. 1998, Stephenson et al. 1999, and Clark et al. 2000). In addition, the multi-model mean discharge has a downward trend in the 20th century. This not only

agrees with the observations but also corresponds to the SST rising in the model simulation. However, in the GHGs increasing SRES scenarios, while the equatorial SST increases gradually over all the 21st century, the Yangtze, Ganges, and Brahmaputra River discharge increase at a much fast speed during the second half of the 21st century. This is opposite to the monsson-NINO3 SST correlation found earlier in both the climate model and observation. It should note that starting from mid-21st century, many GHGs and aerosol concentrations would already exceed their peak values and begin to fall down except for CO2 and N2O (Figure 4.2). What is the coupled mechanism that increases the summer Asian monsoon precipitation and overrides the equatorial SST effect that should weaken the South and East Asia monsoon?

From Figure 5.9, Table 5.1, and Table 5.2, we find that, during the early 21st century, all rivers under all scenarios have a close mean and variation value as in the 20th century even though the GHGs and aerosols concentrations are already at high levels and keep increasing. This suggests we should control the greenhouse emission, especially the CO2. As it may take several decades long for the high-level GHGs concentration to take effect and introduce considerable climate changes, the restriction on CO2 emission should be considered at a high priority.

CHAPTER 6

CONCLUSIONS

Seasonal discharge variability and their relationship with SST are examined for the Ganges, Brahmaputra, Yangtze, Blue Nile, and Murray-Darling rivers to investigate the discharge predictability from SST variations. In addition, the intraseasonal variability among the first two river discharges and monsoon precipitation is also analyzed. The next 100-year discharges of these rivers are estimated from the IPCC-AR4 CMIP3 modeled precipitation via the connection built between modeled precipitation and observed discharge during the 20^{th} century.

The characteristics of the discharge of the Ganges and Brahmaputra rivers where they enter Bangladesh from India have been examined. Intraseasonal monsoon precipitation variability possesses a strong signal in discharge with both basins being approximately in phases.

The association of discharge with intraseasonal variability with basin discharge suggests that there are predictable elements on these time scales. In fact, following the band-passed rainfall over the two basins provides a rudimentary forecast of about two pentads. Correlation and composite analysis show that there is a significant negative linear relationship between equatorial Pacific SST and the Ganges River discharge from zero to three-month lead consistent with the influence of ENSO on Indian precipitation. In addition, SSTs in the southwest Pacific Ocean SST shows a high positive correlation with Ganges discharge > 0.6 that exists with lags for two seasons. These associations

would suggest future predictability of the Ganges discharge with at least a two-month lead time.

No significant Brahmaputra JAS discharge relationship was found with tropical SSTs in either the Pacific or the Indian oceans. The strong relationship found by earlier studies appears to come from the inclusion of year 1998 in the data analysis when excessive discharge occurred simultaneously with very warm Indian Ocean SSTs. With the exclusion of this one year, the strong lagged associations disappear and are replaced by minor and insignificant simultaneous correlations in the tropical Indian Ocean. It may well be that the extremely warm tropical Indian Ocean during 1998 somehow changed the circulation features of the monsoon to produce the above average precipitation in the river basins. Irrespective, there is no evidence that this association, if it exists, is indicative of long-term associations between the tropical Indian Ocean and Brahmaputra discharge.

In a manner similar to Ganges and Brahmaputra River, the wet season discharge variabilities of the Yangtze and Blue Nile rivers at the mouth are examined. A smaller correlation is found with equatorial SST compared to the Ganges. Their wet season discharges are negatively related with eastern equatorial Pacific Ocean and Indian Ocean SSTs. However, no significant leading SST-discharge relationship is found. The modeled Murray-Darling River discharge is strongly related to the equatorial Pacific Ocean SST variation.

The coupled AOGCM models under IPCC-AR4 CMIP3 project provide less inter-model deviation for temperature projection than for precipitations over all five river basins considered in this study. The Q-Q technique converts modeled precipitation to

river discharge with reduced inter-model biases and successfully reproduces the observational discharge in the 20th century. Furthermore, with the same link built between modeled precipitation and observed discharge, the future 21st century river discharge of Yangtze, Ganges, Brahmaputra, and Blue Nile are simulated under different SRES scenarios. During this procedure, only contributions from those models capable of reproducing the observational annual cycle are counted.

Three Asian monsoon-affected rivers, the Yangtze, Ganges, and Brahmaputra rivers are response-sensitive to an increase of GHG and aerosol concentrations. In addition, the change in discharge is very similar to the trend in CO2 concentration. A 15-25% discharge increment at the end of the 21st century is found for the high GHGs concentration scenarios (SRESA1B and SRESA2). Under the same scenarios, the risk of flooding, expressed as probability of extreme events, increases up to 5-12 times. The occurrence of the flooding at other level also increases dramatically. Blue Nile River's multi-model mean discharge does not suggest any sign of change with large inter-model deviations.

Differed from other rivers, the Murray-Darling River, with a rather small flow rate, does not possess a good fitting between discharge annual cycle and precipitation cycle. Thus, the annual mean precipitation is reconstructed instead of wet season discharge. The result is not sensitive to different SRES scenarios.

Among all SRES scenarios, the fixed-GHGs and -aerosols concentration scenario (COMMIT), as an idealized "control" experiment, projects the most similar next-100 year discharge/precipitation with the 20th century observations. In addition, this scenario has the best model agreement for all the rivers and all SRES scenarios.

Future research work includes seeking the basis for the statistical SST pattern between the southwest Pacific SST and summer Ganges discharge, and between the spring SST to the east coast of Japan and June Brahmaputra discharge. The latter is possibly due to the SST forcing on the winter storm activities in East Asia and the increase in snow pack as suggested by Shaman et al (2005).

Estimations of other major river future discharges, including those rivers with major lag between rainfall peak and discharge or without a seasonal discharge cycle, are expected. The issue is whether the increase of river discharge will keep up the increase of population, (i.e. the future water supply per capita), would be analyzed.

APPENDIX A: FEATURES OF MODELS

Table A.1 Model characteristics of the IPCC-AR4 CMIP3 project (from Redall et al, 2007, IPCC-AR4, WG1 page 597-599).

Table 8.1. *Selected model features. Salient features of the AOGCMs participating in the MMD at PCMDI are listed by IPCC identification (ID) along with the calendar year ('vintage') of the first publication of results from each model. Also listed are the respective sponsoring institutions, the pressure at the top of the atmospheric model, the horizontal and vertical resolution of the model atmosphere and ocean models, as well as the oceanic vertical coordinate type (Z: see Griffies (2004) for definitions) and upper boundary condition (BC: free surface or rigid lid). Also listed are the characteristics of sea ice dynamics/structure (e.g., rheology vs 'free drift' assumption and inclusion of ice leads), and whether adjustments of surface momentum, heat or freshwater fluxes are applied in coupling the atmosphere, ocean and sea ice components. Land features such as the representation of soil moisture (single-layer 'bucket' vs multi-layered scheme) and the presence of a vegetation canopy or a river routing scheme also are noted. Relevant references describing details of these aspects of the models are cited.*

Model ID, Vintage	Sponsor(s), Country	Atmosphere Top Resolution[a] References	Ocean Resolution[b] Z Coord., Top BC References	Sea Ice Dynamics, Leads References	Coupling Flux Adjustments References	Land Soil, Plants, Routing References
1: BCC-CM1, 2005	Beijing Climate Center, China	top = 25 hPa T63 (1.9° x 1.9°) L16 Dong et al., 2000; CSMD, 2005; Xu et al., 2005	1.9° x 1.9° L30 depth, free surface Jin et al., 1999	no rheology or leads Xu et al., 2005	heat, momentum Yu and Zhang, 2000; CSMD, 2005	layers, canopy, routing CSMD, 2005
2: BCCR-BCM2.0, 2005	Bjerknes Centre for Climate Research, Norway	top = 10 hPa T63 (1.9° x 1.9°) L31 Déqué et al., 1994	0.5°–1.5° x 1.5° L35 density, free surface Bleck et al., 1992	rheology, leads Hibler, 1979; Harder, 1996	no adjustments Furevik et al., 2003	Layers, canopy, routing Mahfouf et al., 1995; Douville et al., 1995; Oki and Sud, 1998
3: CCSM3, 2005	National Center for Atmospheric Research, USA	top = 2.2 hPa T85 (1.4° x 1.4°) L26 Collins et al., 2004	0.3°–1° x 1° L40 depth, free surface Smith and Gent, 2002	rheology, leads Briegleb et al., 2004	no adjustments Collins et al., 2006	layers, canopy, routing Oleson et al., 2004; Branstetter, 2001
4: CGCM3.1(T47), 2005	Canadian Centre for Climate Modelling and Analysis, Canada	top = 1 hPa T47 (~2.8° x 2.8°) L31 McFarlane et al., 1992; Flato, 2005	1.9° x 1.9° L29 depth, rigid lid Pacanowski et al., 1993	rheology, leads Hibler, 1979; Flato and Hibler, 1992	heat, freshwater Flato, 2005	layers, canopy, routing Verseghy et al., 1993
5: CGCM3.1(T63), 2005		top = 1 hPa T63 (~1.9° x 1.9°) L31 McFarlane et al., 1992; Flato 2005	0.9° x 1.4° L29 depth, rigid lid Flato and Boer, 2001; Kim et al., 2002	rheology, leads Hibler, 1979; Flato and Hibler, 1992	heat, freshwater Flato, 2005	layers, canopy, routing Verseghy et al., 1993
6: CNRM-CM3, 2004	Météo-France/Centre National de Recherches Météorologiques, France	top = 0.05 hPa T63 (~1.9° x 1.9°) L45 Déqué et al., 1994	0.5°–2° x 2° L31 depth, rigid lid Madec et al., 1998	rheology, leads Hunke-Dukowicz, 1997; Salas-Mélia, 2002	no adjustments Terray et al., 1998	layers, canopy,routing Mahfouf et al., 1995; Douville et al., 1995; Oki and Sud, 1998
7: CSIRO-MK3.0, 2001	Commonwealth Scientific and Industrial Research Organisation (CSIRO) Atmospheric Research, Australia	top = 4.5 hPa T63 (~1.9° x 1.9°) L18 Gordon et al., 2002	0.8° x 1.9° L31 depth, rigid lid Gordon et al., 2002	rheology, leads O'Farrell, 1998	no adjustments Gordon et al., 2002	layers, canopy Gordon et al., 2002
8: ECHAM5/MPI-OM, 2005	Max Planck Institute for Meteorology, Germany	top = 10 hPa T63 (~1.9° x 1.9°) L31 Roeckner et al., 2003	1.5° x 1.5° L40 depth, free surface Marsland et al., 2003	rheology, leads Hibler, 1979; Semtner, 1976	no adjustments Jungclaus et al., 2005	bucket, canopy, routing Hagemann, 2002; Hagemann and Dümenil-Gates, 2001
9: ECHO-G, 1999	Meteorological Institute of the University of Bonn, Meteorological Research Institute of the Korea Meteorological Administration (KMA), and Model and Data Group, Germany/Korea	top = 10 hPa T30 (~3.9° x 3.9°) L19 Roeckner et al., 1996	0.5°–2.8° x 2.8° L20 depth, free surface Wolff et al., 1997	rheology, leads Wolff et al., 1997	heat, freshwater Min et al., 2005	bucket, canopy, routing Roeckner et al., 1996; Dümenil and Todini, 1992

Table 8.1 (continued)

Model ID, Vintage	Sponsor(s), Country	Atmosphere Top Resolution[a] References	Ocean Resolution[b] Z Coord., Top BC References	Sea Ice Dynamics, Leads References	Coupling Flux Adjustments References	Land Soil, Plants, Routing References
10: FGOALS-g1.0, 2004	National Key Laboratory of Numerical Modeling for Atmospheric Sciences and Geophysical Fluid Dynamics (LASG)/Institute of Atmospheric Physics, China	top = 2.2 hPa T42 (~2.8° x 2.8°) L26 Wang et al., 2004	1.0° x 1.0° L16 eta, free surface Jin et al., 1999; Liu et al., 2004	rheology, leads Briegleb et al., 2004	no adjustments Yu et al., 2002, 2004	layers, canopy, routing Bonan et al., 2002
11: GFDL-CM2.0, 2005	U.S. Department of Commerce/ National Oceanic and Atmospheric Administration (NOAA)/Geophysical Fluid Dynamics Laboratory (GFDL), USA	top = 3 hPa 2.0° x 2.5° L24 GFDL GAMDT, 2004	0.3°–1.0° x 1.0° depth, free surface Gnanadesikan et al., 2004	rheology, leads Winton, 2000; Delworth et al., 2006	no adjustments Delworth et al., 2006	bucket, canopy, routing Milly and Shmakin, 2002; GFDL GAMDT, 2004
12: GFDL-CM2.1, 2005		top = 3 hPa 2.0° x 2.5° L24 GFDL GAMDT, 2004 with semi-Lagrangian transports	0.3°–1.0° x 1.0° depth, free surface Gnanadesikan et al., 2004	rheology, leads Winton, 2000; Delworth et al., 2006	no adjustments Delworth et al., 2006	bucket, canopy, routing Milly and Shmakin, 2002; GFDL GAMDT, 2004
13: GISS-AOM, 2004	National Aeronautics and Space Administration (NASA)/ Goddard Institute for Space Studies (GISS), USA	top = 10 hPa 3° x 4° L12 Russell et al., 1995; Russell, 2005	3° x 4° L16 mass/area, free surface Russell et al., 1995; Russell, 2005	rheology, leads Flato and Hibler, 1992; Russell, 2005	no adjustments Russell, 2005	layers, canopy, routing Abramopoulos et al., 1988; Miller et al., 1994
14: GISS-EH, 2004		top = 0.1 hPa 4° x 5° L20 Schmidt et al., 2006	2° x 2° L16 density, free surface Bleck, 2002	rheology, leads Liu et al., 2003; Schmidt et al., 2004	no adjustments Schmidt et al., 2006	layers, canopy, routing Friend and Kiang, 2005
15: GISS-ER, 2004	NASA/GISS, USA	top = 0.1 hPa 4° x 5° L20 Schmidt et al., 2006	4° x 5° L13 mass/area, free surface Russell et al., 1995	rheology, leads Liu et al., 2003; Schmidt et al., 2004	no adjustments Schmidt et al., 2006	layers, canopy, routing Friend and Kiang, 2005
16: INM-CM3.0, 2004	Institute for Numerical Mathematics, Russia	top = 10 hPa 4° x 5° L21 Alekseev et al., 1998; Galin et al., 2003	2° x 2.5° L33 sigma, rigid lid Diansky et al., 2002	no rheology or leads Diansky et al., 2002	regional freshwater Diansky and Volodin, 2002; Volodin and Diansky, 2004	layers, canopy, no routing Alekseev et al., 1998; Volodin and Lykosoff, 1998
17: IPSL-CM4, 2005	Institut Pierre Simon Laplace, France	top = 4 hPa 2.5° x 3.75° L19 Hourdin et al., 2006	2° x 2° L31 depth, free surface Madec et al., 1998	rheology, leads Fichefet and Morales Maqueda, 1997; Goosse and Fichefet, 1999	no adjustments Marti et al., 2005	layers, canopy, routing Krinner et al., 2005
18: MIROC3.2(hires), 2004	Center for Climate System Research (University of Tokyo), National Institute for Environmental Studies, and Frontier Research Center for Global Change (JAMSTEC), Japan	top = 40 km T106 (~1.1° x 1.1°) L56 K-1 Developers, 2004	0.2° x 0.3° L47 sigma/depth, free surface K-1 Developers, 2004	rheology, leads K-1 Developers, 2004	no adjustments K-1 Developers, 2004	layers, canopy, routing K-1 Developers, 2004; Oki and Sud, 1998
19: MIROC3.2(medres), 2004		top = 30 km T42 (~2.8° x 2.8°) L20 K-1 Developers, 2004	0.5°–1.4° x 1.4° L43 sigma/depth, free surface K-1 Developers, 2004	rheology, leads K-1 Developers, 2004	no adjustments K-1 Developers, 2004	layers, canopy, routing K-1 Developers, 2004; Oki and Sud, 1998

Table 8.1 (continued)

Model ID, Vintage	Sponsor(s), Country	Atmosphere Top Resolution[a] References	Ocean Resolution[b] Z Coord., Top BC References	Sea Ice Dynamics, Leads References	Coupling Flux Adjustments References	Land Soil, Plants, Routing References
20: MRI-CGCM2.3.2, 2003	Meteorological Research Institute, Japan	top = 0.4 hPa T42 (~2.8° x 2.8°) L30 Shibata et al., 1999	0.5°–2.0° x 2.5° L23 depth, rigid lid Yukimoto et al., 2001	free drift, leads Mellor and Kantha, 1989	heat, freshwater, momentum (12°S–12°N) Yukimoto et al., 2001; Yukimoto and Noda, 2003	layers, canopy, routing Sellers et al., 1986; Sato et al., 1989
21: PCM, 1998	National Center for Atmospheric Research, USA	top = 2.2 hPa T42 (~2.8° x 2.8°) L26 Kiehl et al., 1998	0.5°–0.7° x 1.1° L40 depth, free surface Maltrud et al., 1998	rheology, leads Hunke and Dukowicz 1997, 2003; Zhang et al., 1999	no adjustments Washington et al., 2000	layers, canopy, no routing Bonan, 1998
22: UKMO-HadCM3, 1997	Hadley Centre for Climate Prediction and Research/Met Office, UK	top = 5 hPa 2.5° x 3.75° L19 Pope et al., 2000	1.25° x 1.25° L20 depth, rigid lid Gordon et al., 2000	free drift, leads Cattle and Crossley, 1995	no adjustments Gordon et al., 2000	layers, canopy, routing Cox et al., 1999
23: UKMO-HadGEM1, 2004		top = 39.2 km ~1.3° x 1.9° L38 Martin et al., 2004	0.3°–1.0° x 1.0° L40 depth, free surface Roberts, 2004	rheology, leads Hunke and Dukowicz, 1997; Semtner, 1976; Lipscomb, 2001	no adjustments Johns et al., 2006	layers, canopy, routing Essery et al., 2001; Oki and Sud, 1998

Notes:

[a] Horizontal resolution is expressed either as degrees latitude by longitude or as a triangular (T) spectral truncation with a rough translation to degrees latitude and longitude. Vertical resolution (L) is the number of vertical levels.

[b] Horizontal resolution is expressed as degrees latitude by longitude, while vertical resolution (L) is the number of vertical levels.

REFERENCES

Adler, R.F., G.J. Huffman, A. Chang, R. Ferraro, P. Xie, J. Janowiak, B. Rudolf, U. Schneider, S. Curtis, D. Bolvin, A. Gruber, J. Susskind, and P. Arkin, The Version 2 Global Precipitation Climatology Project (GPCP) Monthly Precipitation Analysis (1979-Present). *J. Hydromet.*, 4,1147-1167, 2003.

Agudelo PA, Curry JA, Analysis of spatial distribution in tropospheric temperature trends, *Geo. Res. Let.*, 31 (22): Art. No. L22207, 2004

Allen MR, Tett SFB, Checking for model consistency in optimal fingerprinting *Climate Dynamics,* 15 (6): 419-434, 1999.

Amarasekera, K.N., R.F. Lee, E.R. Williams, and E.A.B. Eltahir, 1997: ENSO and the natural variability in the flow of tropical rivers, *J. Hydrology*, 200 (1-4): 24-39, 1997.

Arkin, P. A, and B. N. Meisner, the relationship between large-scale convective rainfall and cloud cover over the western hemisphere during 1982-1084, *Monthly Weather Review*, 115, 51-74, 1987.

Barnett DN, Brown SJ, Murphy JM, et al., Quantifying uncertainty in changes in extreme event frequency in response to doubled CO2 using a large ensemble of GCM simulations, *Climate Dynamics,* 26 (5): 489-511, 2006.

Benestad RE, Can we expect more extreme precipitation on the monthly time scale? *J. Climate,* 19 (4): 630-637, 2006.

Berri, G.J., M.A. Ghietto and N.O. García 2002: The influence of ENSO in the flows of the Upper Paraná River of South America over the past 100 years, *J. Hydromet.,* 3(1): 57-65.

Bodo, B. A., Annotations for monthly discharge data for world rivers (excluding former Soviet Union). NCAR, 85 pp. [Available online at http://dss.ucar.edu/datasets/ds552.1/docs/.], 2001

Boroneant C, Plaut G, Giorgi F, et al. Extreme precipitation over the Maritime Alps and associated weather regimes simulated by a regional climate model: Present-day and future climate scenarios, THEORETICAL AND APPLIED CLIMATOLOGY 86 (1-4): 81-99, 2006.

Charney, J. G. and J. Shukla, *Predictability of monsoons. Monsoon Dynamics*, edited by J. Lighthill, pp. 99-110,Cambridge University Press, 1981.

Chang CP, Zhang YS, Li T, Interannual and interdecadal variations of the East Asian summer monsoon and tropical Pacific SSTs. Part I: Roles of the subtropical ridge, *J. Climate*, 13 (24): 4310-4325, 2000.

Chang CP, Zhang YS, Li T, Interannual and interdecadal variations of the East Asian summer monsoon and tropical Pacific SSTs. Part II: Meridional structure of the monsoon, *J. Climate,* 13 (24): 4326-4340, 2000.

Chaves RR, Ross RS, Krishnamurti TN, Weather and seasonal climate prediction for South America using a multi-model superensemble, *Int. J. Climatology*, 25 (14): 1881-1914, 2005.

China Daily on October 8, 2005, Flood Season Claims 1,292 Lives, accessed on July 20, 2007 from http://www.china.org.cn/english/features/flood/144401.htm

Chowdhury, M.R., 2003: The El Niño-Southern Oscillation (ENSO) and seasonal flooding – Bangladesh, *Theor. Appl. Climatol.*, 76,105-124.

Chowdhury, MD. R., and N. Ward, Hydro-meteorological variability in the greater Ganges-Brahmaputra-Meghna basins, *Int. J. Climatology*, 24, 1495-1508, 2004.

Clark, C. O., J. E. Cole, and P. J. Webster, 2000: SST and Indian summer rainfall: predictive relationships and their decadal variability. *J. Climate*., 13, 2503-2519.

Clark, C. O., P. J. Webster, and J. E. Cole, The Indian Ocean dipole and the prediction of East African precipitation, *J. Climate*, 16, 548-554, 2003.

Collins, W.D., C. M. Bitz, M. Blackmon, G. B . Bonan, C. S. Bretherton, J. A. Carton, P. Chang, S. Doney, J. J. Hack, T. Henderson, J. T. Kiehl, W. G. Large, D. McKenna, B. D. Santer, and R. Smith, The Community Climate System Model version 3 (CCSM3), *J. Climate*, 19 (11): 2122-2143, 2006.

Coupled Model Inter-comparison Project Phase three (CMIP3) data source, https://esg.llnl.gov:8443/index.jsp, accessed on Feb 2, 2007.

Curry, J.A., P.J. Webster and G.J. Holland, Mixing Politics and Science in Testing the Hypothesis That Greenhouse Warming Is Causing a Global Increase in Hurricane Intensity. *Bull. Amer. Met. Soc.*, 87 (8), 1025-1037, 2006.

Dai AG, Giorgi F, Trenberth KE，Observed and model-simulated diurnal cycles of precipitation over the contiguous United States，*J. Geo. Res.-Atmos*, 104 (D6): 6377-6402, 1999.

Dai AG, Trenberth KE, Estimates of freshwater discharge from continents: Latitudinal and seasonal variations, *J. Hydromet.*, 3 (6): 660-687, 2002.

Dai AG, Trenberth KE, The diurnal cycle and its depiction in the Community Climate System Model, *J. Climate*, 17 (5): 930-951, 2004.

Dai A, Fung IY, DelGenio AD, Surface observed global land precipitation variations during 1900-88, *J. Climate*, 10 (11): 2943-2962, 1997.

Dutta SC, Ritchie JW, Freebairn DM, et al., Rainfall and streamflow response to El Nino Southern Oscillation: a case study in a semiarid catchment, Australia, *Hydrological Sciences Journal-Journal Des Sciences Hydrologiques*, 51 (6): 1006-1020, 2006.

Eldaw, A.K., J.D. Salas, and L.A. Garcia, 2003: Long-Range Forecasting of the Nile River Flows Using Climatic Forcing, *J. Appl. Meteor.*, 42, 890-904.

Fang HW, Rodi W, Three-dimensional calculations of flow and suspended sediment transport in the neighborhood of the dam for the Three Gorges Project (TGP) reservoir in the Yangtze River, *J. Hydraulic Research*, 41 (4): 379-394, 2003.

Fasullo, J., and P. J., Webster, Hydrologic signatures relating the Asian summer monsoon and ENSO, *J. Climate*, 15, (21), pp. 3082–3095, 2002.

Global Runoff Data Centre (GRDC) station catalogue, accessed on Feb 2 2007 from http://grdc.bafg.de/servlet/is/910/20070807_GRDC_Stations.zip?command=downloadContent&filename=20070807_GRDC_Stations.zip

Harzallah, A. and R. Sadourny, Observed lead-lag relationships between Indian summer monsoon and some meteorological variables, *Climate Dynamics,* 13 (9): 635-648, 1997.

Hegerl, G.C., F. W. Zwiers, P. Braconnot, N.P. Gillett, Y. Luo, J.A. Marengo Orsini, N. Nicholls, J.E. Penner and P.A. Stott, 2007: Understanding and Attributing Climate Change. In: *Climate Change 2007: The Physical Science Basis. Contribution of Working Group I to the Fourth Assessment Report of the Intergovernmental Panel on Climate Change* [Solomon, S., D. Qin, M. Manning, Z. Chen, M. Marquis, K.B. Averyt, M. Tignor and H.L. Miller (eds.)]. Cambridge University Press, Cambridge, United Kingdom and New York, NY, USA.

Hopson, Thomas M, Operational Flood-Forecasting for Bangladesh, Ph.D. thesis, University of Colorado, 2005.

Hoyos, Carlos D, Intraseasonal Variability: Processes, Predictability and Prospects for Prediction, Ph.D. thesis, Georgia Institute of Technology, 2006.

Hoyos, C. and P. J. Webster, The Role of Intraseasonal Variability in the Nature of Asian Monsoon Rainfall, *J. Climate,* 20(17): 4402-4424, 2007.

Hubbard M, MERLO N, MAXWELL S, et al., REGIONAL FOOD SECURITY STRATEGIES - THE CASE OF IGADD IN THE HORN OF AFRICA, *Food Policy*, 17 (1), 1992

Jian, J. , Webster P., et al., Predictability of Ganges and Brahmaputra river dishcarge on intraseasonal and seasonal time scales, submitted to *J of Climate*, 2007.

IPCC-AR4 MRI,http://www.mri-jma.go.jp/Dep/cl/cl4/IPCC-AR4/simulations2.html, accessed on Feb 2, 2007.

IPCC data distribution Centre, http://www.ipcc-data.org/sres/ddc_sres_emissions.html

IPCC Synthesis report, Summary for policy makers, accessed on July 15, 2007 from http://www.ipcc.ch/pub/un/syreng/spm.pdf

IPCC third assessment report (TAR), accessed on July 30, 2001 from http://www.grida.no/climate/ipcc_tar/.

IPCC second assessment report (SAR), accessed on July 20, 2007 from http://www.ipcc.ch/pub/sa(E).pdf.

IPCC first assessment report, Scientific Assessment of Climate Change, JT Houghton, GJ Jenkins and JJ Ephraums, Cambridge University Press, UK. pp. 365, 1992.

Hastenrath, S., On the prediction of India monsoon rainfall anomalies, *J. Clim. Appl. Meteorol.*, 26, 847-857, 1987.

Hirsch, R. M., J. R. Slack, and R. Smith, Techniques of trend analysis for monthly water quality data, *Water Resource Research*, 8, 107–121, 1982.

Karl TR, Trenberth KE, Modern global climate change, *Science*, 302 (5651): 1719-1723, 2003.

Kendall, M. and Jean Dickinson Gibbons, 10th edition, *Rank Correlation Methods,* Edward Arnold, 1990.

Kendall, M. G., *A New Measure of Rank Correlation*, Biometrika , 30, 81-93, 1938.

Krishnamurti TN, Kishtawal CM, LaRow TE, Bachiochi DR, Zhang Z, Williford CE, Gadgil S, Surendran S, Improved weather and seasonal climate forecasts from multimodel superensemble, *Science*, 285 (5433): 1548-1550, 1999.

Krishnamurti TN, Stefanova L, Chakraborty A, Kumar TSVV, Cocke S, Bachiochi D, Mackey B, Seasonal forecasts of precipitation anomalies for North American and Asian monsoons, J. METEOROLOGICAL SOCIETY OF JAPAN 80 (6): 1415-1426, 2002.

Krishnamurti TN, Mitra AK, Kumar TSVVK, et al., Seasonal climate forecasts of the South Asian monsoon using multiple coupled models, *Tellus Series A-Dyn. Meterol. and Ocean.*, 58 (4): 487-507, 2006.

Kumar, K. K., Rajagapolan, B., Cane, M. A., On the weakening relationship between the Indian monsoon and ENSO. *Science*, 284 (5423): 2156-2159, 1999.

Labat, D., Ronchail, J., Callede, et al., Wavelet analysis of Amazon regime variability, *Geo. Res. Let.,* 31 (2) Article No, L02501, 2004.

Labat, D., Ronchail, J., Guyot, J. L., Recent advances in wavelet analysis: part 2: Amazon, Parana, Orinico and Congo discharges. *J. Hydrology,* 324 (1-4), 239-311, 2005.

Lawrence, D, and P. J. Webster, Interannual variability of intraseasonal oscillation in the Asian monsoon region. *J. Climate*, 14(3), 2910-2922, 2001.

Lawrence, D, and P. J. Webster, The boreal summer intraseasonal oscillation and the South Asian monsoon. *J. Atmos. Sci*., 59, 1593-1606, 2002.

Le Treut, H., R. Somerville, U. Cubasch, Y. Ding, C. Mauritzen, A. Mokssit, T. Peterson and M. Prather, Historical Overview of Climate Change. In: *Climate Change 2007: The Physical Science Basis. Contribution of Working Group I to the Fourth Assessment Report of the Intergovernmental Panel on Climate Change* [Solomon, S., D. Qin, M. Manning, Z. Chen, M. Marquis, K.B. Averyt, M. Tignor and H.L. Miller (eds.)]. Cambridge University Press, Cambridge, United Kingdom and New York, NY, USA, 2007.

Livezey, R.E. and W.Y. Chen, Statistical field significance and it's determination by Monte Carlo Techniques, *Monthly Weather Review*, 111, 46-59, 1983.

Livezey, R. E., Variability of skill of long-range forecasts and implications for their use and value, *Bull. Amer. Met. Soc.*, 71, 288--299, 1990.

Mann, H.B., Non-parametric tests against trend, *Econometrica*, 13, 245-259, 1945.

MATTSSON JO, RAPP A, The RECENT DROUGHTS IN WESTERN ETHIOPIA AND SUDAN IN A CLIMATIC CONTEXT, *Ambio,* 20 (5): 172-175, 1991.

Meehl, G.A., T.F. Stocker, W.D. Collins, P. Friedlingstein, A.T. Gaye, J.M. Gregory, A. Kitoh, R. Knutti, J.M. Murphy, A. Noda, S.C.B. Raper, I.G. Watterson, A.J. Weaver and Z.-C. Zhao, Global Climate Projections. In: *Climate Change 2007: The Physical Science Basis. Contribution of Working Group I to the Fourth assessment Report of the Intergovernmental Panel on Climate Change* [Solomon, S., D. Qin, M. Manning, Z. Chen, M. Marquis, K.B. Averyt, M. Tignor and H.L.

Miller (eds.)], Cambridge University Press, Cambridge, United Kingdom and New York, NY, USA, 2007.

Meehl, CMIP2 announcement in 1997, accessed on July 30, 2007 from http://www-pcmdi.llnl.gov/projects/cmip/announ.php.

Meehl GA, Boer GJ, Covey C, Latif M, Stouffer RJ, The coupled model intercomparison project (CMIP), *Bull. Amer. Met. Soc.,* 81: 313–318, 2000.

Meehl, G. A., W. M. Washington, C. M. Ammann, J. M. Arblaster, T. M. L. Wigley, and C. Tebaldi, Combinations of natural and anthropogenic forcings in twentieth-century climate. *J. Climate,* 17, 3721–3727, 2004.

Mirza MMQ, Warrick RA, Ericksen NJ, The implications of climate change on floods of the Ganges, Brahmaputra and Meghna rivers in Bangladesh, *Climate Change,* 57 (3): 287-318, 2003.

The New Zealand Herald on November 8, 2006, Australia's dry horrors "worst for 1000 years", accessed on July 20, 2007 from http://subs.nzherald.co.nz/section/story.cfm?c_id=2&objectid=10409680

Paleoclimate Modeling Inter-comparison Project (PMIP), accessed on July 1st, 2007 from http://pmip.lsce.ipsl.fr/

Paleoclimate Modeling Intercomparison Project (PMIP): *proceedings of the third PMIP workshop*, Canada, 4-8 october 1999, in WCRP-111, WMO/TD-1007, edited by P. Braconnot, pp 271, 2000.

Paleoclimate Modeling Inter-comparison Project Phase 2 (PMIP2), accessed on July 1st, 2007 from http://www.lsce-cea.fr/pmip2

Palmer TN, Ralsanen J, Quantifying the risk of extreme seasonal precipitation events in a changing climate, *Nature*, (6871): 512-514, 2002.

People's Daily on July 31, 2007, The direct economical loss has reached 52.5 million RMB this year (in Chinese), accessed on August 3, 2007 from http://paper.people.com.cn/rmrb/html/2007-07/31/content_14139652.htm

PMIP2, Crucifix, M., P. Braconnot, S.P. Harrison, B. Otto-Bliesner, Second phase of Paleoclimate Modelling Intercomparison Project, *EOS*, Vol 86, No. 28, 2005.

Randall, D.A., R.A. Wood, S. Bony, R. Colman, T. Fichefet, J. Fyfe, V. Kattsov, A. Pitman, J. Shukla, J. Srinivasan, R.J. Stouffer, A. Sumi and K.E. Taylor, Climate Models and Their Evaluation. In: *Climate Change 2007: The Physical Science Basis. Contribution of Working Group I to the Fourth Assessment Report of the Intergovernmental Panel on Climate Change* [Solomon, S., D. Qin, M. Manning,

Z. Chen, M. Marquis, K.B. Averyt, M.Tignor and H.L. Miller (eds.)], Cambridge University Press, Cambridge, United Kingdom and New York, NY, USA, 2007.

Special Report on Emissions scenarios (SRES), http://www.ipcc.ch/pub/sres-e.pdf and http://www.grida.no/climate/ipcc/emission/, accessed on June 20, 2007.

Trenberth KE, Dai AG, Rasmussen RM, et al.， The changing character of precipitation, *Bull. Amer. Met. Soc.*, 84 (9): 1205, 2003.

Räisänen J, Palmer TN, A probability and decision-model analysis of a multimodel ensemble of climate change simulations, *J. Climate,* 14 (15): 3212-3226, 2001.

Räisänen J, CO2-induced changes in interannual temperature and precipitation variability in 19 CMIP2 experiments, *J. Climate,* 15 (17): 2395-2411, 2002.

Räisänen J, Impact of increasing CO2 on monthly-to-annual precipitation extremes: analysis of the CMIP2 experiments CLIMATE DYNAMICS 24 (2-3): 309-323, 2005.

Räisänen J, How reliable are climate models? TELLUS SERIES A-DYNAMIC Meteorology and Oceanography, 59 (1): 2-29, 2007.

Ramírez, J.M., and J.I. Vélez, Estrategias para la estimacion automatica de direcciones de drenaje a partir de modelos digitales de terreno. *Avances en Recursos Hidráulicos.* Vol. 9, 45-63, 2002.

Saji, N. H., B.N. Goswami, P.N. Vinayachandran, and T. Yamagata, A dipole mode in the tropical Indian Ocean, *Nature,* 401, 6751, 360-363, 1999.

Senior CA, Jones RG, Lowe JA, et al. Predictions of extreme precipitation and sea-level rise under climate change, *Philosophical Transactions: Mathematical, Physical and Engineering Sciences*, 360 (1796): 1301-1311, 2002.

Shaman, J., M. Cane, and A. Kaplan, The relationship between Tibetan snow depth, ENSO, river discharge and the monsoons of Bangladesh, *Inter. J. of Remote Sensing,* 26, 17, 3735-3748, 2005.

Shukla, J., Predictability of the tropical atmosphere, the tropical oceans and TOGA, *in Proceedings of the International Conference on the Tropical Ocean-Global Atmopshere (TOGA) Programme*, Vol. 2., WCRP-91, pp.725-730, World Climate Research Programme, Geneva, Switzerland, 1995.

Shukla, J. and D.A. Paolina, The southern oscillation and long range forecasting of the summer monsoon rainfall over India, *Monthly Weather Review*, 111, 1830-1837, 1983.

Shukla, J., and M. J. Fennessy, Simulation and predictability of monsoons, *in Proceedings of the International Conference on Monsoon Variability and Prediction,* Tech. Rep. WCRP--84, 567--575, World Climate Research Programme, Geneva, Switzerland, 1994.

Sikka, D., and S. Gadgil, On the maximum cloud zone and the ITCZ over Indian longitudes during the southwest monsoon, *Monthly Weather Review*, 108, 1840–1853, 1980.

SIMPSON HJ, CANE MA, HERCZEG AL, et al., ANNUAL RIVER DISCHARGE IN SOUTHEASTERN AUSTRALIA RELATED TO EL-NINO SOUTHERN OSCILLATION FORECASTS OF SEA-SURFACE TEMPERATURES, *Water Resources Research*, 29 (11): 3671-3680, 1993.

SIMPSON HJ, CANE MA, LIN SK, et al. FORECASTING ANNUAL DISCHARGE OF RIVER MURRAY, AUSTRALIA, FROM A GEOPHYSICAL MODEL OF ENSO, *J. Climate,* 6 (2): 386-391, 1993.

Smith, T. M., and R.W. Reynolds, 2003: Extended Reconstruction of Global Sea Surface Temperatures Based on COADS Data (1854-1997). *J. Climate*, 16, 1495-1510.

Solomon, S., D. Qin, M. Manning, R.B. Alley, T. Berntsen, N.L. Bindoff, Z. Chen, A. Chidthaisong, J.M. Gregory, G.C. Hegerl, M. Heimann, B. Hewitson, B.J. Hoskins, F. Joos, J. Jouzel, V. Kattsov, U. Lohmann, T. Matsuno, M. Molina, N. Nicholls, J. Overpeck, G. Raga, V. Ramaswamy, J. Ren, M. Rusticucci, R. Somerville, T.F. Stocker, P. Whetton, R.A. Wood and D. Wratt, Technical Summary. In: *Climate Change 2007: The Physical Science Basis. Contribution of Working Group I to the Fourth Assessment Report of the Intergovernmental Panel on Climate Change* [Solomon, S., D. Qin, M. Manning, Z. Chen, M. Marquis, K.B. Averyt, M. Tignor and H.L. Miller (eds.)], Cambridge University Press, Cambridge, United Kingdom and New York, NY, USA, 2007.

Stephenson, D. B., K. R. Kumar, F. J. Doblas-Reyes, J.-F. Royer, F. Chauvin and S. Pezzulli, Extreme Daily Rainfall Events and Their Impact on Ensemble Forecasts of the Indian Monsoon, *Monthly Weather Review,* Vol. 127, No. 9, 1954-1966, 1999.

Subbiah, A., Ed., Initial report on the Indian monsoon drought of 2002, Asian Disaster Preparedness Center, *Technical Report*, Bangkok, Thailand, 29 pp, 2004.

Tanaka, H.L., N. Ishizaki, and D. Nohara, 2005: Intercomparison of the intensities and trends of Hadley, Walker and monsoon circulations in the global warming projections. *Scientific Online Letters on the Atmosphere*, **1**, 77–80.

Tawfik, M., Linearity versus non-linearity in forecasting Nile River flows, *Advances in Engineering Software*, 34 (8), 515-524, 2003.

Torrence, C. and P. J. Webster, The Annual Cycle of Persistence in the El Niño-Southern Oscillation. *Quart. J. Roy. Meteor. Soc.*, 124, 1985-2004, 1998.

Torrence, C., and P. J. Webster, Interdecadal changes in the ENSO-Monsoon System. *J. Climate.*, 12, 2679-2690, 1999.

Trenberth, K.E., P.D. Jones, P. Ambenje, R. Bojariu, D. Easterling, A. Klein Tank, D. Parker, F. Rahimzadeh, J.A. Renwick, M. Rusticucci, B. Soden and P. Zhai, Observations: Surface and Atmospheric Climate Change. In: *Climate Change 2007: The Physical Science Basis*. Contribution of Working Group I to the Fourth Assessment Report of the Intergovernmental Panel on Climate Change [Solomon, S., D. Qin, M. Manning, Z. Chen, M. Marquis, K.B. Averyt, M. Tignor and H.L. Miller (eds.)]. Cambridge University Press, Cambridge, United Kingdom and New York, NY, USA, 2007.

Trenberth KE, Shea DJ, Relationships between precipitation and surface temperature, *Geo. Res. Let.,* 32 (14): Art. No. L14703, Jul 19 2005.

Troup, A. J., The Southern Oscillation. *Quar. J. Roy. Meteor. Soc.*, 91, 490-506, 1965.

Vavrus S, Walsh JE, Chapman WL, et al. The behavior of extreme cold air outbreaks under greenhouse warming, *Int J. Climatol*, 26 (9): 1133-1147, 2006.

Wang B, Wu RG, Li T, Atmosphere-warm ocean interaction and its impacts on Asian-Australian monsoon variation, *J. Climate,* 16 (8): 1195-1211, 2003.

Wang, G., and E.A.B. Eltahir, Use of ENSO information in medium- and long-range forecasting of the Nile floods. *J. Climate,* 12, 1726–737, 1999.

Webster, P. J., Mechanisms of Monsoon Transition: Surface Hydrology Effects, *J. Atmos. Sci*., 40, 2110-2124, 1983.

Webster, P.J., V.O. Magana , T.N. Palmer, J. Shukla, R.A. Tomas, M. Yanai, and T. Yasunari, Monsoons, Processes, Predictability, and the Prospects for Prediction, *J. Geophys Res*., 103 c7, 14451-14510, 1998.

Webster, P.J., A. Moore, J.P. Loschnigg, and R.R. Leban, Coupled ocean-atmosphere dynamics in the Indian Ocean during 1997-98, *Nature,* 401, 23, 356-360, 1999.

Webster, P. J, and C. Hoyos, Prediction of Monsoon Rainfall and River Discharge on 15-30 day Time Scales, *Bull. Amer. Met. Soc.*, 85 (11): 1745-1765, 2004.

Webster, P. J., T. Hopson, C. Hoyos, A. Subbiah, H-. R. Chang, and R. Grossman, A three-tier overlapping prediction scheme: Tools for strategic and tactical decisions in the developing world, In *Predictability of Weather and Climate*, Ed. T. N. Palmer, Cambridge University Press, 2006.

Whitaker, D.W., S.A. Wasimi, and S. Islam, The El Niño-Southern Oscillation and long-range forecasting of flows in the Ganges, *Int. J. Climatology*, 21, 77-87, 2001.

Wikipedia, "China flooding" (in Chinese), accessed on July 30, 2007 from http://zh.wikipedia.org/wiki/中国洪水

Wu BY, Weakening of Indian summer monsoon in recent decades, *Adv. Atmos. Sci*, 22 (1): 21-29, 2005.

Xu KQ, Brown C, Kwon HH et al., Climate teleconnections to Yangtze river seasonal streamflow at the Three Gorges Dam, China, *Int. J. Climatology*, 27 (6): 771-780, 2007.

Xu M, Chang CP, Fu CB, et al., Steady decline of east Asian monsoon winds, 1969-2000, Evidence from direct ground measurements of wind speed, *J. Geophys. Res-Atmos*, 111 (D24): Art. No. D24111, DEC 23 2006

Xue F, Interannual to interdecadal variation of East Asian summer monsoon and its association with the global atmospheric circulation and sea surface temperature, *Adv. Atmos. Sci.*, 18 (4): 567-575, 2001.

Yasunari, T., Impact of Indian monsoon on the coupled atmosphere/ocean system in the tropical Pacific, *Meteorol. and Atmos. Phys.*, 44, 29-41, 1990.

Yukimoto S, Endoh M, Kitamura Y, et al., ENSO-like interdecadal variability in the Pacific Ocean as simulated in a coupled general circulation model, *J. Geophysical Research-Oceans*, 105 (C6): 13945-13963, 2000.

Zhang Q, Xu CY, Jiang T, et al., Possible influence of ENSO on annual maximum streamflow of the Yangtze River, China, *J. Hydrology*, (2-4): 265-274 FEB 15 2007

Zhang Y, Xu YL, Dong WJ, et al. A future climate scenario of regional changes in extreme climate events over China using the PECIS climate model, *Geo. Res. Let.,* 33 (24): Art. No. L24702, 2006.